Title
Delayed Gamma-Ray Assay for Nuclear Safeguards

Author
Mozin, Vladimir

Publication Date
2011

Peer reviewed|Thesis/dissertation

Delayed Gamma-Ray Assay for Nuclear Safeguards

By

Vladimir Mozin

A dissertation submitted in partial satisfaction of the

requirements for the degree of

Doctor of Philosophy

in

Engineering – Nuclear Engineering

in the

Graduate Division

of the

University of California, Berkeley

Committee in charge:

Professor Jasmina Vujic, Chair
Dr. Stephen J. Tobin
Professor Kai Vetter
Professor James Siegrist

Fall 2011

Delayed Gamma-Ray Assay for Nuclear Safeguards

by

Vladimir Mozin

Abstract

Delayed Gamma-Ray Assay for Nuclear Safeguards

by

Vladimir Mozin

Doctor of Philosophy in Engineering – Nuclear Engineering

University of California, Berkeley

Professor Jasmina Vujic, Chair

This dissertation addresses the need for new non-destructive assay instruments capable of quantifying the fissile isotopic composition of spent nuclear fuel and of independently verifying the declared amounts of special nuclear materials at various stages of the nuclear fuel cycle. High-energy delayed gamma-ray spectroscopy can provide the ability to directly assay fissile and fertile isotopes in the highly radioactive environment of the spent fuel assemblies and to achieve the safeguards goal of measuring nuclear material inventories for spent fuel handling, interim storage, reprocessing facilities, and final disposal and repository sites.

The delayed gamma-ray assay concept is investigated within this context with the objective of assessing whether the delayed gamma-ray assay instrument can provide sufficient sensitivity, isotope specificity and accuracy as required in nuclear material safeguards applications. Preliminary system design analysis indicates that the delayed gamma-ray response is affected by multiple parameters: type and intensity of the interrogating source, the configuration of the interrogation setup, the time pattern of the interrogation, and the resolution and count rate limit of the gamma-ray detection system.

In order to handle the variety of factors associated with the delayed gamma-ray assay of spent nuclear fuel, a high-fidelity response modeling technique is introduced. The new algorithm seamlessly combines transport calculations with analytical decay/depletion, and discrete gamma-ray source reconstruction codes. Its performance was benchmarked in the dedicated experimental campaign involving accelerator-driven photo-neutron sources and samples containing fissile and fertile isotopes.

Analytical estimations of the intensity of the delayed gamma-ray response and the passive background rate are utilized to develop a concept of the non-destructive instrument for the assay of spent nuclear fuel. The modeling technique is then applied to more detailed parametric study. These simulations included extensive spent fuel inventories, and accounted for realistic assay configurations and instrumentation. The results of this preliminary analysis indicate that the delayed gamma-ray assay of spent nuclear fuel assemblies can be performed with available neutron generator and detection technology.

The sensitivity of the delayed gamma-ray spectra to the actinide content of the spent nuclear fuel is investigated. The simplest analysis of the delayed gamma-ray response is based on the analysis of integrated count rates and peak ratios. More powerful analytical and numerical methods are likely needed for determining the relative concentrations of fissile and fertile isotopes in samples with complex compositions.

Contents

List of Figures

List of Tables

Chapter 1

Introduction

1.1 Nuclear Nonproliferation and Safeguards

The anticipated expansion of commercial nuclear power generation, often associated with the nuclear renaissance, inevitably involves potential risks of materials diversion and the misuse of technologies for undeclared weapons production and terrorist activities. Sustainable development and the security of nuclear energy are contingent upon creating appropriate control mechanisms to prevent these threats.

Debates revolving around proliferation concerns have been prominent since the early days of nuclear technology. Nuclear power was originally presented in the form of a weapon of mass destruction and emerged only later as an energy source. This double-use perception has continued to taint the notion of civilian nuclear power throughout history. With respect to operating nuclear facilities in various countries, the concern is that peaceful activities could be diverted to the nuclear weapons program by a mere political decision. Nevertheless, it was always clear that the process of nuclear power development is unstoppable. A gradual but constant expansion of nuclear power generation capacity could be observed across the globe over the last several decades, and today particularly in developing nations.

As early as 1953, President Eisenhower presented the politically controversial program “Atoms for Peace” to the United Nations (U.N.) [1]. In doing so, he introduced the idea of international control over peaceful nuclear activities and fissile materials. After intensive international negotiations, a statute of the new

international control organization – the International Atomic Energy Agency (IAEA) was adopted in 1957. The goals of the agency were at the time and are to this day to facilitate the peaceful applications of nuclear energy and to prevent its use for any military purpose. To this end, the IAEA statute introduced the concept of nuclear safeguards (INFCIRC/66, also known as "Classical safeguards") [2], according to which a country recipient of nuclear technology makes it subject to IAEA inspections and regulations.

The Nuclear Nonproliferation Treaty (NPT) adopted in 1970 has further improved the control regime over nuclear technology. The discriminatory nature of the NPT is manifested in the fact that all countries except for 5 nuclear weapon states have to renounce the pursuit of nuclear military programs in exchange for a right to benefit from the development of peaceful nuclear applications. The comprehensive safeguards agreement (INFCIRC/153) [3] outlined the role of the IAEA as an independent control mechanism of nuclear programs in these countries. This safeguards agreement allowed IAEA inspections only of the declared nuclear activities. This has proven to be an effective tool for the countries in compliance with the NPT, but is severely limited when it comes to detecting covert activities.

After the discovery of the clandestine Iraqi nuclear program in the early 1990s, a new format for safeguards was negotiated and adopted as a prerequisite for any nuclear cooperation. The new agreement known as the "Additional Protocol" (INFCIRC/540) [4] provided the IAEA with extended capabilities for detecting undeclared activities using unannounced inspections with a variety of technical and political means. The U.S. Nuclear Regulatory Commission (NRC) and the U.S. Department of Energy (DOE) have implemented new technical and institutional measures in the U.S. to unify safeguards requirements with the IAEA and to standardize material control and accountancy procedures within the government complex.

In the aftermath of the September 11th, 2001 terrorist attacks, a new kind of threat emerged. The expansion of the terrorist network all over the world has increased the risk that nuclear materials may be acquired by means of theft or clandestine

diversion through a state sponsor. These materials can be further used for the production of crude nuclear explosive devices or in radioactive dispersal devices often referred to as a "dirty bombs". These risks increase in countries where nuclear material control and accountancy systems have not kept up with the growth of the nuclear program.

Presently, many nations have announced plans to exercise their right of expanding nuclear power use to ensure social and energy stability for their own economic systems. Many of these countries do not have the appropriate infrastructure and experience with controlling nuclear materials and technological processes. Thus, monitoring such an expansion would become the responsibility of the international community. Under these conditions, the primary challenges associated with nuclear proliferation from expanding commercial nuclear power and nuclear fuel cycle technologies can be formulated as follows:

- A threat of nuclear terrorism by means of nuclear material theft, or supplied by a rogue state sponsor.
- Covert diversion of nuclear materials from civilian nuclear fuel cycle facilities for weapons production.
- The creation of a clandestine nuclear weapons program parallel to the existing civilian nuclear fuel cycle.

Meeting these threats will require the development of new methodologies and instrumentation in support of the safeguards regime. New techniques that can more quickly and accurately survey nuclear materials at various facilities around the world are required to support already existing and future political agreements. This material control and accountancy technology can be implemented by means of the IAEA safeguards inspections or can become a part of multi-lateral agreements on nuclear cooperation.

1.2 Spent Nuclear Fuel Safeguards

The IAEA defines the objective of the "Comprehensive Safeguards" agreement as "…*the timely detection of diversion of significant quantities of nuclear materials*

from peaceful nuclear activities to the manufacture of nuclear weapons or of other nuclear explosive devices or for purposes unknown, and the deterrence of such diversion by the risk of early detection" [3]. The "Additional Protocol" further extends this objective to "…*the detection of undeclared nuclear materials and activities in a State*" [4]. Therefore, the overall goal of the safeguards regime is to assure that nuclear materials are not used outside the civilian programs by means of diversion from the known (declared) facilities, or by maintaining concealed (undeclared) activities. For the declared nuclear programs, the IAEA develops technical procedures in accordance with a facility- and a technology-specific model (also called a generic safeguards approach). Undeclared activities can occur both at the declared facilities and at the covert installations, and identifying them often requires intelligence-gathering measures in support of the technical safeguards.

The key concern with expanding commercial nuclear power generation is that it can be used for diversion or undeclared production of weapons-grade materials, specifically highly enriched uranium (HEU) or plutonium. Fuel enrichment, fabrication, reactor operation, spent fuel storage, reprocessing, and mixed oxide (MOX) production are considered the most vulnerable stages of the nuclear fuel cycle. Enrichment facilities that produce low-enriched uranium can be converted to HEU generation. Spent nuclear fuel handling facilities are vulnerable to diversion of the plutonium accumulated during the reactor operation.

In order to detect the diversion of significant quantities of plutonium from the commercial nuclear fuel cycle in a timely manner, the IAEA identifies material amounts and time rates for the various forms of nuclear materials. Each element or isotope with proliferation potential is characterized by a Significant Quantity (SQ) – "*the approximate amount of nuclear material for which the possibility of manufacturing a nuclear explosive device cannot be excluded*" [5]. In addition, the IAEA defines a timeliness goal for these nuclear materials as a target SQ diversion detection time. This time is determined individually for each material category based on complexity, amount, and time requirements necessary for its conversion into the weapons-usable form. SQs and timeliness goals are generally lower for the "direct-use" materials that can be diverted to the manufacture of

nuclear explosive devices without transmutation or further enrichment. Table 1.1 compares the IAEA safeguards goal quantities for the most important nuclear materials and forms.

Table 1.1. A comparison of IAEA safeguards goal quantities for the most important nuclear materials.

Material form	Type	Category	SQ	Timeliness
Enrichment plant safeguards				
UF_6 (LEU[b]), Natural and Depleted U	Unirradiated	Indirect use	75 kg U-235	1 year
UF_6 (HEU[a])	Unirradiated	Direct use	25 kg U-235	1 month
Light water reactor safeguards				
LEU fresh fuel	Unirradiated	Indirect use	75 kg U-235	1 year
HEU fresh fuel	Unirradiated	Direct use	25 kg U-235	1 month
MOX fresh fuel	Unirradiated	Direct use	8 kg total Pu[c]	1 month
Reactor core fuel	Irradiated	Direct use	8 kg total Pu[c]	3 months
Spent fuel	Irradiated	Direct use	8 kg total Pu[c]	3 months

[a] U-235 + U-233 ≥ 20%
[b] U-235 + U-233 < 20%
[c] Pu-238 < 80%

According to Table 1.1, plutonium-containing materials are the highest priority for safeguards, both because of their low SQ and relatively short conversion times that affect the timeliness goals. Since HEU is not typically present in the conventional nuclear fuel cycle, plutonium material streams are the primary source for direct-use material diversion. Irradiated nuclear fuel handling and reprocessing facilities thus require intense safeguards to reduce the risks of proliferation. Although the weapon potential of plutonium with a complex

isotopic composition obtained in high-burnup spent fuel is still widely debated, the present concept is applied to all variations of Pu-containing materials in the nuclear fuel cycle.

The intense radioactivity of irradiated spent nuclear fuel is not considered an adequate protection for its plutonium content. With a relatively modest infrastructure, it can be radiochemically separated with decontamination factors sufficient for further weapon production. The annual worldwide spent nuclear fuel (SNF) discharge rate is approximately 10,500 tons of heavy metal containing on average 1% of elemental plutonium [6]. This amount corresponds to over 13,000 SQ of plutonium produced annually in terms of IAEA goal quantities. Some of the discharged fuel is reprocessed, however most of it is stored in water-filled pools, with a small fraction in dry cask storage. Under these conditions, several likely scenarios for plutonium diversion may be considered: (1) diversion of the full SNF assembly (gross defect), (2) removal of individual pins from an assembly and substitution with dummy ones (partial defect), and (3) theft of nuclear fuel material at the start of the reprocessing operation when spent fuel changes its physical form.

At spent nuclear fuel storage facilities where sampling and destructive analysis is not available, fuel inventories and plutonium content are derived approximately using burnup-depletion codes and from characteristics of the reactor operation history. Due to complicated structure and exposure rates, the integrity of nuclear materials in the fuel is most often controlled through visual inspections and methods involving the gross-count of passive emissions. This “containment and surveillance” safeguards approach involves per-item accountancy and integrity verification of the spent fuel assemblies and does not have the capacity to directly control plutonium inventories. The accuracy of the computer codes used to estimate plutonium concentration in the fuel is only on the order of 5 to 10% [7]. This uncertainty level increases considerably when the fuel reactor history is atypical or unknown.

When spent nuclear fuel is moved to a reprocessing plant, the same containment and surveillance methods are used until fuel assemblies are transferred to the head

of the separation process. At this stage, assemblies are sheared, fuel is dissolved and leached out, and destructive analysis is performed on a sample of the resulting aqueous solution. Although nuclear materials inventory in the solution can be established with a nominal accuracy of approximately 1%, it is obtained as an average for several assemblies, and does not account for any losses occurring in the process. Uncertainties in material streams associated with transition from "per item" to "per mass" accountancy make the head of the reprocessing cascade extremely vulnerable to plutonium diversion.

The problem of safeguarding fissile materials in spent nuclear fuel can be effectively mitigated by improving the regulators knowledge about an assemblies' content at any point in time after discharge from a reactor. Studies of techniques for accurately measuring spent fuel inventories are currently underway [8,9] with particular emphasis being placed on the development of non-destructive assay methods.

1.3 Importance of Non-destructive Assay

Presently, destructive assay which is based primarily on physical and chemical instrumentation analysis, continues to be the most reliable tool for nuclear material accountancy tasks at nuclear fuel cycle facilities. It provides a high degree of accuracy and reliability in cases when representative samples can be collected from the established material flows. However, this approach to materials security is limited by the associated costs, personnel exposures, and labor-intensive procedures. As the number of nuclear fuel cycle facilities continues to increase and new technologies are developed, the application of destructive assay becomes more complicated and makes full coverage of nuclear material inventories prohibitively expensive. Under these conditions and in cases when "ad hoc" investigations (performed without disrupting the established technological process) are required, non-destructive assay (NDA) techniques emerge as a more attractive option when compared to traditional radiochemical analysis.

A number of NDA instruments are presently being used for spent fuel characterization. Among these instruments are the Cherenkov Viewing Device [10], Fork Detector [11], and Safeguards MOX Python detector [12]. These passive assay instruments measure indirect signatures of nuclear materials contained in spent fuel assemblies in the form of light and gamma-ray emissions from decaying fission products, and neutron emissions primarily from the accumulated curium. The application of these instruments is mostly limited to verification of the relative burnup, cooling time, and fuel material integrity (absence of partial defects). Such measurements can be related to inventory calculations with burnup/depletion codes. However, plutonium content determination is still very difficult because of the many variables associated both with reactor history and measured data.

Direct measurements of nuclear materials can be achieved using active interrogation techniques when an external source is used to induce actinide-specific responses and override the passive background. Neutron and high-energy photon interrogating sources are commonly considered for inducing unique prompt and delayed signatures capable of direct assay of the fissile and fertile materials. Generally, active non-destructive assay techniques offer important response flexibility controlled by the changing parameters of the interrogating source and detector system. Unlike active assay, the following attributes are not found in passive techniques:

- Adjustable response intensity;
- Distinguishable isotope-specific signatures;
- Analysis of several material characteristics in the same interrogation setup;
- Capability to isolate target signatures and suppress interfering signals;
- Assay of materials in the presence of a considerable radioactive background.

Despite these advantages, no active NDA instruments are used for spent nuclear fuel safeguards applications at this time. These methods require high-intensity interrogation sources and elaborate assay setups that likely have to be integrated into existing and newly constructed spent fuel handling facilities. As the need for

the accurate determination of plutonium content rises, increased efforts are emerging to deploy active NDA techniques for routine safeguards verifications.

1.4 Delayed Gamma-Ray Assay Potential

Delayed gamma-ray interrogation techniques offer the attractive capability of non-destructive direct measurement and quantification of fissile and fertile isotopes in spent nuclear fuel. This technique is based on inducing fissions by interrogation with neutrons or photons and the subsequent detection of delayed gamma-rays emitted from the fission products. The response analysis relies on the difference in rates at which gamma-emitting isotopes are produced in fission events. The intensities of detected individual delayed gamma-ray peaks in measured spectra are governed by fission product yield distributions and provide a signature for each fissionable element present in the assayed material.

Earlier research on the delayed gamma-ray (DG) method was primarily experimental. Possible applications included: determining the qualitative presence of fissile or fertile isotopes [13], waste packages characterization [14,15], transport containers screening [16], and uranium enrichment measurements [17]. More recent publications [18-20] offer empirical studies of the DG applicability to nuclear forensics and the determination of the residual fission rates in irradiated nuclear fuel elements. These works demonstrate the potential of the delayed gamma-ray technique as an assay method for simplified cases, but fail to effectively deal with the complexities of the DG responses and to offer generalized assay principles and analysis techniques necessary for safeguards and accountancy applications.

1.5 Dissertation outline

This dissertation addresses the need for new non-destructive assay instruments for quantifying the actinide composition of spent nuclear fuel and independent verification of the declared quantities of special nuclear materials at key stages of

the fuel cycle. It discusses the importance of the non-destructive assay techniques for quantitative measurements of fissile and fertile isotopic compositions in safeguards applications. Subsequently, the delayed gamma-ray active interrogation technique is introduced with the overall objective of assessing whether this assay principle can provide sufficient sensitivity, isotope specificity and accuracy as required in nuclear material safeguards.

Chapter 2 outlines the theoretical background behind the proposed assay method. It begins with a description of the induced fission process and the associated effects applicable for the non-destructive assay. Compared to other detectable signatures, delayed gamma-rays are characterized by higher abundance, and demonstrate rich time and energy emission patterns. The specificity of the delayed gamma-ray responses to the isotope undergoing fission is illustrated by the analysis of the fission yield sets from the evaluated data libraries. The time and energy distributions of the associated delayed gamma-ray emissions are discussed, and two practical assay modes are identified. The "long" assay concept considers inducing fissions with an interrogation source and detection of delayed gamma-rays emitted from the fission products in two consecutive extensive time periods. The "pulsed" mode refers to the measurement of the short-lived delayed gamma-ray emissions repetitively during the idle cycle of the intermittent interrogating source.

Based on theoretical considerations, the design variables of the assay instrument are established as (1) nature and energy of the interrogating source, (2) detector system arrangement, and (3) interrogation time regime. Analysis and optimization of these three components is required to evaluate the feasibility of the technique under real assay conditions. The development of the delayed gamma-ray response analysis technique with the intent of extracting quantities of individual isotopes in the assayed material is identified as another research goal.

Chapter 3 introduces a high-fidelity delayed gamma-ray response modeling technique developed specifically for this research effort. It incorporates modified versions of existing Monte Carlo-based transport (MCNPX) and analytical decay/depletion (CINDER) codes with a newly-developed Discrete Gamma-ray

Source DEFinition (DGSDEF) code. This four-step hybrid calculation method offers unconstrained spatial, energy and time resolution and relies on extensive datasets for the reconstruction of the discrete passive and induced photon source terms and detector responses. The code package uses the latest data libraries containing multi-group neutron cross-sections, fission yield sets, decay constants and branching ratios obtained from a variety of sources, including international data libraries and evaluation codes.

Preliminary benchmarking and validation of this modeling technique was accomplished in a dedicated experimental campaign at the Idaho Accelerator Center. Delayed gamma-ray activation tests involved accelerator-driven neutron sources and samples of fissile and fertile materials and their combinations with a variety of interrogation setups. The code performance in reconstructing empirically acquired passive and delayed gamma-ray spectra is analyzed in Chapter 4. A good agreement between the measured and calculated delayed gamma-ray peak intensities and positions was observed for the "long" interrogation mode.

In Chapter 5, a framework for the modeling of the spent nuclear fuel delayed gamma-ray response is developed. Constraints arising from the limited spent nuclear fuel library inventories and the limitations of the simulation approach are analyzed. Analytical estimations are used to establish the initial parameters of the assay setup configuration, interrogation source intensity, and detector count rate limits. These instrument components are then further evaluated using the four-step response modeling technique. The overall feasibility of the delayed gamma-ray response acquisition in spent nuclear fuel assay is demonstrated. A sensitivity study of the assay parameters has yet to be completed. The modeling results were produced primarily for the "long" interrogation time pattern, while evaluation of the "pulsed" mode is still underway.

Chapter 6 provides an overview of the delayed gamma-ray response analysis methods and investigates the sensitivity of the signatures to the total fissile content and individual isotopic concentrations in the assayed materials. An exact analytical expression governing the peak area ratios in the delayed gamma-ray

spectrum of mixed samples is derived. The sensitivity of the peak area ratios to the spent fuel inventories is subsequently demonstrated using the modeling technique results. A formal numerical method is proposed for determining the relative concentrations of fissile and fertile isotopes in samples with complex compositions.

Chapter 2

Theoretical Considerations

2.1 Fission Process

Delayed gamma-ray assay is based on the detection of delayed photon emissions following induced fissions in the interrogated material. Induced fission is the primary effect used for assaying fissionable actinides in situations when active interrogation is acceptable. Along with (n,2n) reactions, it is the most important multiplicative process [21]. It can be directly used for non-destructive assay of the primary fissile (U-233, U-235, Pu-239, Pu-241) and fertile (U-238, Th-232) isotopes of the nuclear fuel cycle. Fission events result in the emission of unique, isotope-specific signatures that can be used for distinguishing fissionable actinides in the assayed materials.

Some passive assay concepts utilize the effect of spontaneous fission; however, the intensity of this process in target fissile and fertile actinides is relatively low. In spent nuclear fuel, useful spontaneous fission responses are often obstructed by spontaneous fissions on other isotopes, such as Pu-238, Pu-240, Pu-242, Am-241, Cm-242, and Cm-244, as well as passive background fissions intrinsically induced by neutrons from (α,n) reactions. Under these conditions, the use of an external interrogating source to actively induce fissions of the assayed isotopes significantly improves the ability to distinguish their characteristic signatures.

In active non-destructive assay, fissions are typically induced by subjecting nuclear materials to neutron or high-energy photon irradiation. Most fissionable nuclei require additional energy to increase the total energy level to overcome the fission barrier or to increase the probability of tunneling through the barrier.

Differences between neutron and photon induced fission are in the incident energy required to initiate fission events, and in the resulting products and emissions.

The probability of a target nucleus undergoing induced fission under irradiation is characterized by a fission cross-section. Figure 2.1 demonstrates the effect of the incident neutron energy on the fission cross-section for the most important fissile and fertile [1] isotopes [22]. Neutron absorption by fissile isotopes creates a compound nucleus with excitation energy above the fission barrier. Consequently, fission can occur with thermal energy neutrons. In the case of fertile U-238, thermal neutron absorption leads to the creation of a compound nucleus with an excitation energy below the fission barrier. Additional kinetic energy of the incoming neutron is required to induce fission (~1 MeV). This threshold energy is one of the important properties of the fertile isotopes that distinguishes them from the fissile ones, and provides an efficient way to discriminate their signal in active neutron assay.

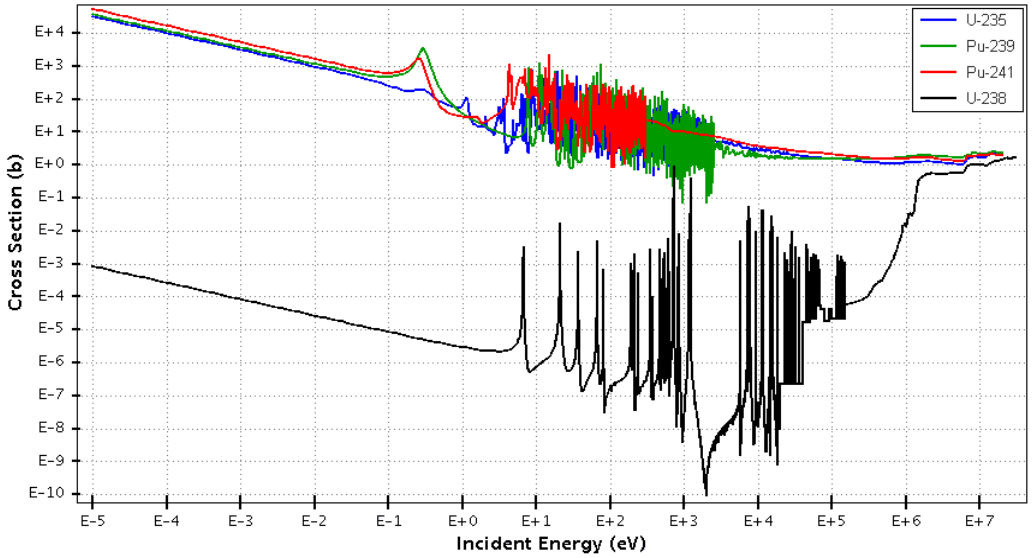

Figure 2.1. Neutron fission cross-section for primary actinides [22].

[1] Here and throughout the remainder of the text "fertile" refers to isotopes which upon capture of a neutron become fissionable.

In the photon-induced fission assay, the required incident photon energy is the difference between the ground state and the fission barrier of the target nucleus. In the event that the incident photon is within the giant dipole resonance, absorption of the incident gamma-ray oscillating electric field causes opposite vibrations of photons and neutrons in the excited nucleus. These vibrations cause increased deformation of the nucleus, which leads to fission. As Figure 2.2 illustrates, this process is similar in all fissionable nuclei, making the shape of the photo-fission cross-section consistent among the fissile and fertile isotopes [22].

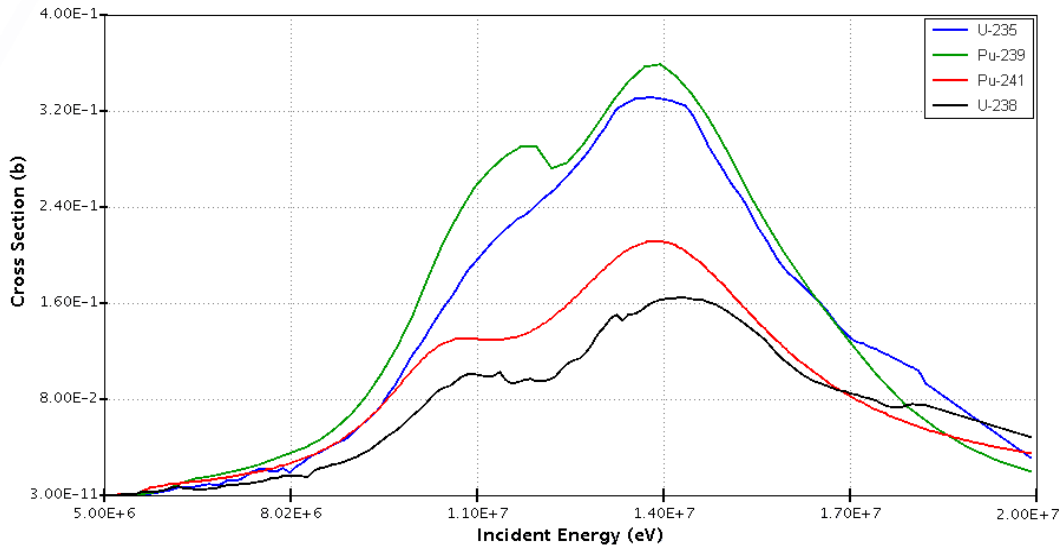

Figure 2.2. Photo-fission cross-sections for primary actinides [22].

Once fission occurs, the overall process is generally consistent, regardless of the inducing radiation. Schematic representation of the induced fission process is shown in Figure 2.3 [21]. Following absorption of the incoming radiation, the heavy nucleus advances its total energy level to an excited state. Assuming that excitation energy is sufficient to overcome the fission barrier, the excited nucleus splits primarily into two fragments. Typically, these fission fragments have an excess of neutrons and have energy levels above their ground states. This results in the emission of prompt neutrons and prompt gamma-rays. Fission fragments

can still be present in the excited states even after the prompt emissions, and their de-excitation leads to the emission of delayed neutrons and delayed gamma-rays. These medium-mass nuclei are often far from the valley of stability and act as precursors to multiple decay chains which lead to more stable nuclides. The majority of delayed emissions are observed from the excited states of daughter nuclides following β-decay of the precursors.

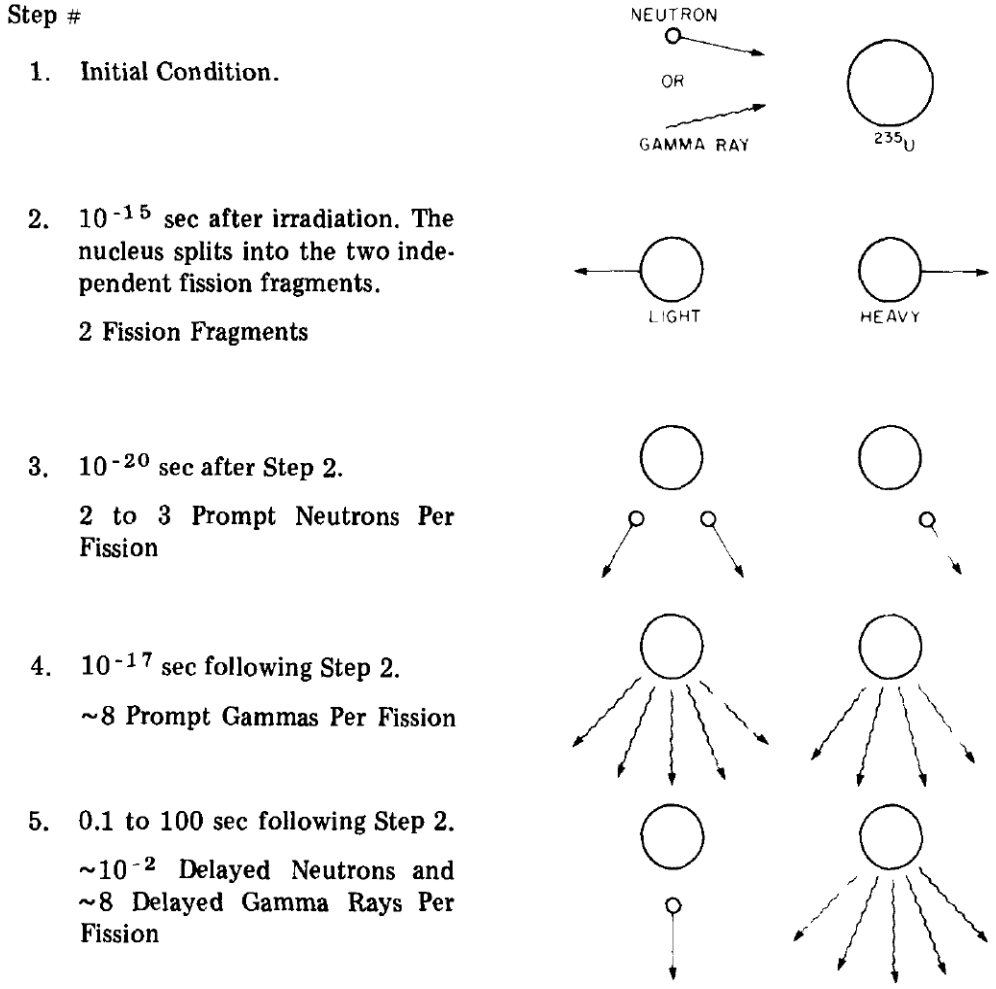

Figure 2.3. Schematics of the fission process [21].

This sequence of fission process events illustrates the origin of four types of responses that can be used in the active non-destructive assay of nuclear materials: prompt neutrons, prompt gamma-rays, delayed neutrons, and delayed gamma-rays. All of these signatures are characterized by unique distributions specific for each actinide and depend on the type and energy of the incident radiation. The commonly used advantage of the delayed signatures over the prompt ones is that they can be detected over a considerable period of time after the induced fissions, and can consequently be distinguished from the interrogating source radiation using time discrimination. Additionally, the yields and temporal behavior of delayed neutrons and photons significantly varies among the fissionable isotopes allowing their unambiguous identification.

Considering all of these factors, the detection of delayed gamma-ray responses emerges as a practical concept for the assay of nuclear materials. Delayed gamma-rays are emitted continuously during the extended time periods after interrogation (seconds to hours), and their detection is not obstructed by the interrogating source. They are more abundant, producing an average of approximately 8 delayed gamma-rays per fission compared to the delayed neutron rate of $\sim 10^{-2}$ emitted generally within a much shorter time. Because the energy of the delayed gamma-ray emissions extends to several MeV, they are less vulnerable to the matrix effects and media surrounding the assayed material. The delayed gamma-ray energy spectra are rich and complex, and characterized by unique distributions of individual line positions and intensities controlled by fission product yields highly specific to each fissionable isotope.

2.2 Fission Yields

Fission events result primarily in the formation of two medium-mass nuclei. The mass distribution of these fission products is highly asymmetric, and partially correlated with the mass of the initial heavy nucleus. Most of the fission products are initially neutron rich, and undergo a series of beta decays to approach stability. In the course of these transformations, nuclei emit gamma-rays with a complex

time- and energy-dependent structure. These beta-delayed gamma-ray emissions constitute a signal that can be utilized for the non-destructive assay.

The delayed gamma-ray spectra observed are dependent on the inventories of the fission products resulting from the induced fissions. These are defined as fission product yield distributions in terms of the number of nuclei of each isotope produced on average per fission event. There are three types of fission product yields generally reported in the literature [23-25].

Independent (or *direct*) fission yields are defined as the probability of formation in fission of an isotope with a certain mass number after prompt emissions, but before any radioactive decay takes place. Determining the direct yields requires separation of the fission products rapidly after a short irradiation period.

Cumulative fission yields refer to the probability of formation of a nuclide of a certain mass after prompt and delayed neutron emission after the decay of its short-lived precursors. In addition to the methods used for direct yields, cumulative yields can be determined by observing the specific radioactivity of the fission products.

Chain fission yields are defined as the probability of formation of all stable nuclides of the same mass number after all prompt and delayed emissions and after complete development of the beta decay chains. Chain yields can be determined with the highest accuracy using mass-spectrometry and other high-precision techniques.

In addition to experimental observations, a number of models were developed for estimating fission yields. An extensive overview of the current yield libraries, research concepts, and methods was published by the IAEA [26]. Presently, most of the yield compilations are defined for the case of neutron-induced fissions, while the data on photon or charged particle induced fissions continues to be extremely sparse.

Asymmetry in the chain fission yields mass distribution for thermal neutron fission in the case of the most important actinides can be seen in Figure 2.4, produced from the data reported in [27]. The heavy fission fragment peaks are reasonably constant for all of these nuclei, while there is considerable variation among the light products. The formation of the heavy products during the fission process is largely influenced by nuclear shell closures, preventing the heavy peak from appreciably shifting for various fissionable nuclei. In contrast, the light fragments are not as dependent on shell closures [28], and receive the majority of the additional nucleons. Among the fissionable isotopes, individual features of the delayed gamma-ray spectra are primarily explained by this shift in the light products peak.

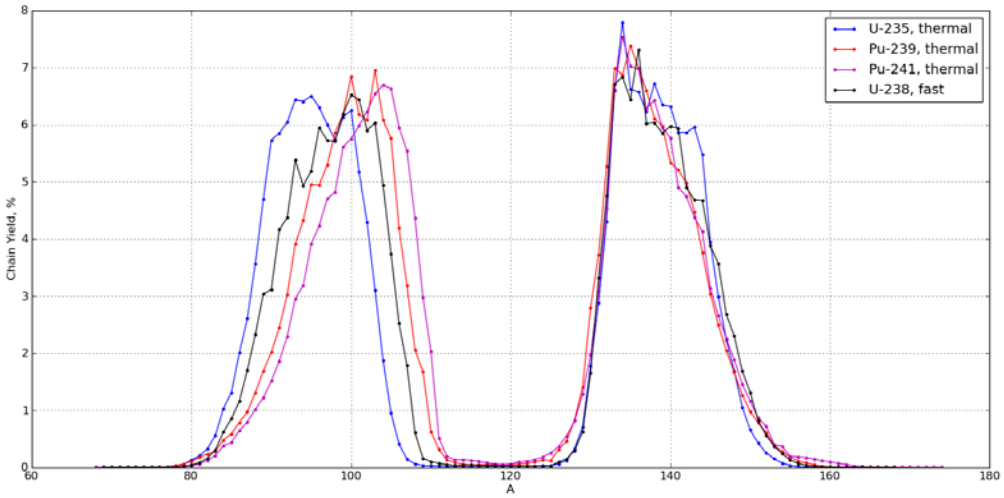

Figure 2.4. Thermal chain fission yields for primary actinides [27].

At high excitation energies, the shell effects on the mass distribution of the fission products are much less important. In cases when fission is initiated by a highly energetic particle, the effect of the shell structure is greatly diminished, resulting in more symmetric mass distributions of the fragments. This effect can be seen in Figure 2.5 where chain fission yield distributions are depicted for fast- and 14 MeV neutron fissions of primary actinides based on the data reported in [27]. It is even more pronounced for a large interval of the incident photon energies in Th-232 photo-fissions in Figure 2.6 [29].

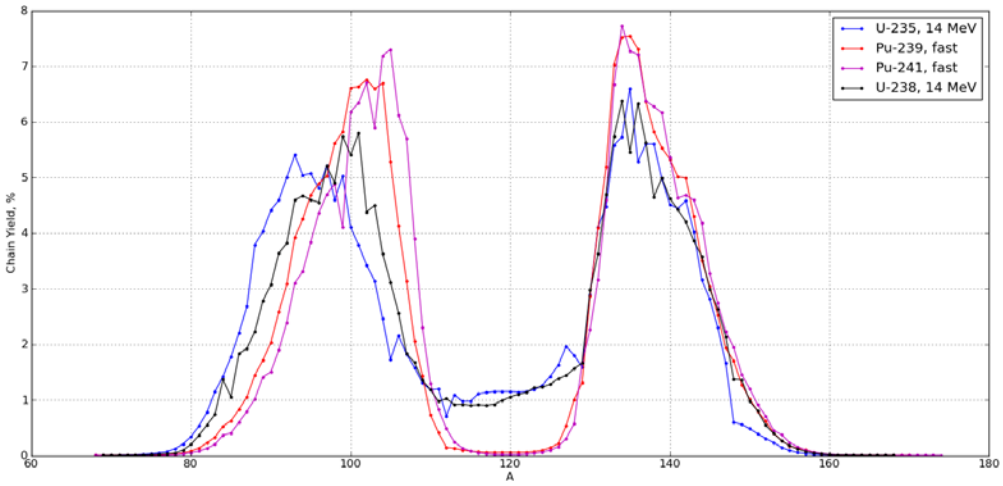

Figure 2.5. Chain fission yields of primary actinides for fast and 14 MeV neutrons [27].

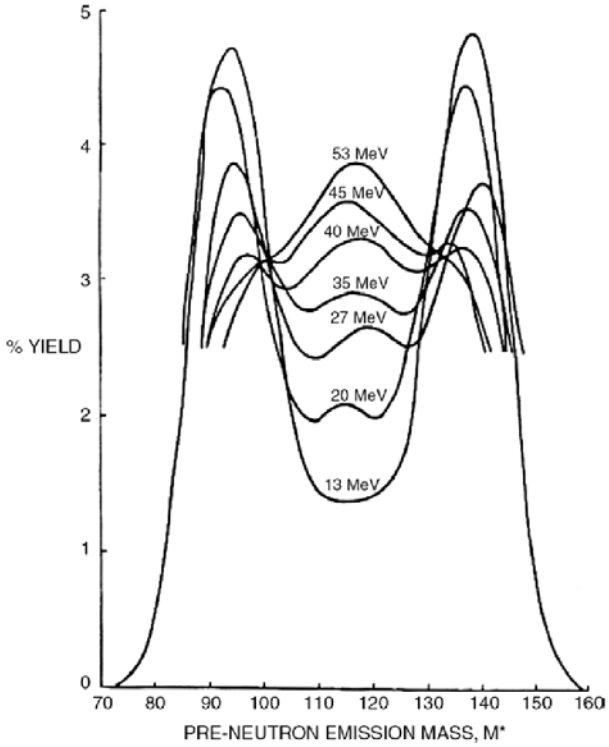

Figure 2.6. Fission products mass distributions for Th-232 photofissions at various incident photon energies [29].

The effect of incident particle energy on the mass distribution of the fission products must always be considered in the active assay. In order to account for the energy dependence, fission yield data for different incident neutron energies is traditionally divided into three large groups: "thermal", "fast", and "high" (14 MeV). The differences in the mass distributions are quite high, so it is natural to expect corresponding energy and intensity variation of the delayed gamma-ray emissions. When an exact number of fissions must be determined, it is important to establish the precise relationship between the incident neutron energy, fission cross-section, and energy-dependent fission yields.

Uncertainties in fission yields reported in various databases vary considerably among different actinides and energy groups. For example, in the fission yield evaluated database [22,25], error limits between ~0.5 to ~20% are adopted based on the number of experiments, time period and methods used to determine each yield set. Presently, the errors in evaluated yield data are considered to be about 1% for primary well-known actinides, and on the order of 30% for the nuclides with fewer measurements [26]. Reported errors are minimal in the peak regions of the yield distributions, and reach their maximum on the wings and in the valley between the peaks. This complicated assortment of data has caused corresponding complexity in the analysis and prediction of the delayed gamma-ray rates and distributions.

2.3 Delayed Gamma-Ray Time Dependence

Fission products and their daughter isotopes have half-lives ranging from fractions of a second to dozens of years. The time distribution of the delayed gamma-ray emissions varies with each decay chain resulting in a unique signature of the fissionable nuclide. Historically, experimentally observed delayed gamma-ray activities of the primary fissile and fertile isotopes were arranged in multiple groups spanning the range of dozens to thousands of seconds [18,30,31]. Since delayed gamma-ray emissions are produced in complex decay chains with multiple members, there is very little physical meaning to the group structure. Nevertheless, delayed gamma-ray group sets were determined for a variety of

source energies and time patterns for use in models and assay system studies [21,32].

Figure 2.7 shows the bulk distribution of fission product half-lives [33] depicted for a subset of isotopes from the ENDF-VI database. This figure provides important considerations for the expected total delayed gamma-ray intensity variation as a factor of the active interrogation parameters. It is reasonable to expect that delayed gamma-ray emissions will be more readily observed from the fission products with half-lives in the mid-range (10 to 1000 sec.) of the distribution shown. The analysis of emissions from isotopes with half-lives shorter than 10 sec. will require interrogation time periods of a comparable length, and will suffer from increased statistical uncertainties. The precision of short decay time measurements can be improved by using interrogating sources of higher intensity or repeated (pulsed) measurement patterns. On the other hand, delayed gamma-ray emissions from isotopes with half-lives greater than a few thousand seconds will have lower intensities for reasonable assay times, resulting in diminished useful signal strength.

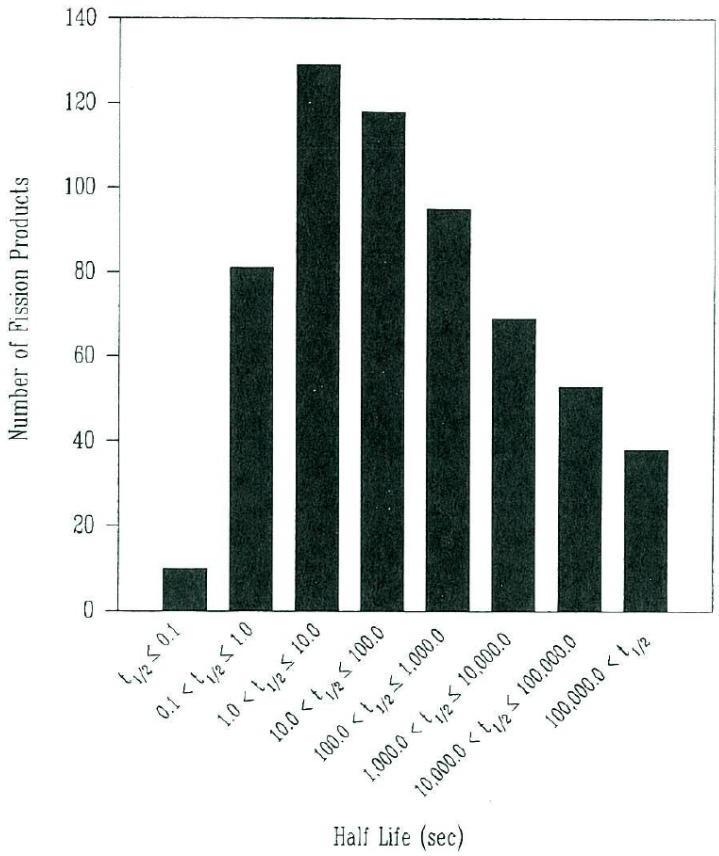

Figure 2.7. Fission product half-lives temporal distribution [33].

Another important consideration is the delayed gamma-ray emission rate variation within individual decay chains. The half-life of isotopes far from the valley of stability is generally less than that of isotopes close to the stability line. As a result, intensities of individual delayed gamma-ray lines vary with time after fission. Early emissions that occur at the beginning of the decay chains will be more specific to the initial inventory of the fission products, and can therefore provide a highly accurate signature of the isotope that undergoes fission. Analysis of these short-time emissions can be more effective for distinguishing delayed gamma-ray responses from fissionable nuclides with very similar mass numbers. However, achieving good statistical precision of such measurements is still problematic. The optimal trade-off between isotope specificity and response statistics has to be determined individually for each assay scenario. Understanding

the time-dependent features in the delayed gamma-ray spectra is essential for extracting accurate information about the initial fission process.

2.4 Delayed Gamma-Ray Assay Concept

The delayed gamma-ray assay principle offers the attractive capability of non-destructive direct measurement and quantification of fissionable isotopes in nuclear materials. This technique is based on inducing fissions by interrogation with neutrons or photons and the subsequent spectroscopy of high-energy beta-delayed gamma-rays emitted from the fission products and their decay daughters. The response analysis relies on the difference in rates at which gamma-emitting isotopes are produced in fission events. The yield distribution of the initial fissile products is specific to each actinide, and the resulting delayed gamma-ray emission spectrum serves as a unique characteristic of the nuclide that undergoes fission. Analysis of detected delayed gamma-ray spectra allows for the qualitative and quantitative identification of actinides. In some cases [17], the gross photon count in certain energy regions can be used for material characterization. For more complex systems, ratios formed using the observed intensities of certain peaks in a high-resolution spectrum can be used to identify the isotopic composition [20].

Delayed gamma-ray spectra recorded after an interrogation with an active source accentuate delayed gamma-ray emissions from fission products with half-lives ranging from fractions of a second to dozens of minutes. This is followed by the detection of high-energy delayed gamma-ray peaks, which are in the energy region free of interferences from passive background, e.g. from spent fuel. To emphasize emissions from the short-lived fission products, interrogation and detection can be performed in pulsed mode, with very short time periods. As discussed previously, the short-lived fission products are expected to result in delayed gamma-ray spectra more sensitive to fissile isotopes than those for longer decay times.

The individual nature of the delayed gamma-ray spectra is a result of the unique fission product yield distribution for each actinide. This effect is often illustrated

by comparing the thermal neutron-induced fission mass-yield cumulative distributions for the fissile isotopes of U-235 and Pu-239, as shown in Figure 2.8 [20,34]. The variation between the two lines in this figure suggests that fission products in a certain mass region (Zone 1) are created preferentially in U-235 fissions, while others (Zone 2) are more characteristic for Pu-239, with a third region (Zone 3) not specific for either isotope. Therefore, ratios of peak intensities between delayed gamma-ray emitted by fission products and their daughter nuclides from each zone can be obtained for pure materials and compared with those of an unknown mixture. This type of analysis requires simple calibration and as shown in [20] is sufficiently accurate for qualitative assay of simple binary systems.

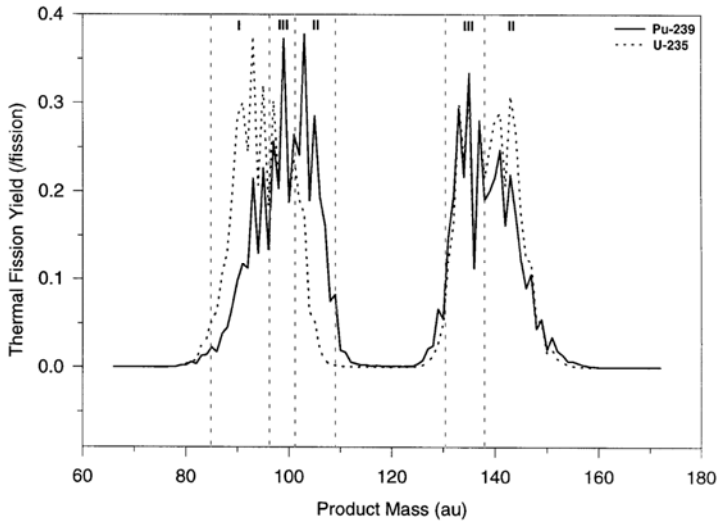

Figure 2.8. Cumulative thermal neutron fission yields for U-235 and Pu-239 [34].

It can be expected that delayed gamma-ray interrogation of spent nuclear fuel follows the same principles; however, it is much more convoluted and requires more accurate accounting of the physical phenomena affecting the goal signatures. When quantitative spent fuel inventory assay is considered, the DG-based technique capability is significantly complicated by the set of factors outlined below.

- Distributions of individual fission product yields are unique but not well separated for the fissile and fertile actinides. Thus, fissions of various types of heavy nuclei result in the formation of almost identical inventories of fission products, with only production rates unique to the original isotope. Figure 2.9 [22] illustrates this effect, showing individual thermal neutron fission yields for the same two fissile isotopes as in Figure 2.8. This means that there are no or very few delayed gamma-ray lines from fission products or their decay daughters specific to a particular actinide. Rather, the intensity of each delayed gamma-ray line is governed by fission reactions on all actinides present in the mixture. In the case of spent nuclear fuel, a very diverse heavy nuclei inventory must be considered in the detected gamma-ray peaks analysis. Yields for certain isotopes have to be well-defined in order to predict individual contributions to the detected signature.

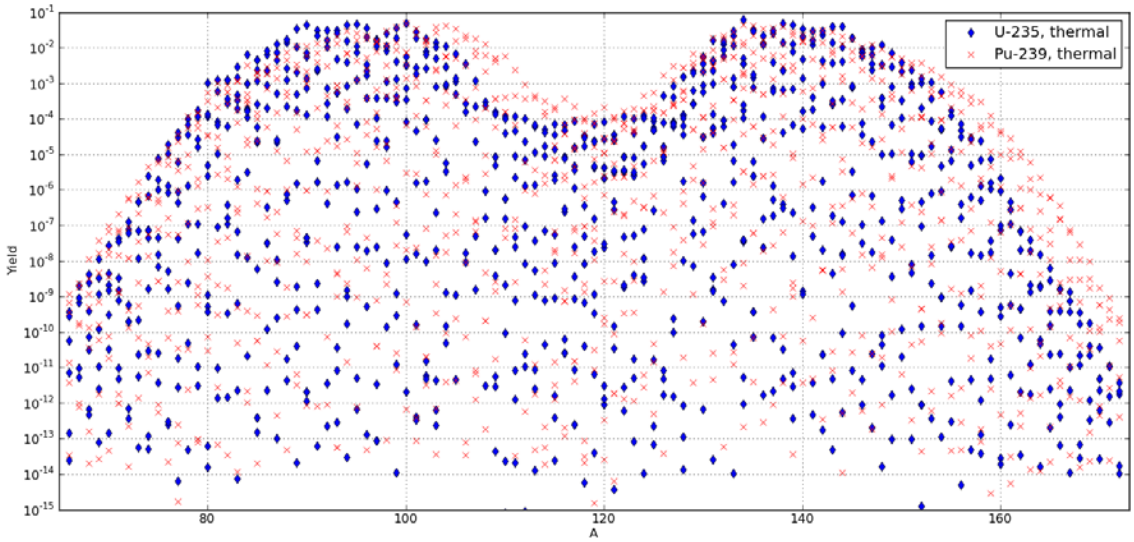

Figure 2.9. ENDF/B-VII U-235 and Pu-239 thermal neutron induced fission product yields. Each point corresponds to an absolute yield of an isotope with unique A and Z [22].

- Fission yield distributions for actinides with similar A are very close. As demonstrated above in Figure 2.3 [27], the mass-yield curves reveal small differences between Pu-239 and Pu-241 thermal, and U-238 fast neutron fission sets, especially when compared with the U-235 thermal set. In spent nuclear fuel assays, fissile U and Pu nuclide signatures have to be distinguished from one another and separated from those of U-238 in order to perform an accurate multi-component system analysis.

- Actively induced fissions, multiplication effects, and spontaneous fission events lead to a sustained population of fission-spectrum neutrons in spent nuclear fuel. Regardless of the interrogating source nature, this always results in a certain amount of fissions on fertile isotopes, especially U-238. These contributions have to be quantified and separated from the resulting delayed gamma-ray signatures.

- Passive photon background from the intrinsic spent fuel radioactivity interferes with the detection of the delayed gamma-ray spectrum. This obstacle requires the capability of predicting optimal regions of interest for DG signatures, as well as a careful selection of the acquisition setup configuration and a detector system adequate for high count rates and desired energy resolutions.

- Configuration of the spent nuclear fuel, structural materials, and interrogation media introduce additional complexity and uncertainty. Periodic structure and heavy material can lead to spatial shielding effects for both the active source and the delayed gamma-ray detector. Assay environment (air, water, borated water) can affect multiplication in the assembly under interrogation. These and other effects may be important and must be accounted for in the final analysis.

On the other hand, the concept of delayed gamma-ray interrogation allows for flexibility in the process that can be used to suppress or intensify the resulting signatures and therefore adjust the instrument to a particular task or application. The main design variables of the delayed gamma-ray NDA are: (1) nature and

energy of the active source, (2) detector type, and (3) interrogation time regime. These are discussed below.

2.4.1 Interrogating Source

In practical applications, fissions in heavy nuclei can be induced by three types of active sources: neutrons, high-energy photons, and accelerated charged particles. In the case of the spent nuclear fuel assay, the intensity of the interrogating source must be high enough to produce sufficiently strong delayed gamma-ray emissions distinguishable above the passive background. Compared with neutron and photon assay sources, intense charged particle sources require extremely complex accelerator systems which are not practical for safeguards applications. Complex interaction effects, a lack of proton fission cross-section libraries, and yield distributions make the application of the active proton interrogation only a distant possibility.

An interrogating neutron flux of sufficient strength for delayed gamma-ray assay can be practically obtained from a deuterium-tritium (D-T) generator, a deuterium-deuterium (D-D) generator, or an accelerator-driven system. In the SNF assay, the interrogating neutron flux can be effectively propagated through the periodic structure of the fuel by means of multiplication effects, particularly if the assay environment is composed of water. Another considerable advantage is that source neutrons can be moderated to thermal and epithermal energies and can therefore induce fissions and delayed gamma-ray signatures primarily from fissile isotopes. This effect was previously demonstrated in Figure 2.1 [22] by comparing fission cross-sections for the most important fissile and fertile isotopes in the spent nuclear fuel inventory. Fertile U-238 is present as a dominant component in spent nuclear fuel and has a fission cross-section that is several orders of magnitude lower in the thermal region, thus making its contribution to the resulting delayed gamma-ray signatures easy to control by tailoring the source neutron energy spectrum. However, induced fissions and multiplication will always result in fast neutron production; therefore high-energy U-238 fissions can never be completely excluded. The interrogating neutron flux is also affected by the presence of

various neutron absorbers in spent nuclear fuel. This effect is not known for any assay conditions.

High-energy photon interrogation can be performed by accelerator-driven bremsstrahlung sources and must reach endpoint energy ranges substantially above the fission threshold. Since threshold energies are very close for fissile and fertile elements (Figure 2.2), fissions cannot be preferably induced in fissile isotopes and the resulting delayed gamma-ray spectrum becomes more complicated. Highly energetic photons can propagate further through the spent nuclear fuel structure than thermal neutrons from the interrogating source. This greater penetration could be a real advantage if measurements were made in air. However, if measurements are made in water or borated water, neutron multiplication provides greater penetration for the interrogating neutron population relative to the photon interrogation conditions.

For spent fuel assay conditions, it is expected that neutron interrogation will likely provide more favorable results since with thermal neutron interrogation, over 90% of the induced fissions occur in the fissile isotopes of interest, hence minimizing the signal from U-238; while with photon interrogation, over 90% of the induced fissions in spent fuel would be in U-238. In spite of these favorable properties of neutron interrogation scenarios, it is worth researching photon interrogation since these sources are more intense and there may still be some delayed gamma-ray peaks from the fissile isotopes that are strong enough to provide information on the mass of the fissile isotopes. Furthermore, the signal from U-238 may be useful in detecting partial mass defects as a result of individual pin diversion from the assembly.

2.4.2 Detector System

In the delayed gamma-ray assay of spent nuclear fuel, the acquisition of the resulting gamma-ray spectrum is considerably obstructed by the passive radioactive background. As shown in Figure 2.10 [7], the background is strongest at low energies, and decreases exponentially up to approximately 2.5 MeV at the

highest energies. As shown further in Chapter 5, only delayed gamma-ray peaks located above this energy will be practical for the assay. Consequently, the detector system for the delayed gamma-ray spectrum acquisition must be compatible with high count rates and have higher efficiency for high-energy photons. On the other hand, a fine energy resolution may not be necessary for the DG assay, and dead time from parasitic low-energy passive emissions can be partially mitigated by collimators and attenuating filters.

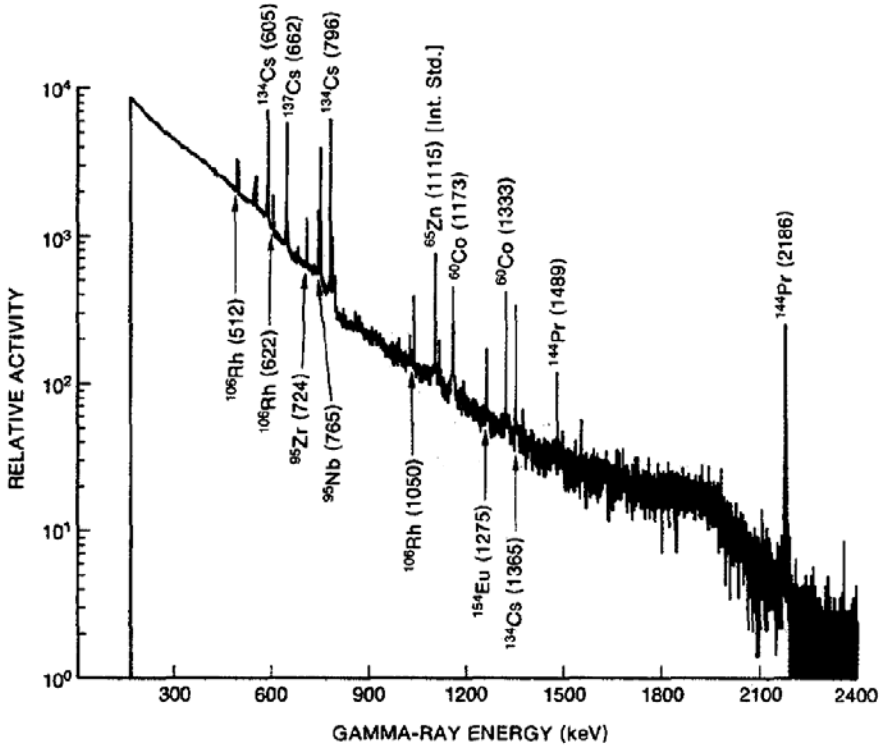

Figure 2.10. Passive gamma-ray spectrum of a PWR assembly with 32 GWd/t burnup and 9 months cooling time [7].

Two types of detectors are being considered in the current research of the delayed gamma-ray assay: (1) high-efficiency high-purity germanium detector (HPGe) systems, and (2) fast $LaBr_3$ scintillators. HPGe detectors offer fine energy resolution (up to 2 to 3 keV at 3 MeV), but their dead time limits are low, and intrinsic photon efficiency drops significantly above approximately 5 MeV. $LaBr_3$

scintillation detectors tolerate much higher count rates (estimated 3 to 4 orders of magnitude higher compared to high-purity germanium detector systems) and are more efficient for high-energy photons at the cost of energy resolution (approximately 30 keV at 3 MeV [56]). Each of these systems requires a specific analysis technique and optimization of the detector setup geometry.

2.4.3 Interrogation Time Regime

The delayed gamma-ray assay technique also suggests two different treatments of the time-factor in the analysis. The conventional "long" mode considers a sequence of relatively extensive time periods during the assay:

- interrogation period using an external source;
- cool-down period with the source switched off; and
- acquisition period when the delayed gamma-ray spectrum is collected in the detectors.

The long mode interrogation is predominantly discussed in the literature and emphasizes delayed gamma-ray signatures from relatively long-lived fission products and their decay daughters with half-lives ranging from minutes to hours. The extent of each time period can be optimized based on the production rates and decay constants of the isotopes in the decay chains leading to emissions of the particular gamma-ray lines. The important advantage of this approach is that cumulative fission yields of the most important fission products involved in the analysis are generally well-known.

The less obvious "pulsed" interrogation mode considers an intermittently operating active source. The detector electronics, and, if needed, a shutter system, are synchronized to acquire the delayed gamma-ray spectrum in between the source periods. The delayed gamma-ray signature in this case consists not only of isolated peaks, but also the rate of accumulation of gross photon counts in certain energy ranges. Very short-lived delayed gamma-ray emitters are produced at rates specific to each fissile isotope and are expected to populate the energy regions of the spectrum at certain rates approaching saturation with each pulse. This method

provides the ability to determine relative fission rates in the fuel; however, the analysis suffers from considerable uncertainties in known short-lived fission product yields. It is also unclear what kind of source strength and detection efficiency are required to achieve satisfactory statistical performance at the very short interrogation time scale. Both time modes are of interest in the current research. The "long" approach performance can be accurately evaluated using the existing physical data, and is therefore considered a priority. The predicted behavior and data quality will still need to be experimentally verified for the "pulsed" technique.

It is obvious that even a basic design of the delayed gamma-ray instrument must account for multiple factors and variable conditions. When combined with the intricate structure of the spent nuclear fuel, accompanying radiation fields, assay media, etc., the level of complexity increases indefinitely. Considering that empirical tests involving actual fuel are impractical at the early design stage, it is imperative that theoretical proof of concept has to be as comprehensive as possible.

Chapter3

Modeling Approach

3.1 Algorithm Description

In order to address the whole complex of factors and variety of parameters associated with the delayed gamma-ray NDA of spent nuclear fuel, an original modeling technique was introduced in this research. Existing codes do not adequately account for the delayed gamma-ray assay effects; therefore a specific code development effort was deemed necessary. As a result, a hybrid Monte Carlo and analytical modeling scheme was developed and adapted to the design and analysis process of the NDA instrument. The new capability offers unconstrained spatial, energy, and time resolution and relies on extensive datasets for the reconstruction of the discrete passive and induced gamma-ray emission intensities and detector responses. Based only on the user-supplied assay geometry, material compositions, interrogating source and detector specifications, the high-fidelity delayed gamma-ray spectra can be obtained in a form similar to the results of actual measurements. The modeling technique is capable of reproducing passive emission background when the interrogation source is omitted from the simulations.

The delayed gamma-ray modeling capability was realized in a sequence of four steps as shown in Figure 3.1. At each step, a stand-alone code is automatically executed with seamless data transfer between each stage. The algorithm relies on independent calculations in an arbitrary transport code, analytical decay/depletion CINDER'90 package [35], and a specifically developed discrete gamma-ray source definition code DGSDEF [36]. A high-level overview of each step is provided below.

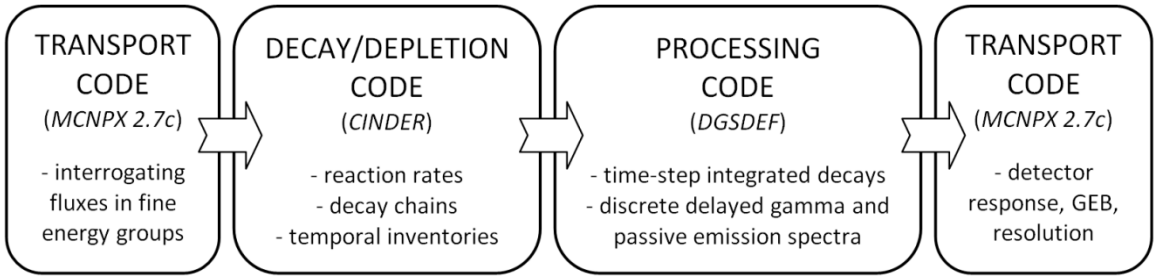

Figure 3.1. Four-step delayed gamma-ray response modeling algorithm.

Step 1. Neutron transport calculations are performed in the simulated interrogation geometry. The neutron flux resulting from the active interrogation is obtained in the 63-group LaBauve energy structure [37] for every arbitrary volume and material predefined in the spent fuel. Although any transport code can be used at this step, it is currently optimized for MCNPX2.7c [38]. A considerable advantage of using MCNPX transport is its effective variance reduction techniques that enhance computational performance, and its capability for massive parallelized calculations.

Step 2. The CINDER decay/depletion code is executed separately for each volume with a unique isotopic inventory with neutron flux defined in Step 1. CINDER performs fast and precise analytical calculations of transmutation processes occurring in the material due to the neutron reactions and radioactive decay. The code operates a data library containing multi-group neutron cross-sections, fission yield sets, decay constants, and branching ratios obtained from a variety of sources, including international data libraries (ENDF, JEF, JENDL) as well as evaluation codes. The Markov decomposition scheme is used to explicitly follow the temporal evolution within multiple decay patterns using an extensive dataset of 3400 nuclides with Z ranging from 1 to 103. Consequently, an integrated number of decays of each isotope can be determined for arbitrary time periods. For the delayed gamma-ray calculation, full isotope inventory and associated integral decay values are extracted for any pre-defined irradiation and detection time period.

Step 3. A newly developed DGSDEF code extracts the time-step integrated decays and complete inventory data from the previous step. By utilizing the ENDF/B-VI decay library [39] containing decay information for 979 isotopes, these data are converted into the discrete gamma-ray spectrum that includes delayed and/or prompt passive emissions. Each gamma-ray line in the source spectrum is characterized by the number of photon emissions during the time period and designated by the emitting nuclide. The calculation is repeated for all individual volumes, and the results are assembled in a single spatially-sensitive discrete source term that is passed to the next step. At this point, various user-defined source modifications and filters can be applied to obtain results for isotope-specific contributions, perform source energy and spatial biasing, optimize the sampling efficiency, etc.

Step 4. The complex discrete photon source is reintroduced into the interrogation geometry and propagated to the acquisition part of the setup using the same transport code. At this point, parameters of a real detector system are applied, including resolution and Gaussian energy broadening (used to simulate the peak-broadening effects exhibited by real radiation detectors), resulting in a representative detected gamma-ray spectrum.

The primary advantage of this calculation scheme is effective processing of extensive amounts of data, performed with full user control over the parameter complexity, input, and transport parameters. The flexible modular structure of the algorithm makes it instantly compatible with any transport code and adaptable for a variety of photon response simulation problems. The following list of features summarizes its capabilities, which are critical for the design of the delayed gamma-ray assay instrument:

- *Provides fast and rigorous calculations.* The mere amount of physical processes associated with the delayed gamma-ray assay is already computationally challenging. The whole variety of these phenomena is simulated comprehensively, and any simplifications are user-controlled. The hybrid calculation approach combines accurate Monte Carlo transport

with fast and precise analytical calculations of complex transmutation processes.

- *Operates a reliable transport scheme*. The effects associated with moderation of the source neutrons, their diffusion through the media, multiplication, elastic and inelastic interactions and photon transport are reproduced in a complex geometry with a state-of-the-art code.

- *Determines reaction rates with a high level of precision*. Fission and activation events are calculated at the limit of the known reliable neutron cross-section data using a fine energy group structure.

- *Comprehensively replicates transformations in the assayed materials*. The code considers extensive isotope-specific data with known fission yields, decay constants and branching ratios and follows most of the possible transmutation chains with associated gamma-ray emissions, produced as a passive background and as a result of active interrogation.

3.2 CINDER Method

The difficulty in calculating the delayed gamma-ray emissions from the fission products arises from a need to specify a large amount of time-dependent isotopic concentrations for each fission product and its decay daughters, and to treat the associated extensive numbers of gamma-ray emissions. The analytical approach to high-fidelity calculation of transmutation processes offered in CINDER is considerably faster and demonstrates higher precision when compared to numerical techniques such as matrix exponential as used in ORIGEN-S code member of the SCALE package [40].

The decay/depletion differential equation describing transmutation processes during and after the active interrogation can be written as:

$$\frac{d\mathrm{N}_m(r,t)}{dt} = -\mathrm{N}_m(r,t)\beta_m + Y_m + \sum_{k\neq m} \mathrm{N}_k(r,t)\gamma_{k\to m}, \tag{3.1}$$

where $\mathrm{N}_m(r,t)$ is the spatially- and time-dependent atom density of an isotope *m*, Y_m is the rate of isotope production from an external source, $\gamma_{k\to m}$ is the probability of isotope *k* transmuting in isotope *m* by means of decay or neutron absorption. β_m is the total loss probability of isotope *m* by transmutation, expressed as:

$$\beta_m = \lambda_m + \sum_j \int \sigma_m^j(E)\Phi(r,E,t)dE, \tag{3.2}$$

where λ_m is the total decay constant of isotope *m*, $\Phi(r,E,t)$ is the spatially-, energy-, and time-dependent neutron flux, and $\sigma_m^j(E)$ is the flux-weighted neutron transmutation cross-section of isotope *m*.

The first term in the expression (3.1) accounts for all losses of isotope *m* due to transmutation processes, such as radioactive decay, and particle reactions resulting in products other than isotope *m* and include absorption, neutron multiplication and inelastic scattering. The second term is the constant isotope production rate such as fission reactions during active interrogation. The third term accounts for the probability of isotope *m* production in the transmutation of other nuclides as a decay daughter or a reaction product. The transmutation rates in this expression depend on the knowledge of the flux, which has to be imported from a transport calculation. The solution of this equation assumes the constant flux-dependent transmutation probabilities during a pre-defined time period (first-order linear differential equation with constant coefficients). Therefore, any temporal history has to be approximated using a vector of consecutive time intervals. To account for spatial effects, the calculation can be performed individually for small homogenized volumes.

A system of equations describing temporal evolution of the full isotopic composition can be extremely large. Moreover, differential equations in the whole

set are coupled through the branching ratios and yield probabilities of the gain and loss coefficients, since each equation in general contains the concentration of other isotopes. Since the type and number of production and loss paths varies for individual isotopes, the corresponding differential equations are changing, making a general solution difficult to obtain.

The solution method for the system of coupled differential equations employed in ORIGEN is a numerical matrix exponential method used for reactor burnup calculations. However, in situations when large isotopic inventories with vastly different nuclide parameters are considered, the matrix of depletion coefficients becomes extremely large. In order to perform the expansion solution, specific approximations have to be used in order to truncate depletion equations. Numerical instabilities can arise from the fact that depletion equations include isotopes with long and short half-lives, with high and low reaction rates depending on the magnitude of the cross-section. Time step intervals have to be accurately defined in order to avoid associated numerical errors.

In the CINDER solution approach, the set of coupled differential equations is reduced to a set of independent, linear differential equations using the Markov decomposition scheme [41,42]. In this method, solutions to the depletion equations are obtained assuming rates of change in partial isotopic concentrations in each independent chain with a single source term, but with all loss mechanisms included. The large set of coupled differential equations is thus reduced to a number of small sets of partial concentration differential equations in a single generalized form. The linear nature of the chain allows for a unique analytical solution assuming constant flux conditions during the time step. The total isotopic concentrations can be obtained by summation of the partial concentrations.

The general solution for a linear sequence of transmutation chains coupled by any sequence of particle absorption or radioactive decay was first derived for use in the CINDER code [43]:

$$\mathrm{N}_n(r,t) = \sum_{m=1}^{n} \prod_{k=m}^{n-1} \gamma_k \left\{ Y_m \left[\frac{1}{\prod_{l=m}^{n} \beta_l} - \sum_{j=m}^{n} \frac{e^{-\beta_{jt}}}{\prod_{i=m,\neq j}^{n} \left(\beta_i - \beta_j\right)} \right] + \mathrm{N}_m^0 \sum_{j=m}^{n} \frac{e^{-\beta_{jt}}}{\prod_{i=m,\neq j}^{n} \left(\beta_i - \beta_j\right)} \right\} \tag{3.3}$$

This expression uses the same notation as equations (3.1) and (3.2).

Using this algorithm, CINDER propagates the initial densities of isotopes and constant production rates to the densities for each daughter nuclide in the decay sequence for spatially homogeneous regions. No pre-defined criteria for the chain termination are required by CINDER, and all possible transmutation paths are followed within the available nuclear data libraries. To limit the decay chain development, CINDER utilizes a test for significance to determine if a further transmutation is insignificant or insufficiently accurate. The test for significance determines a quantity of "passby" to quantify transmutation of the *n*-th isotope in a decay chain and determine if the amount of decay is significant for the subsequent isotopes in the path. The passby is calculated as a time-step integrated number of transmutations of isotope *n*, i.e. the quantity of atoms transmuted over the time period:

$$P_n(t) = \int_0^t N_n(t')\beta_n dt'. \tag{3.4}$$

The user-supplied control value of passby is used to determine whether the chain should be terminated or continued to the next generation of transmutation products. The sum of passby values for the same isotope from all partial concentration chains corresponds to the total number of decays for this isotope during the time period. Full isotopic inventory and associated decay numbers are passed from CINDER to DGSDEF during the execution of the delayed gamma-ray modeling algorithm shown in Figure 3.1.

Transmutation calculations performed in CINDER are based on the associated libraries of physical data. Data sets relevant to the delayed gamma-ray assay

modeling include neutron absorption cross-sections, neutron fission yields, and decay constants for each nuclide transmutation path with branching ratios to ground and isomeric states. The data libraries were assembled from a variety of sources including international data repositories and evaluation codes over the course of many years. Extensive experimental validation of these data was performed by the authors of CINDER [44]. The breakdown of data operated by the present version of the code is provided in Table 3.1 [35]. The CINDER library includes 3400 isotopes in ground and isomeric states, 98 nuclides with spontaneous and neutron induced fission yields (at thermal, fast, and high energy) for 1325 fission products. Reaction cross-sections are organized in a 63-group energy structure as defined by LaBauve [37]. A wide variety of this data is used in the delayed gamma-ray modeling process.

Table 3.1. Content of CINDER Data Libraries [35].

Maximum neutron energy, MeV	25
Neutron group cross-sections	63
Total nuclides	3400
Stable nuclides	259
Unstable nuclides	3141
Ground state nuclides	2762
1st isomeric state nuclides	583
2nd isomeric state nuclides	55
Spontaneous or induced fission products	1325
Nuclides decaying by spontaneous fission	58
Nuclides decaying by delayed neutron emission	271
Nuclides with reaction paths	736
Nuclides with neutron fission paths	67
Total non-fission reaction paths	15269
Total non-fission decay paths	4041

3.3 DGSDEF Method

The newly developed Discrete Gamma-ray Source DEFiniton (DGSDEF) code [36] was written specifically for the delayed gamma-ray modeling algorithm. It provides a seamless calculation capability for passively and actively induced prompt and delayed gamma-ray source terms. For each material volume in the model, DGSDEF prepares and executes a CINDER calculation. At each pre-defined time step, DGSDEF extracts the full isotopic inventory along with the time-step integrated number of decays of each isotope obtained as a sum of passbys. As a result of the calculation, a space-, time- and energy-dependent gamma-ray source term is formulated. The emission rate of each gamma-ray is then calculated as a product of the number of decays of each isotope during the time step, and the probability that each decay will produce a photon of a given energy. The fully defined emission source term is passed to the transport code for the detector response calculation.

To reproduce the gamma-ray emission source term, DGSDEF operates with the library containing details on the decay data of 979 isotopes, including decay modes and radioactivity spectra as extracted from the ENDF/B-VI evaluation [39]. The gamma-ray spectral emission data in this library is formulated in the form of discrete lines and continuous distributions in 10-keV bin format. DGSDEF primarily uses the discrete line data to formulate the gamma-ray emission source, with an option to include the continuous emission term data. The content of the decay library is summarized in Table 3.2 from a more comprehensive description in [45].

Table 3.2. Content of the Decay Data Library [45].

Total isotopes	979
Isotopes with discrete gamma-ray emissions	526
Isotopes with continuous gamma-ray emissions	292
Isotopes with mixed sets of emissions	161
Total gamma-ray emission lines	282,035
Discrete gamma-ray emission lines	24,199
Continuous gamma-ray emission lines	257,836

Chapter 4

Experimental Benchmarking

4.1 Motivation

The complex structure of the modeling algorithm required an extensive benchmarking effort involving the analysis of literature data and a specifically organized experimental campaign. The goals of the verification included the following:

- Demonstrate the applicability of the four-step modeling methodology for predicting the delayed gamma-ray responses and identify parameters affecting the performance of the simulation approach.

- Compare measured and predicted delayed gamma-ray responses for the primary fissile and fertile isotopes to validate nuclear data libraries associated with the calculation process.

- Produce experimental data sets from simple and complex samples of nuclear materials to develop response analysis methods, and investigate the conceptual parameters of the delayed gamma-ray assay.

The initial evaluation was performed on the published data. One of the examples for the reported experimental measurements of a DG spectrum from the neutron interrogation of an HEU sample [20] is demonstrated here. In this experiment, a small sample (~40 g) of HEU metal was irradiated for 100 s using a moderated Cf-252 source. Figure 4.1 (top) shows the detected delayed gamma-ray spectrum after 1050 s cooling period followed by 350 s of acquisition time, which is

presented in its original form, without any scale along the vertical axis. Therefore, model calculations for this case are normalized to the number of fissions (approximately 10^8 fissions/g), as estimated in the experiment.

Representative experimental parameters were modeled using the four-step delayed gamma-ray response modeling algorithm described in Chapter 3. The automatically generated discrete gamma-ray spectrum obtained in the third step is shown in Figure 4.1 (middle). For the given conditions, 1403 decaying isotopes were identified by transmutation calculations in CINDER. 849 nuclides matched the decay library data on the following step of the calculation performed in DGSDEF. As a result, the simulated spectrum is composed of 6382 discrete lines in the energy range between 0.8 and 1.55 MeV. Although most of these lines are obviously insignificant, no rejection logic was required, both because of the fast calculation and to preserve the absolute precision of the model. It is also visible that several peaks were misidentified in the original publication.

Figure 4.1 (bottom) demonstrates the simulated detector response for the setup specifications and configuration approximated in the MCNPX model. This calculation was performed assuming a uniform detector resolution of 1 keV with appropriate crystal dimensions and realistic Gaussian energy broadening parameters using the pulse-height tally. Because the exact measured spectra for these experiments were not available, only a visual comparison of peak amplitudes between measured and calculated results was possible. Under these conditions, the simulated spectra were found to be in a good agreement with the experimental data, and solid results observed at this point provided grounds for the specifically-organized experimental campaign.

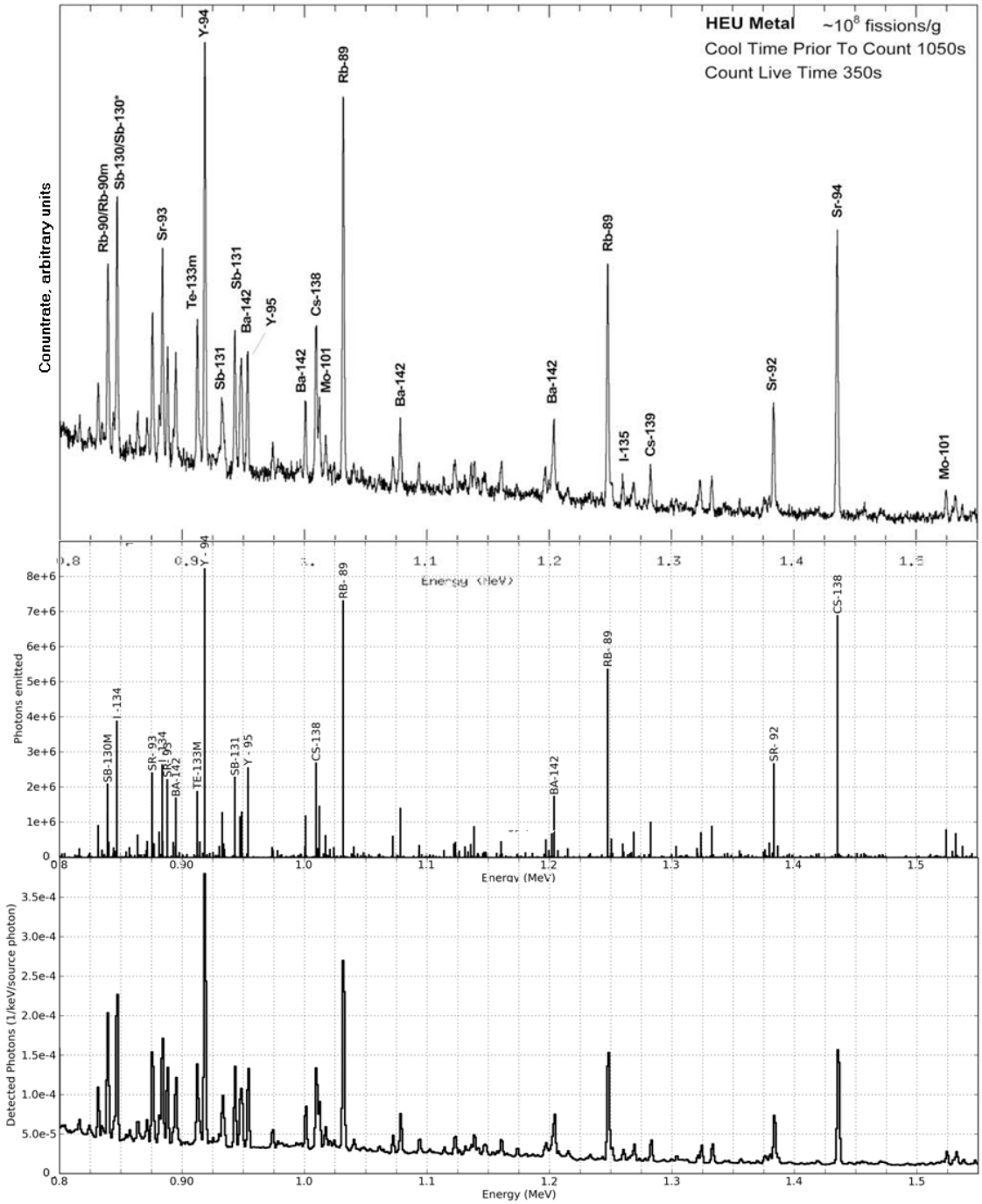

Figure 4.1. Literature data benchmarking of the HEU delayed gamma-ray response: experimentally observed (top) [20], calculated discrete emission spectrum (middle), and simulated detector response (bottom).

4.2 Experimental Arrangement

The primary effort of the experimental campaign was accomplished in several sessions at Idaho State University's Idaho Accelerator Center (IAC) in Pocatello, Idaho. This experimental program is currently in progress, and only a subset of the experimental results is discussed in this chapter. In the course of the experimental measurements at IAC, a variety of neutron and high-energy photon sources were applied to induce fissions in targets containing pure fissile and fertile materials, and their combinations. The high-precision detector setups were used to acquire delayed gamma-ray responses both in "long" and "pulsed" interrogation modes. Due to the limited scope of this dissertation that considers a basic concept of delayed gamma-ray interrogation (moderated neutron source, "long" time interrogation regime), the results of only the three most relevant experiments are discussed here. The full extent of the empirical results and the performance of extended modeling technique will be subjects of future joint publications.

Figure 4.2 depicts the original linear accelerator (LINAC)-driven pulsed neutron source that was designed for the IAC experiments. In this setup, the electron beam accelerated to 5 MeV, is impinged on a 4.2 g/cm^2 thick tungsten radiator to produce a bremsstrahlung photon source. After passing through the aluminum electron filter, the photons are intercepted by a beryllium converter where neutrons are produced by means of (gamma,n) reactions on Be-9 isotopes with a threshold energy of approximately 1.7 MeV, as seen from the Be-9 neutron stripping cross-section depicted in Figure 4.3 [22]. The resulting neutron flux is primarily thermal and epithermal, due to the fact that the bremsstrahlung photon distribution is dominant in the low-energy region, with an exponential decrease to the endpoint energy of 5 MeV (Figure 4.4). The maximum photon energy is below the fission threshold; therefore, delayed gamma-ray signatures in the interrogated samples are induced in low-energy neutron fissions only. The total neutron production was estimated to be approximately 5x10^9 neutrons per second with the accelerator running at 20 microampere electron current. The neutron source design parameters were calculated using the MCNPX 2.7.b transport code and experimentally verified by activation of gold witness foils in the interrogation setup. The latter was performed by introducing thin gold foils with a known mass

at various positions along the beryllium cylinder. After the irradiation period, the amount of thermal neutron flux incident on the foil was estimated from the detected area of the 411 keV peak from the Au-198 isotope decay. Modeling of the gold foil activation was also performed using the 4-step algorithm, with a good agreement between measured and calculated results.

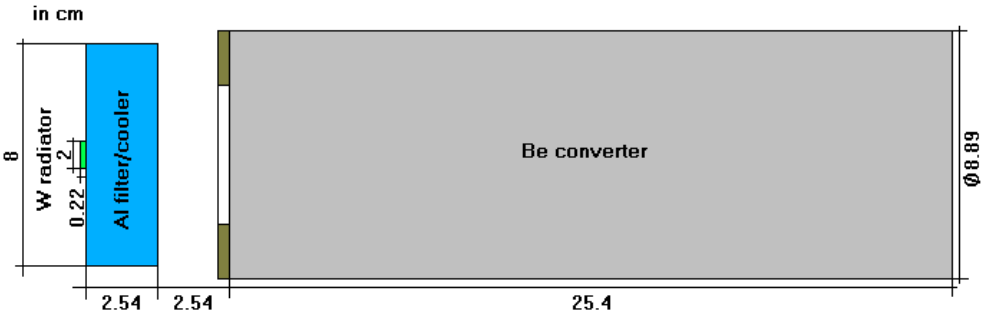

Figure 4.2. Schematic of the LINAC-driven low energy photo-neutron source designed for IAC experimental measurements.

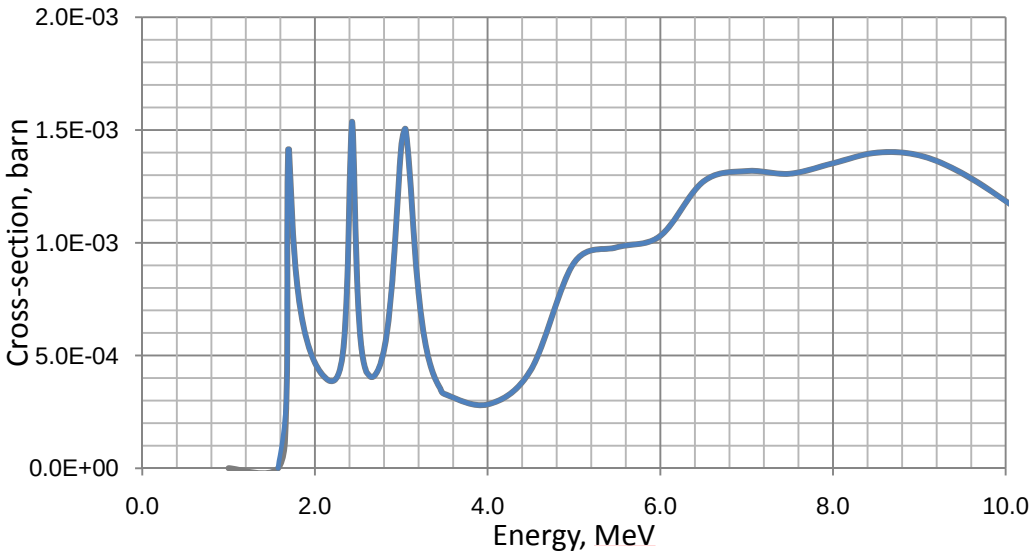

Figure 4.3. ENDF/B-VII Be-9(gamma,n)Be-8 cross-section [22].

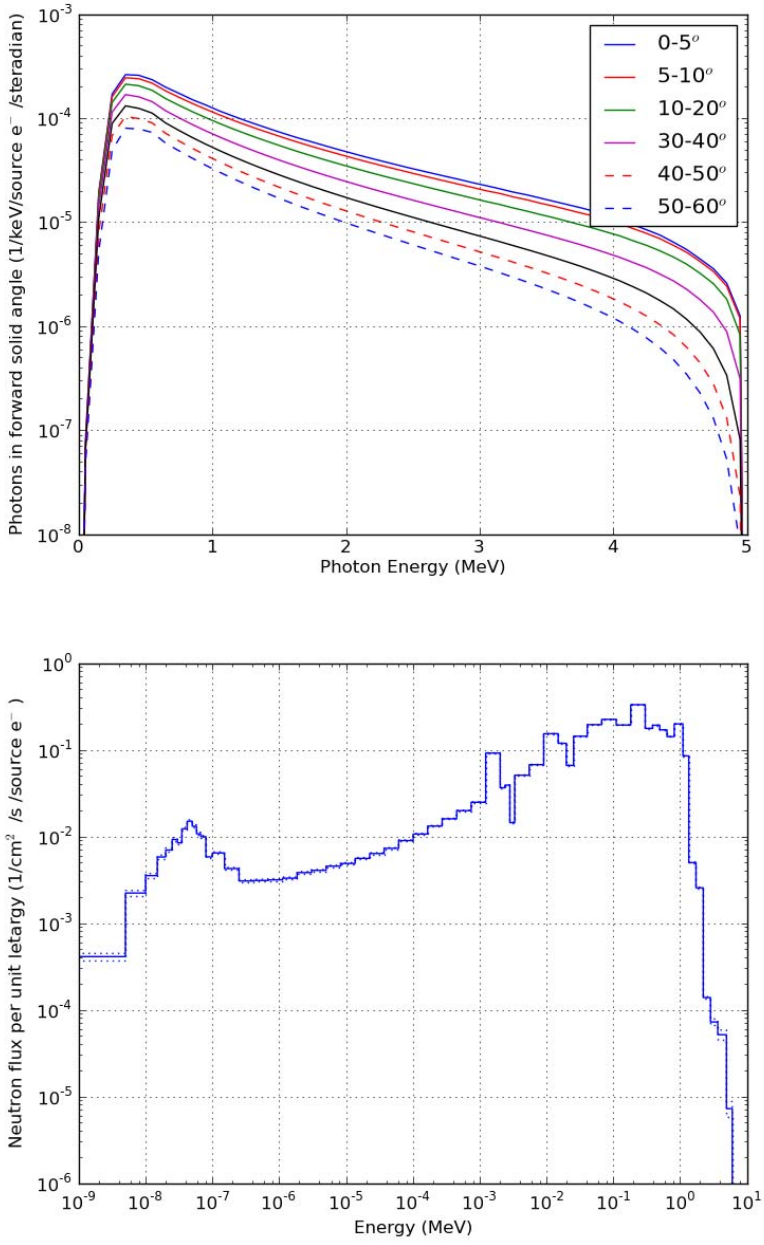

Figure 4.4. Calculated bremsstrahlung photon flux spectrum in forward angular bins at 5 MeV LINAC electron beam energy (top). Calculated 64-group neutron flux produced in Be converter (bottom).

The three experiments discussed below, followed the same type of "long" delayed gamma-ray interrogation pattern:

- The sample of interrogated material is placed into the acquisition setup where the passive spectrum with background is acquired.
- The sample is placed into the interrogation setup and irradiated with a neutron flux.
- After the electron beam is shut down, the activated sample is moved back to the acquisition setup, generally with a one to two minute time delay.
- The activated spectrum is acquired for an extended period of time in the detector setup.

The obtained photon spectrum is then normalized to a count rate, and the passive background is subtracted. The resulting delayed gamma-ray spectrum is then compared with the one predicted using the four-step delayed gamma-ray modeling technique.

The experimental parameters were reproduced as inputs for the simulation algorithm. For the cases discussed here, the pulsed nature of the neutron source was disregarded because of the high LINAC repetition rate, and the interrogating flux was normalized to the integral electron current. The modeling technique provides for easy access to the intermediate calculation results, such as interrogation fluxes, reaction rates, photon source terms, individual isotopic contributions and others. Some of these additional results are shown along with the total predicted and measured spectra.

The acquisition setup utilized a shielded 40% efficiency high-purity germanium (HPGe) detector, with a standoff distance of 23cm from the activated sample. When necessary for count rate dead time control, lead sheets were introduced between the sample and the detector. The energy calibration of the detector was performed before and after each measurement using a set of standard sources and data from the Table of Radioactive Isotopes [46]. Each energy calibration measurement was analyzed and fit to a second-order polynomial using a linear least-squares method.

As shown in Table 4.1, the energy resolution calibration of the detector was performed using the spectral data of isolated peaks from the standard sources. The energy broadening effects exhibited by HPGe detectors are characterized by the standard deviation and error of the Gaussian fit for each individual peak. The energy dependence of the peak full width at half-maximum (FWHM) is given by the following expression for Gaussian energy broadening [68]:

$$FWHM(E) = a + b \cdot \sqrt{E + c \cdot E^2}, \tag{4.1}$$

where E is the energy, and a, b, c are the fitting parameters. Fitting coefficients were determined by fitting the measured broadening data using the weighted least-squared fitting routine with the results shown in Figure 4.5. The experimentally determined detector parameters were reproduced in the MCNPX model at the detector response calculation stage.

Table 4.1. Energy resolution calibration data for the detector used in the experiments.

Peak Energy, keV	**Measured FWHM, keV**
356.02	2.250
661.62	2.600
911.20	2.926
1,173.00	3.429
1,274.00	3.506
1,332.50	3.563
2,614.00	5.337

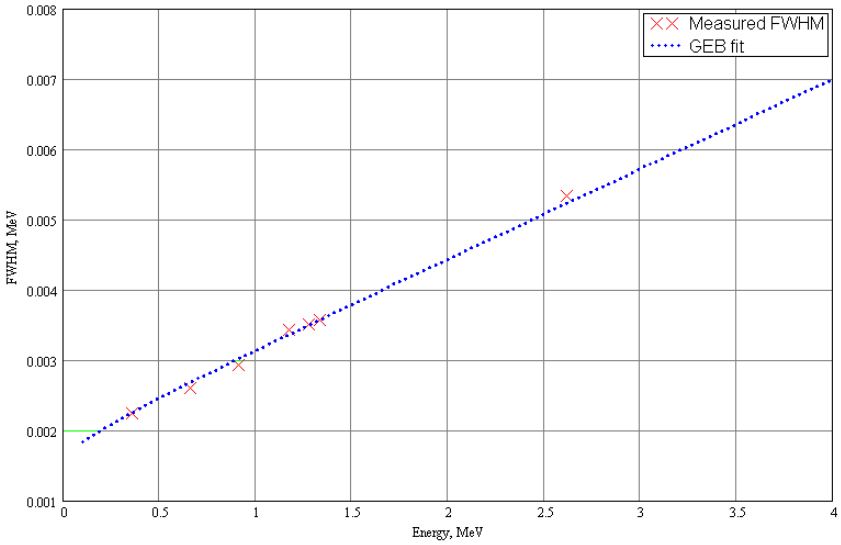

Figure 4.5. Gaussian energy broadening fit for the detector used in the experiments.

4.3 Depleted Uranium Plate Experiment

In this experiment, a depleted uranium plate with the following determined parameters was used:

- Dimensions: 9.1 x 9.1 x 0.635 cm.
- Weight: 1.2 kg.
- Composition as shown in Table 4.2.

Table 4.2. Composition of DU plates used in experiments.

Isotope	Content, at. %
U-235	0.2
U-238	99.8

The investigated sample was placed in the interrogation setup with a layer of polyethylene for additional neutron moderation. The delayed gamma-ray assay was performed according to the following time pattern: 30 minutes irradiation

time at approximately 20 microAmpere LINAC current; 30 seconds transfer time to the acquisition setup, and 55.8 minutes of live detection time with a maximum dead time of less than 2.5%. A photograph of the experimental setup along with a 3D-rendering of the MCNPX model are shown in Figure 4.6. An overlay of measured and calculated delayed gamma-ray spectra is demonstrated in Figure 4.7 along with calculated isotopic contributions to the total response. The bottom of the figure also depicts the discrete gamma-ray emission spectrum calculated in the DU plate at the 3rd step of the modeling algorithm. This spectrum contains more than 12,000 individual lines in the energy interval shown. The total calculated and measured spectra were analyzed using the ORTEC Maestro [47] interactive peak fitting program where several individual peak areas were extracted. The numerical results of spectra comparison are shown in Table 4.3 and demonstrate a satisfactory stability in ratios between the same peak areas, as well as ratios of peak pairs in measured and calculated spectra.

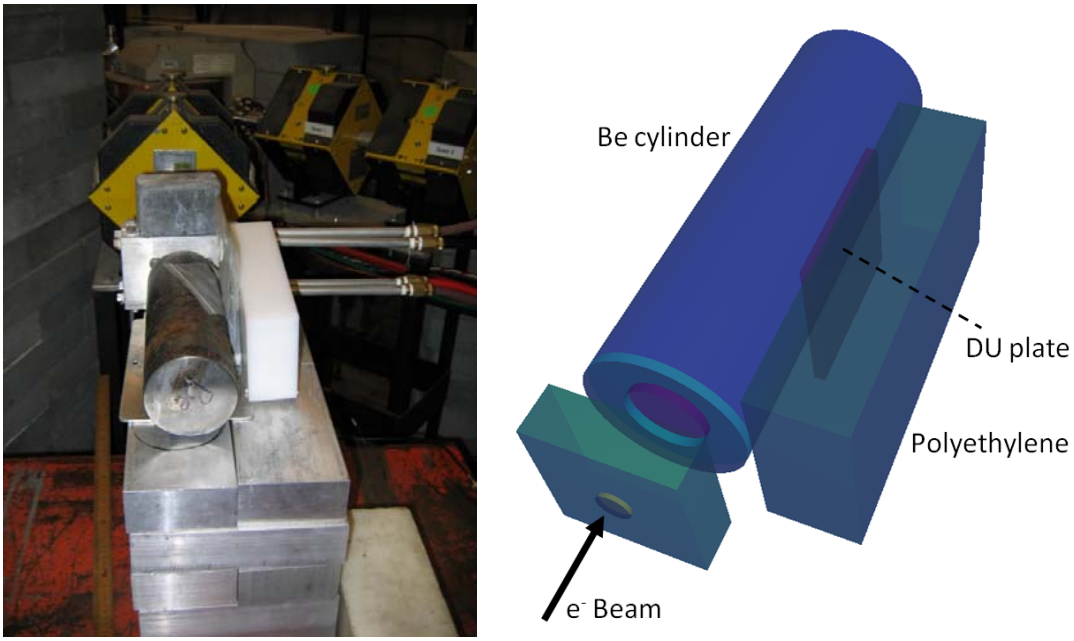

Figure 4.6. A photograph of the DU plate experimental setup, and a 3D-rendering of the MCNPX model.

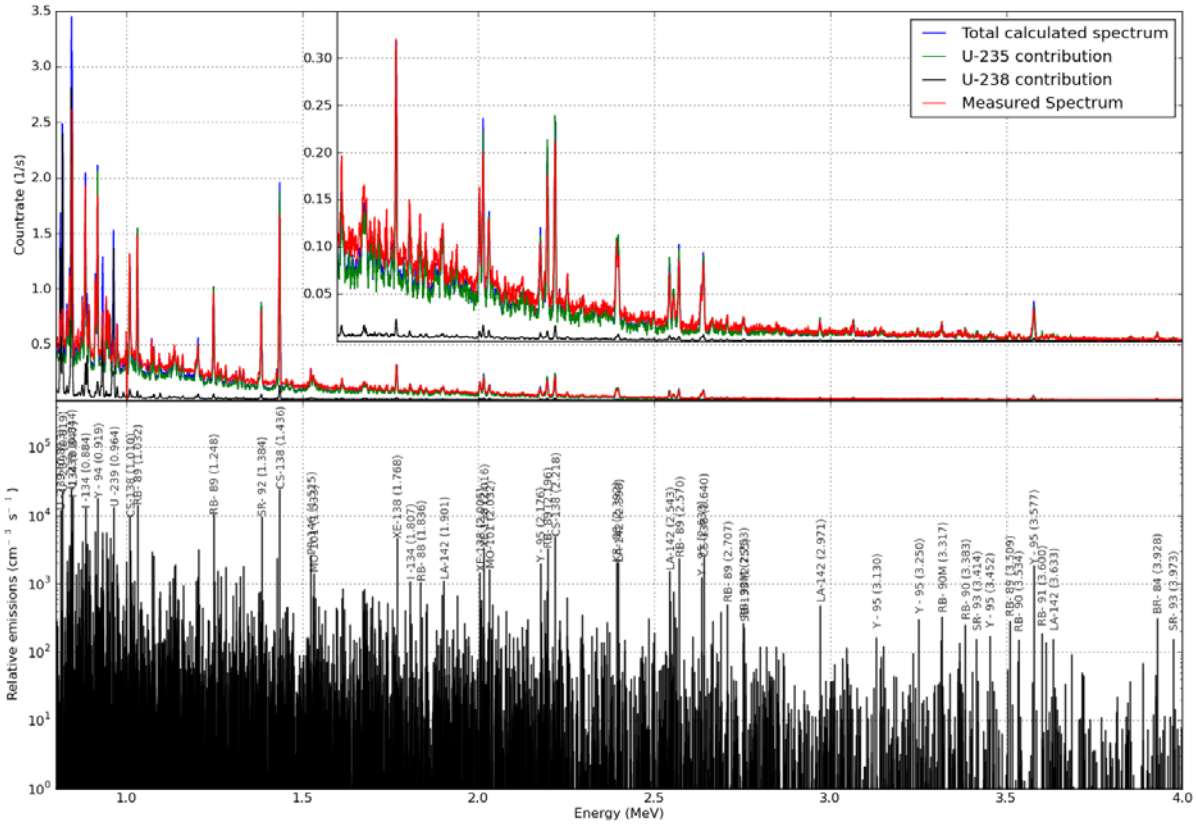

Figure 4.7. An overlay of measured and calculated delayed gamma-ray spectra for the DU plate experiment with calculated isotopic contributions to the total response (top). Calculated discrete gamma-ray emission spectrum (bottom).

Table 4.3. A comparison of the measured and calculated peak areas and peak pair ratios for the DU plate experiment.

Peak centroid position, MeV	**Primary contributors**	**Peak areas from interactive fit, counts/s**		**Difference Calculated/Measured**
		Measured	**Calculated**	
0.847	I-134 (0.847)	17.56 ± 0.17	15.76 ± 0.09	0.90 ± 0.012
0.884	I-134 (0.884), Tc-104 (0.884)	14.21 ± 0.16	13.03 ± 0.09	0.92 ± 0.013
0.920	Y-94 (0.919)	4.26 ± 0.16	4.07 ± 0.13	0.96 ± 0.049
0.934	Sb-131 (0.933)	4.22 ± 0.12	3.8 ± 0.08	0.90 ± 0.036
1.010	Cs-138 (1.010)	10.29 ± 0.09	9.24 ± 0.12	0.90 ± 0.016
1.032	Rb-89 (1.032)	3.33 ± 0.12	3.14 ± 0.10	0.94 ± 0.048
1.248	Rb-89 (1.248)	3.44 ± 0.07	3.26 ± 0.09	0.95 ± 0.034
1.436	Cs-138 (1.436)	15.27 ± 0.22	13.98 ± 0.07	0.92 ± 0.015
1.768	Xe-138 (1.768)	1.45 ± 0.06	1.29 ± 0.05	0.89 ± 0.055
2.218	Cs-138 (2.218)	1.78 ± 0.04	1.6 ± 0.04	0.90 ± 0.033
Average peak ratio difference:				0.92 ± 0.101
Peak Pair Ratios Comparison				
Arbitrary peak pairs	**Ratio in the measured spectrum**	**Ratio in the calculated spectrum**		**Difference Calculated/Measured**
0.884/1.436	0.93 ± 0.02	0.93 ± 0.01		1.00 ± 0.02
1.436/0.847	0.87 ± 0.02	0.89 ± 0.01		1.02 ± 0.02
0.847/2.218	9.87 ± 0.02	9.85 ± 0.03		1.00 ± 0.00
2.218/1.768	1.23 ± 0.05	1.24 ± 0.05		1.01 ± 0.05
1.768/1.032	0.44 ± 0.05	0.41 ± 0.05		0.94 ± 0.18
1.032/1.124	0.97 ± 0.04	0.96 ± 0.04		1.00 ± 0.06

According to the results obtained from the modeling technique, most of the delayed gamma-ray response originates from the U-235 isotope present in the depleted uranium target. Although the U-235 content is very small (~0.2wt%), its fission rate is considerably higher than for U-238 because of the mostly thermal interrogating neutron flux. Overall, a good agreement between the measured and calculated response spectra can be observed.

4.4 Three Pu Coupons Experiment

The investigated sample in this experiment consisted of three Pu disks in copper cladding combined with the following parameters:

- Dimensions: 2.45 cm diameter, 0.11 cm thickness, including a 0.05 cm layer of Cu cladding on the surface of each coupon as shown in Figure 4.8.
- Weight: 1.033 g of Pu each.
- Composition as shown in Table 4.4.

Table 4.4. Composition of Pu coupons used in experiments.

Isotope	Content, wt. %
Pu composition, density 19.4 g/cc	
Pu-239	94.3
Pu-240	5.3
Pu-241	0.2
Am-241	0.2
Cu cladding composition, density 8.92 g/cc	
Cu-63	69.17
Cu-65	30.83

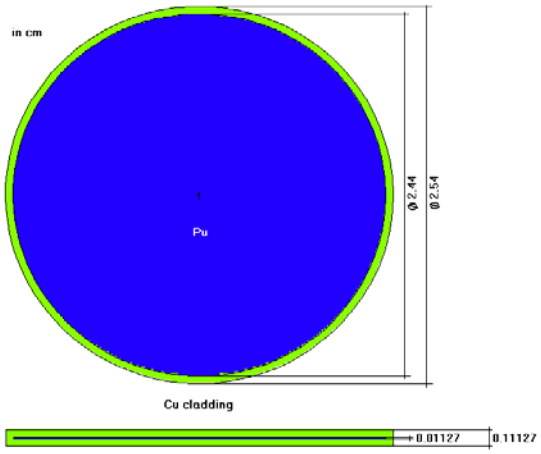

Figure 4.8. Schematic drawing of a Pu coupon target.

Three coupons were attached to a polyethylene block and subject to 30 minutes irradiation time at approximately 20 microAmpere LINAC current, followed by 40 seconds transfer time, and 54 minutes live detection time. A photograph of the experimental setup and a 3D-rendering of the MCNPX model are shown in Figure 4.9. Measured and calculated delayed gamma-ray spectra, along with calculated individual coupon contributions and discrete gamma-ray emission spectrum are demonstrated in Figure 4.10. A comparison of the peak area ratios and ratios of peak pairs between measured and calculated spectra is shown in Table 4.5.

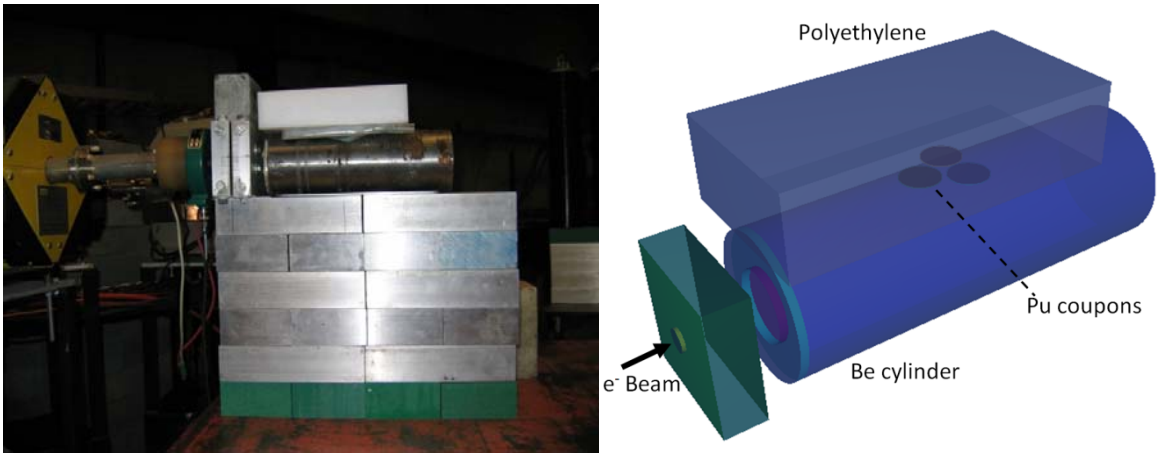

Figure 4.9. A photograph of the 3 Pu coupons experimental setup, and a 3D-rendering of the MCNPX model.

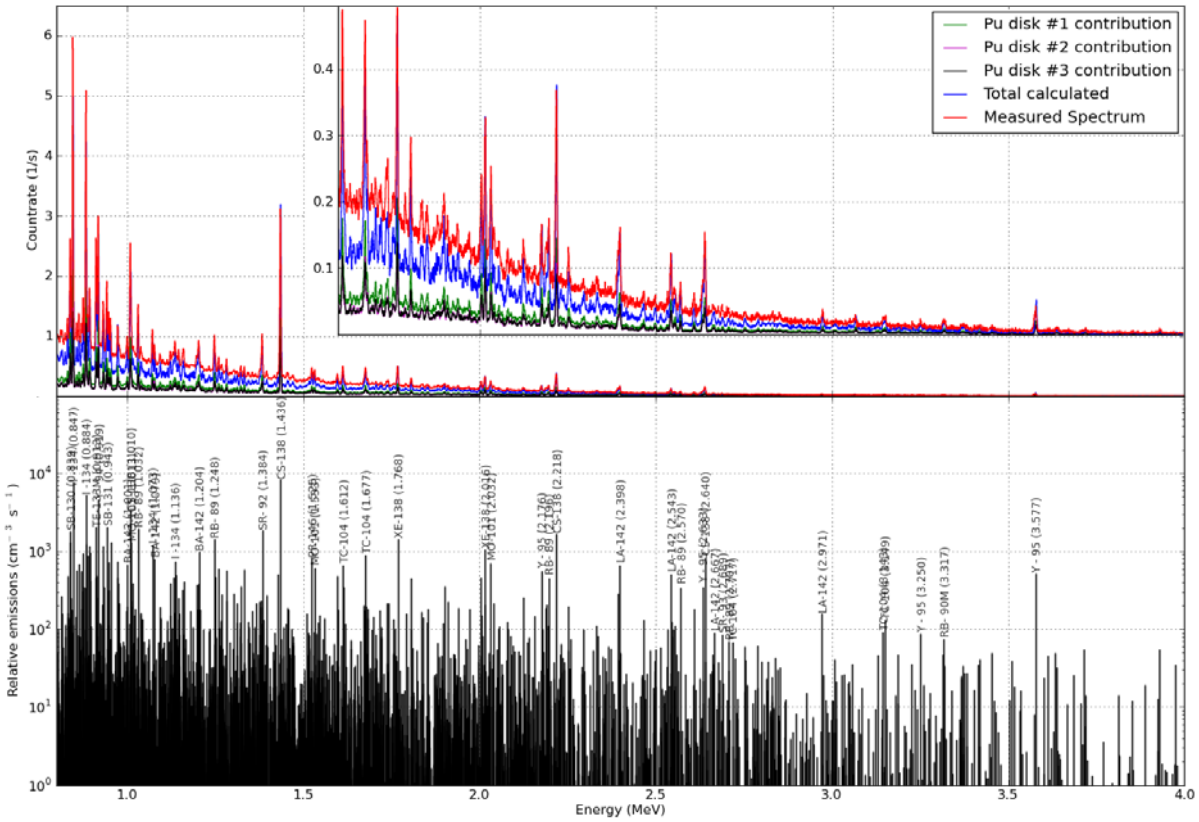

Figure 4.10. An overlay of the measured and calculated delayed gamma-ray spectra for the 3 Pu coupons experiment with calculated individual coupon contributions to the total response (top). Calculated discrete gamma-ray emission spectrum (bottom).

Table 4.5. A comparison of measured and calculated peak areas and peak pair ratios for the 3 Pu coupons experiment.

Peak centroid position, MeV	**Primary Contributors**	**Peak areas from interactive fit, counts/s**		**Ratio Calculated/Measured**
		Measured	**Calculated**	
0.884	I-134 (0.884)	2.88 ± 0.06	3.6 ± 0.06	1.25 ± 0.025
0.919	Y-94 (0.919)	3.49 ± 0.05	4.28 ± 0.06	1.23 ± 0.019
1.009	Cs-138 (1.010), Mo-101 (1.013)	2.66 ± 0.05	3.26 ± 0.05	1.23 ± 0.025
1.031	Rb-89 (1.032)	4.49 ± 0.06	5.46 ± 0.05	1.22 ± 0.017
1.248	Rb-89 (1.248), Mo-101 (1.251)	4.01 ± 0.07	4.79 ± 0.06	1.19 ± 0.021
1.384	Sr-92 (1.384), Mo-101 (1.383)	3.1 ± 0.06	3.83 ± 0.06	1.24 ± 0.026
1.436	Cs-138 (1.436)	7.65 ± 0.07	9.3 ± 0.07	1.22 ± 0.012
1.768	Xe-138 (1.768)	1.32 ± 0.04	1.61 ± 0.04	1.22 ± 0.040
2.218	Cs-138 (2.218)	1.11 ± 0.03	1.3 ± 0.03	1.17 ± 0.037
Average peak ratio difference:				1.22 ± 0.095

Peak Ratios Comparison			
Arbitrary peak pairs	**Ratio in the measured spectrum**	**Ratio in the calculated spectrum**	**Difference Calculated/Measured**
0.919/1.009	1.31 ± 0.02	1.31 ± 0.02	1.00 ± 0.02
1.009/1.436	0.35 ± 0.02	0.35 ± 0.02	1.01 ± 0.08
1.436/1.768	5.80 ± 0.03	5.78 ± 0.03	1.00 ± 0.01
1.768/0.884	0.46 ± 0.04	0.45 ± 0.03	0.98 ± 0.10
0.884/1.031	0.64 ± 0.02	0.66 ± 0.02	1.03 ± 0.05
1.031/1.384	1.45 ± 0.02	1.43 ± 0.02	0.98 ± 0.02

Although there is good agreement between the peak positions and peak area ratios in measured and calculated spectra, a discrepancy can be observed in the low-energy continuum. This effect is discussed later in this chapter.

4.5 DU + 3 Pu Coupons Experiment

A separate experiment was performed as a combination of the previous two with the goal of detecting the combined Pu-239 and U-235 delayed gamma-ray signatures. A DU plate and three Pu coupons were combined with a polyethylene block and irradiated for 30 minutes at approximately 20 microAmpere LINAC current, with 35 seconds transfer time, and a 52 second live detection period. A photograph of the experimental setup and a 3D-rendering of the MCNPX geometry are shown in Figure 4.11. An overlay of measured and calculated delayed gamma-ray spectra with individual Pu and DU targets contributions is shown in Figure 4.12. Table 4.6 demonstrates a comparison of the peak area ratios and the ratios of peak pairs between measured and calculated spectra.

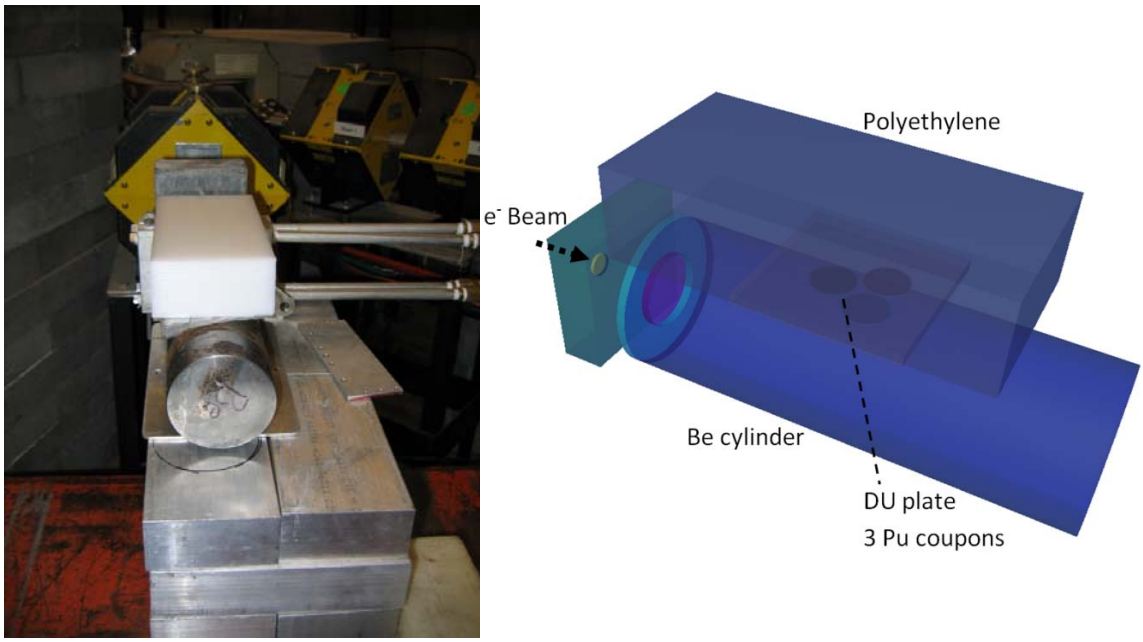

Figure 4.11. A photograph of the DU + 3 Pu coupons experimental setup, and a 3D-rendering of the MCNPX model.

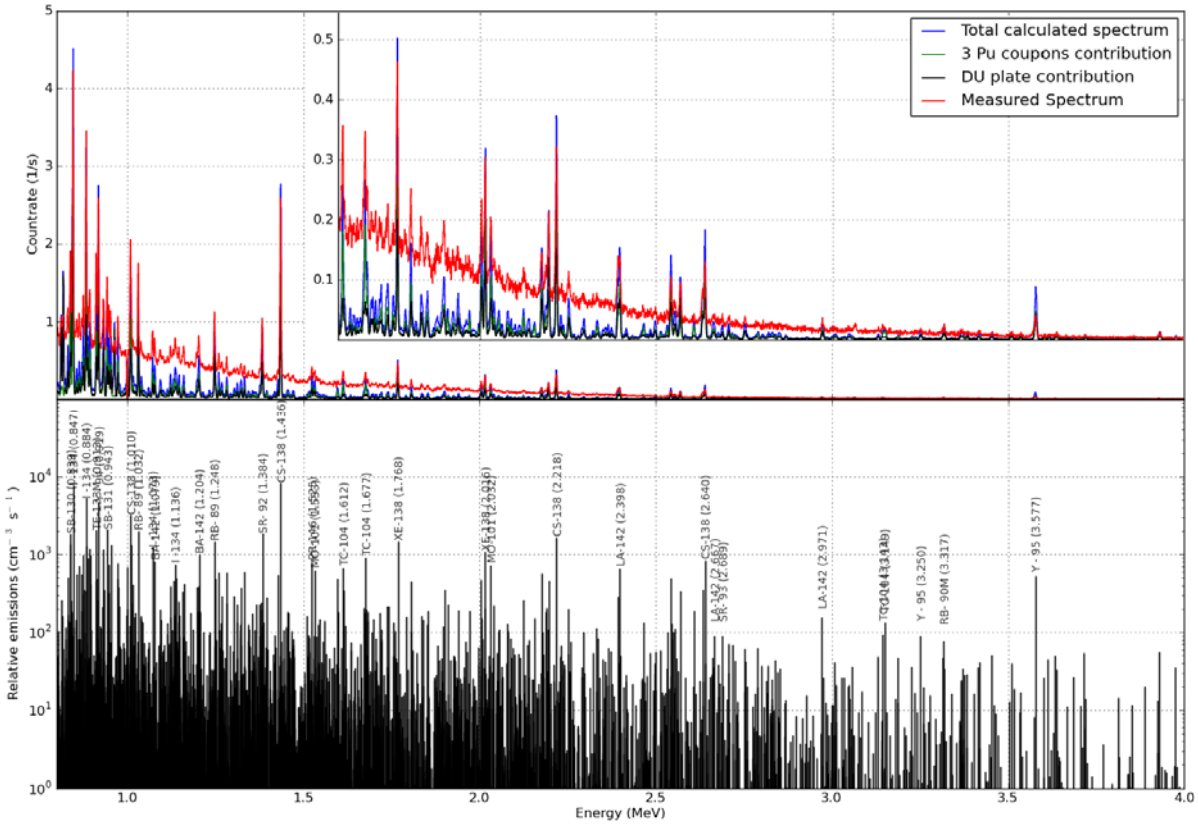

Figure 4.12. An overlay of the measured and calculated delayed gamma-ray spectra for the DU + 3 Pu coupons experiment with calculated individual DU and PU target contributions to the total response (top). Calculated discrete gamma-ray emission spectrum (bottom).

Table 4.6. A comparison of the measured and calculated peak areas and the peak pair ratios for the DU + 3 PU coupons experiment.

Peak centroid position, MeV	**Peak areas from interactive fit, counts/s**		**Ratio Calculated/ Measured**	**Calculated Fractional Peak Area Contributions**	
	Measured	**Calculated**		**3 Pu Disks**	**DU Plate**
0.847	12.18 ± 0.09	14.35 ± 0.10	1.18 ± 0.010	0.311 ± 0.003	0.674 ± 0.002
0.884	11.31 ± 0.14	13.43 ± 0.12	1.19 ± 0.015	0.329 ± 0.004	0.659 ± 0.002
0.919	3.55 ± 0.05	4.15 ± 0.06	1.17 ± 0.021	0.448 ± 0.003	0.541 ± 0.002
1.010	6.87 ± 0.11	8.09 ± 0.13	1.18 ± 0.023	0.388 ± 0.006	0.609 ± 0.004
1.031	4.46 ± 0.11	5.24 ± 0.07	1.17 ± 0.029	0.614 ± 0.014	0.405 ± 0.005
1.248	4.43 ± 0.09	5.35 ± 0.05	1.21 ± 0.023	0.609 ± 0.007	0.389 ± 0.008
1.384	3.85 ± 0.08	4.62 ± 0.08	1.20 ± 0.028	0.537 ± 0.007	0.448 ± 0.008
1.436	12.3 ± 0.10	14.7 ± 0.08	1.20 ± 0.010	0.409 ± 0.003	0.606 ± 0.002
1.768	1.75 ± 0.06	2.19 ± 0.04	1.25 ± 0.037	0.427 ± 0.015	0.56 ± 0.011
2.218	1.5 ± 0.04	1.86 ± 0.03	1.24 ± 0.035	0.418 ± 0.017	0.576 ± 0.012
Average peak ratio difference:			1.20 ± 0.095		

Peak Ratios Comparison			
Arbitrary peak pairs	**Ratio in the measured spectrum**	**Ratio in the calculated spectrum**	**Difference Calculated/Measured**
0.847/0.884	1.08 ± 0.01	1.07 ± 0.01	0.99 ± 0.02
0.884/1.010	1.65 ± 0.02	1.66 ± 0.02	1.01 ± 0.02
1.010/1.248	1.55 ± 0.03	1.51 ± 0.02	0.98 ± 0.02
1.248/1.384	1.15 ± 0.03	1.16 ± 0.02	1.01 ± 0.03
1.384/2.218	2.57 ± 0.03	2.48 ± 0.02	0.97 ± 0.02
2.218/1.436	0.12 ± 0.03	0.13 ± 0.02	1.04 ± 0.27

A comparison of the calculated and measured delayed gamma-ray spectra in each experiment demonstrates a good match for peak intensities and positions. In addition, manually calculated individual peak area ratios determined by peak fitting, are in good agreement with the real and predicted spectra. The discrepancy in photon continuum at low energy is currently attributed to the lack of the electron source term from energetic beta decays in the target. Electron emissions in the activated material produce bremsstrahlung photons in the sample itself and in the detector shielding that contribute to the continuum in this region. Among the three cases shown above, the continuum was best matched for the DU plate sample. This is consistent with the beta decay being the primary source of the disagreement in the continuum, since the bremsstrahlung photons produced by beta particles are readily attenuated in the thick sample, decreasing the rate at which they contribute to the detector.

When compared directly as in Figure 4.13, areas of the same peaks in the measured and calculated spectra demonstrate a consistent negative or positive bias. This discrepancy in the peak intensities arises from (1) the inconsistencies between the real and modeled detector setup geometry and irradiated sample position, and (2) the idealized detector response model which does not account for the effects from signal processing electronics, nor damage and impurities in the detector crystal. The model performance in this case can be evaluated by comparing the area ratios between peak pairs observed in experimental and modeled spectra. Figure 4.14 shows that in each experiment, a very good agreement is demonstrated for this criterion with an almost exact match for calculated and measured ratios of arbitrary peaks.

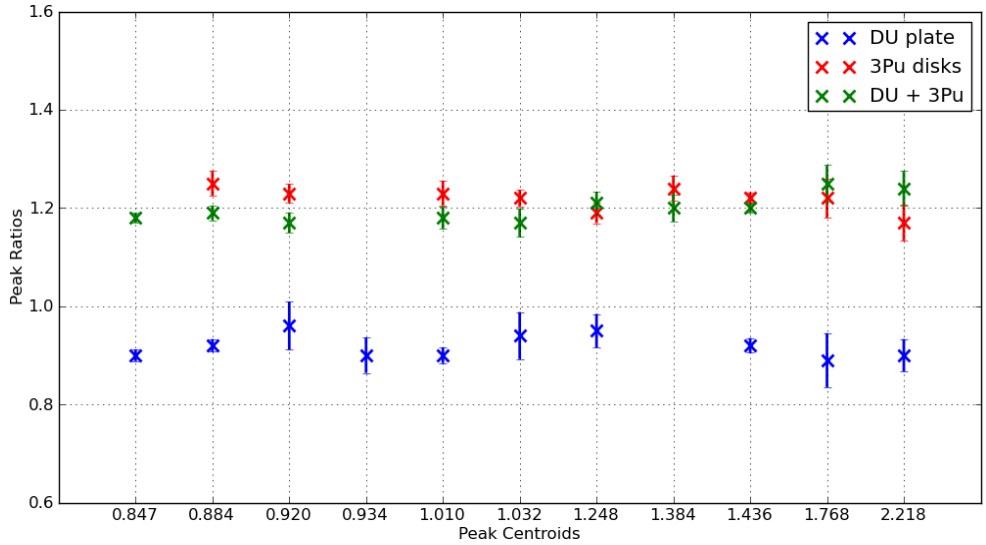

Figure 4.13. Ratios of peak areas between measured and calculated delayed gamma-ray spectra for three experiments.

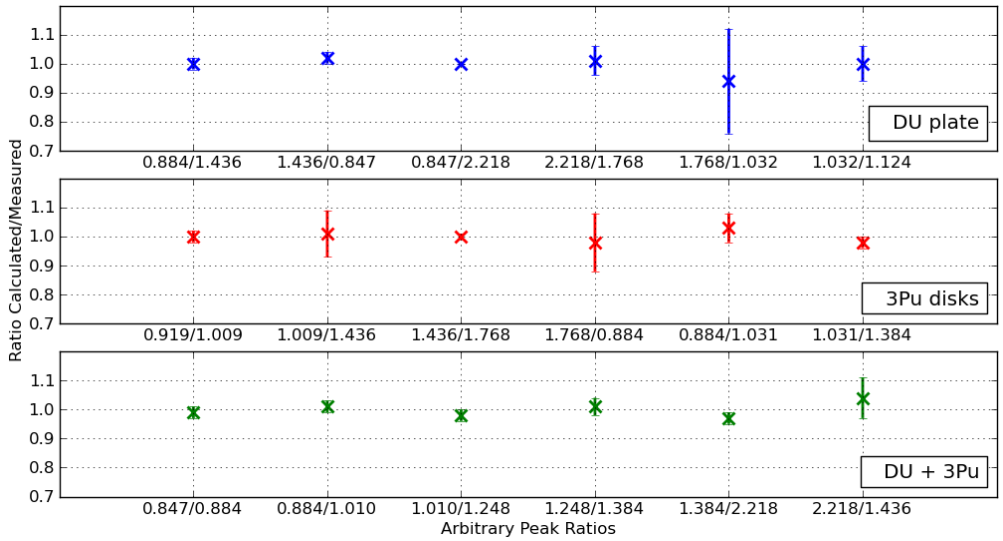

Figure 4.14. Ratios of peak pair ratios between measured and calculated delayed gamma-ray spectra for three experiments.

4.6 Passive Source Experiments

The idealized transport model and the assumptions associated with the electron, photon, and neutron transport can also become a source of small discrepancies. Interrogating flux and detector response modeling performed in MCNPX are the most time-consuming stages of the simulation. To improve the effectiveness of these calculations, an intensive variance reduction is required. A set of experiments using passive calibration gamma-ray sources was performed to gain confidence in the accuracy of the calculation approach.

To improve the efficiency of the MCNPX detector response calculations, the following variance reduction measures were implemented.

- *Pseudo-deterministic transport*. At each production or interaction point, the probability of a photon scatter and transmission towards the detector is performed using a partially deterministic scheme, resulting in a fast transport through parts of the geometry. For example, in the MCNPX transport code this effect is achieved by using DXTRAN spheres and F5 type tallies.

- *Photon population control*. Since only high-energy delayed gamma-ray lines are considered for the assay analysis, photons below a certain energy level can be eliminated from the transport, saving considerable amounts of calculation time.

- *Angular source biasing*. A higher fraction of the otherwise isotropic photon source is emitted towards the detector resulting in faster accumulation of photon histories. For every setup geometry case, the sensitivity to the angular biasing is manually analyzed, and the results are normalized to the emission probability of the uniform source.

- *Source probability biasing*. The delayed gamma-ray source terms include thousands of discrete gamma-ray lines with emission probabilities varying

by several orders of magnitude. The biasing function provides a uniform sampling probability for all photon lines from the source definition.

- *Source filtering*. Discrete gamma-ray lines with a number of emissions during an acquisition period below a certain threshold will not meaningfully contribute to the detected spectrum. These lines can be eliminated from the source definition, improving the overall sampling efficiency.

The full extent of these variance reduction techniques was applied for detector response calculations of known isotopic sources. Each passive spectrum was acquired on the same detector system as the delayed gamma-ray results, normalized to the average count rate and corrected for the background. The source parameters were supplied to Step 2 of the modeling algorithm and a calculated spectrum was produced. Figure 4.15 demonstrates measured and calculated spectra for a subset of Co-60, Eu-152, and Y-88 isotopic sources with peak intensities compared in Table 4.7. For the cases involving passive photon sources without intense beta-emitters, the continuum is accurately reproduced. Also, a good agreement is observed in the peak areas, which unambiguously validates the modified detector response calculation approach.

Table 4.7. Measured and calculated peak areas for the passive source experiments.

Peak centroid position, MeV	Peak areas from interactive fit, counts/s		Ratio Calculated/Measured
	Measured	Calculated	
Co-60			
1.137	22.61 ± 0.18	24.66 ± 0.19	1.09 ± 0.01
1.333	19.59 ± 0.17	21.65 ± 0.18	1.11 ± 1.01
Eu-152			
0.778	3.99 ± 0.05	4.87 ± 0.05	1.22 ± 0.02
0.867	1.19 ± 0.04	1.46 ± 0.04	1.23 ± 0.04
0.964	3.82 ± 0.04	4.63 ± 0.05	1.21 ± 0.01
1.085	2.80 ± 0.04	3.41 ± 0.04	1.22 ± 0.02
1.112	3.24 ± 0.04	3.88 ± 0.04	1.20 ± 0.02
1.408	3.98 ± 0.04	4.89 ± 0.04	1.23 ± 0.01
Y-88			
0.898	1.01 ± 0.02	1.17 ± 0.02	1.16 ± 0.03
1.836	0.62 ± 0.02	0.68 ± 0.02	1.11 ± 0.04

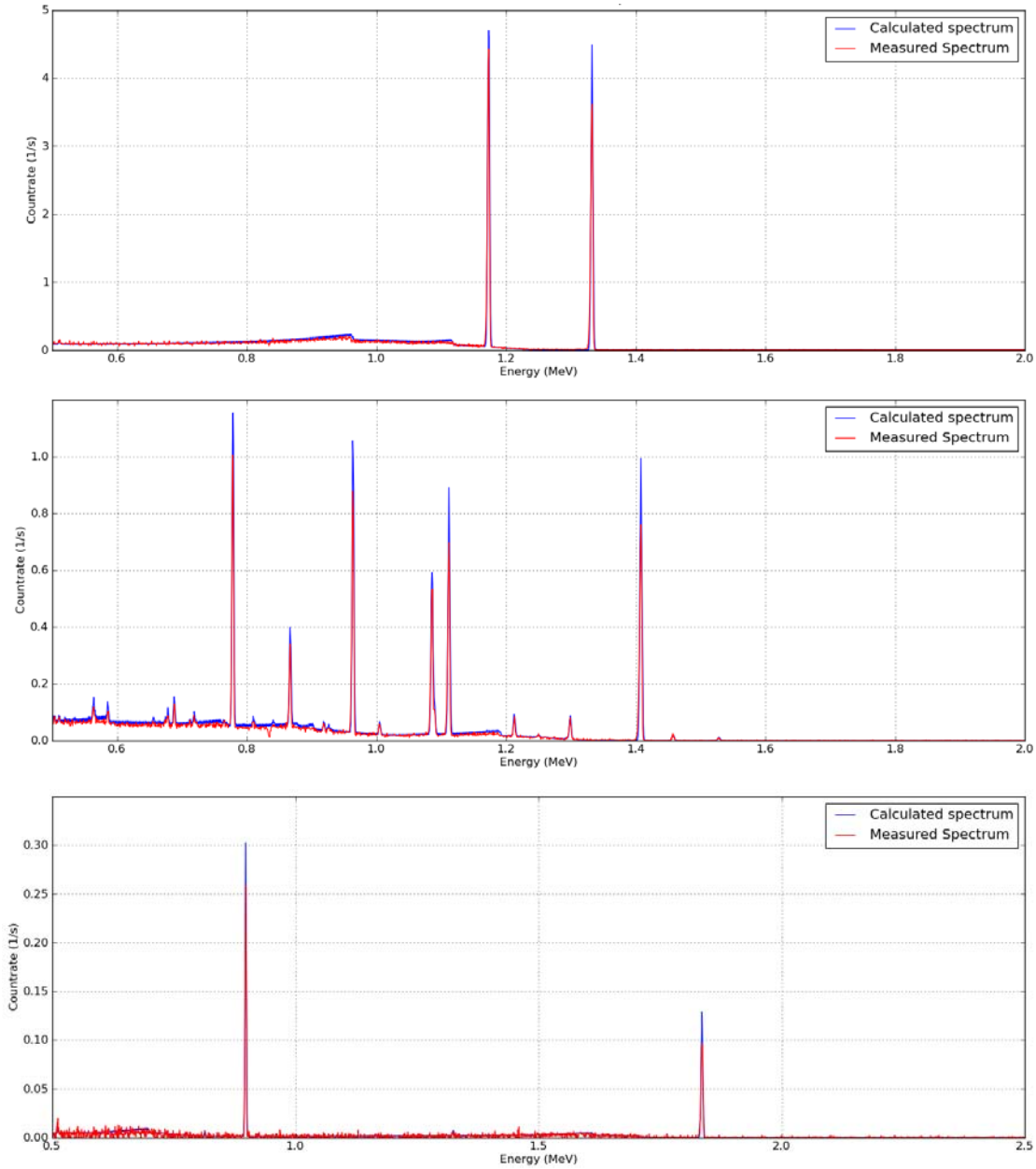

Figure 4.15. Passive source experiments results: Co-60 (top), Eu-152 (middle), Y-88 (bottom).

The results of the IAC benchmarking experiments confirm the satisfactory performance of the four-step calculation approach and, most importantly, the physical data involved. In this case, a good data library performance was expected, since cumulative neutron fission yields for long-lived fission products of main actinides are known with a high level of confidence. The experimental campaign currently continues [48,49] in order to characterize the limits of the data by varying the interrogation time, neutron energy structure, and the source type, utilizing targets with more complex compositions. A parallel benchmarking effort considers obtaining data from several sites where measurements of spent nuclear fuel have been taken. In this respect, the modeling code was already successfully applied to predict the gamma-ray source term and the passive continuum for the spent fuel sample measurements obtained for the X-Ray Fluorescence assay instrument [50].

Chapter 5

Spent Fuel Assay Instrument Design Considerations

5.1 Design Methods and Limitations

Chapter 4 demonstrates the capabilities of a high-fidelity modeling technique developed specifically for delayed gamma-ray response calculations in complex benchmarking setups. This approach can be readily expanded for assay simulations of the spent nuclear fuel assemblies. However, a number of factors limit the design scope of the present research.

One important constraint is posed by the simulation time requirements. Despite the optimization techniques implemented in the four-step modeling scheme, simulation of the delayed gamma-ray spent nuclear fuel assay is still computationally intense. Detailed results require high-resolution spatial and energy model parameters which are applied to extensive isotopic inventories. At present, up to 48 hours may be necessary to produce a delayed gamma-ray response spectrum for a single assembly. Out of this time, 6 to 8 hours on a single processor are required to define the multi-group neutron interrogating fluxes in small volumes defined in the fuel, assuming a moderated D-T active source (Step 1 of the modeling scheme). Transmutation calculations and spatially dependent source reconstructions take 8 to 10 hours on a single processor (Step 2 and 3). The limiting stage of calculations is the detector response run and delayed gamma-ray spectrum reconstruction requiring 10 to 24 hours on about 100 processors per each individual spectrum (Step 4); as an example, Figure 4.7 demonstrated 4 spectra: measured total, calculated total, calculated U-235, and U-238 contributions. Such time requirements are problem-specific and affected by the problem geometry and

fidelity level required. Presently, it is desirable to reduce the time needed to conduct the calculations by fixing the geometry of the interrogation setup and investigating only the variation of the delayed gamma-ray response with spent nuclear fuel parameters.

Other factors that should be considered are the limitations associated with the quality of spent nuclear fuel models. Delayed gamma-ray response simulations performed for this dissertation use spent fuel libraries specifically developed for the safeguards instrumentation development project at Los Alamos National Laboratory [51,52]. These libraries contain inventory and geometry models of generic 17 x 17 pins Westinghouse assemblies (Table 5.1, and Figure 5.1) with detailed fuel compositions of a representative pressurized water reactor after irradiation. Spent fuel inventories were obtained using the MCNPX transport calculations and were coupled with the CINDER90 burnup/depletion code. The first version of the library contained a total of 64 assemblies with different parameters: four initial enrichments (IE), four burnup levels (BU), and four cooling times (CT), as summarized in Table 5.2.

Spent nuclear fuel library #1 was used throughout the initial stage of the research. However, due to the memory constraints of the burnup/depletion scheme, the original inventories were limited to the approximately 100 isotopes most important for the criticality calculations. This number of isotopes is not sufficient to account for passive gamma-ray emissions from the spent fuel that can interfere with the delayed-gamma-ray response. In simulations involving spent fuel library #1, the problem was partially mitigated by extracting the limited isotopic inventories at an assembly discharge point, and allowing additional cooling time using CINDER in order to obtain more extensive inventories by developing all possible radioactive equilibriums. Passive gamma-ray emission spectra reproduced for these inventories were still missing high-intensity high-energy lines (above ~2 MeV) commonly observed in spent fuel.

The deficiency in the composition of the spent fuel in library #1 was not addressed until later in the research, when a new library #2 [52] was introduced. It was obtained with higher fidelity in spatial and isotopic fuel inventories by using more

realistic irradiation schemes. Over 2,000 individual isotopes were extracted for each material volume for the passive and delayed gamma-ray response modeling.

The difference between spent fuel libraries #1 and #2 is illustrated in Figure 5.2 by comparing the calculated passive discrete gamma-ray emission spectra for 45 GWd/t, 4% IE, 5 years CT assembly. The top spectrum in this figure was obtained for a fuel inventory from library #1, and the middle spectrum was produced with additional cooling as described above. The bottom spectrum was produced for the same assembly with inventory from spent fuel library #2. A considerable difference in passive emissions can be observed in the energy region between 2 and 3.5 MeV. Although library #2 appears to have more adequate spent fuel inventories, its overall accuracy is still under investigation. Simulation results demonstrated further in this chapter were obtained using the inventories of library #1 and #2, and should be considered preliminary at this stage of research.

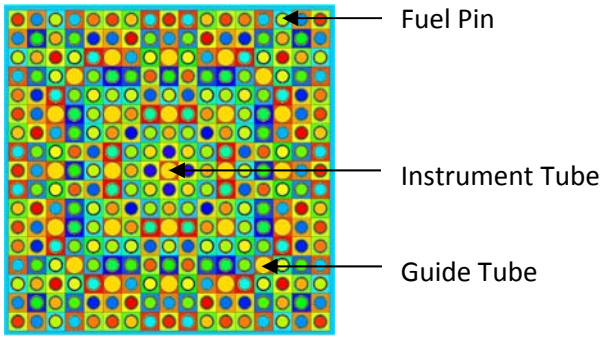

Figure 5.1. The planar cross-section of the spent nuclear fuel assembly MCNPX model [51].

Table 5.1. The parameters of the 17 x 17 Westinghouse fuel assembly from the spent fuel library [52].

Parameter	Data
Assembly general data	
Lattice	17 x 17
Number of fuel rods	264
Number of guide tubes	24
Number of instrument tubes	1
Fuel rod data	
Type of fuel pellet	UO_2 (10.4538 g/cc)
Rod pitch	1.26 cm
Clad thickness	0.065 cm (assumed gap closure)
Pellet radius	0.410 cm
Active fuel length	365.76 cm
Fuel temperature	900 K
Clad temperature	620 K
Clad material	Zircaloy-4 (5.8736 g/cc)
Guide and instrument tube data	
Inner radius	0.571 cm
Outer radius	0.613 cm
Material	Zircaloy-4 (5.8736 g/cc)

Table 5.2. Parameters of spent nuclear fuel assemblies in the library.

Parameter	Available cases
U-235 enrichment	2%, 3%, 4%, 5%
Burnup	15, 30, 45, 60 GWd/tU
Cooling time	1, 5, 20, 80 years

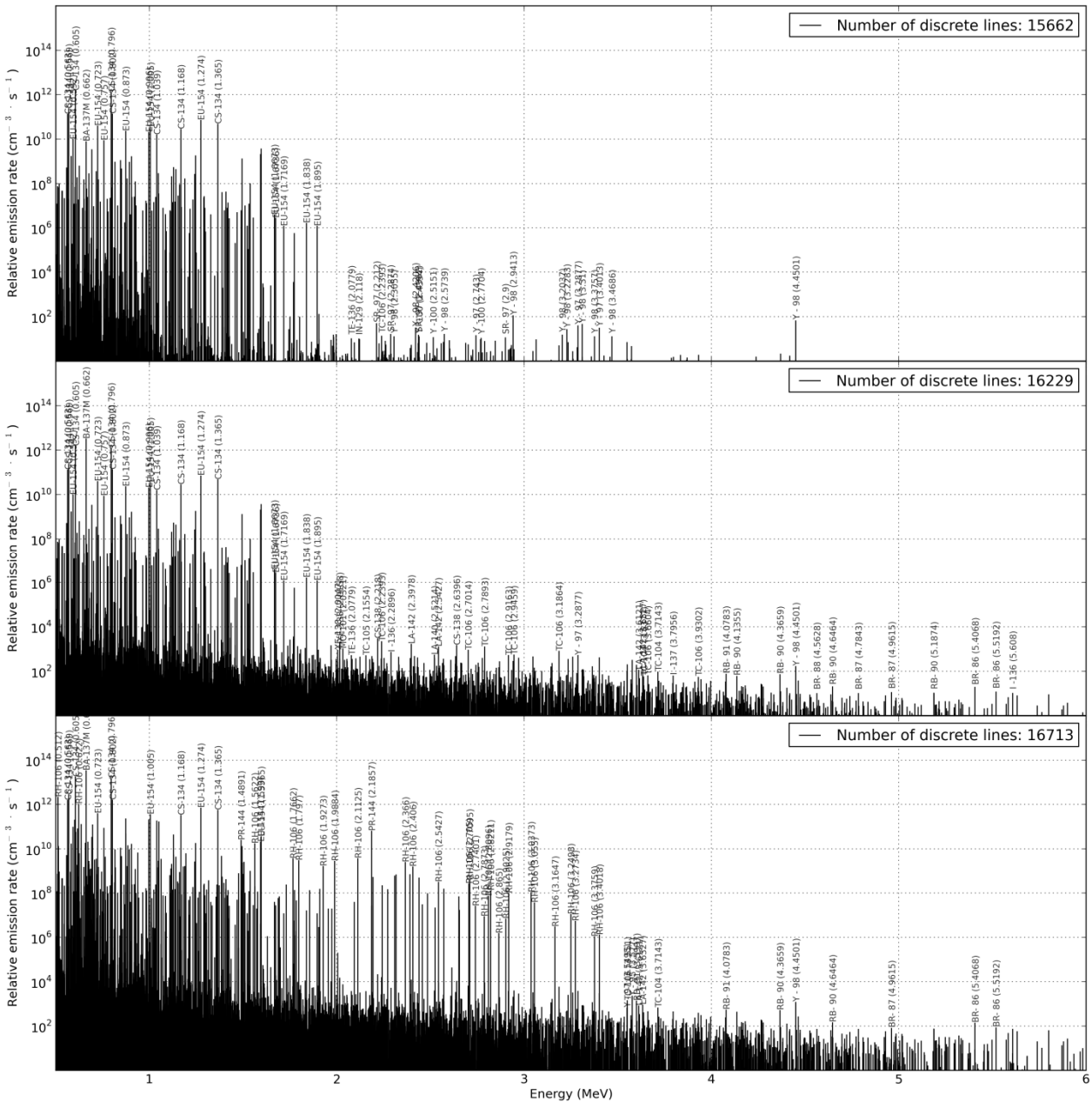

Figure 5.2. A comparison of passive discrete gamma-ray emission spectra calculated for the spent nuclear fuel assembly from libraries #1 and #2 with 45 GWD/t burnup, 4% initial enrichment, 5 years cooling time. Original NGSI library #1 inventory (top). Library #1 assembly with inventory at discharge and additional 5 years cooling period (middle). Library #2 inventory (bottom).

The above considerations require a more strict definition of the parameter space in which the delayed gamma-ray assay instrument capabilities are currently being investigated. The current limitations of the research effort's design scope are outlined below.

- *Geometry*. The interrogation and acquisition setups geometry are fixed for the assay simulations of a whole range of spent fuel assemblies. The adopted configuration includes a single neutron source and a single detector with collimator and attenuating filters. Although passive background and the amount of fissile isotopes vary considerably depending on the assembly parameters, optimization of the assay setup will be performed at later stages of the conceptual design research.

- *Source*. The interrogating neutron source is defined as a high-intensity moderated 14.1 MeV D-T generator, compatible with designs of other active interrogation NDA instruments. The moderation layers include tungsten and beryllium with dimensions calculated in [53,54].

- *Time*. The time regime is established at 15 minutes interrogation time, arbitrary 1 minute delay time, and 15 minutes photon spectrum acquisition time. This regime corresponds to the most conventional "long" delayed gamma-ray assay mode. Modeling of this assay type is more accurate due to the reliable yield data for the long-lived fission products and associated decay chains. After establishing the analysis technique and identifying the key delayed gamma-ray signatures, the time optimization can be performed.

- *Energy region*. The target delayed gamma-ray lines are located in the energy region above 3 MeV. Below this limit, the analysis is obstructed by interferences from the passive spent fuel background.

- *Detector type*. A high-efficiency, HPGe detector type is selected with the goal of utilizing the increased resolution for the identification of delayed gamma-ray peaks. However, considering the count rate limitations of the

HPGe systems, lower-resolution fast $LaBr_3$ scintillators may be considered at a later time.

These constraints of the delayed gamma-ray assay setup were used to demonstrate delayed gamma-ray responses for a variety of simulated spent nuclear fuel assemblies, the optimization of assay parameters, and the development of analysis techniques. A detailed discussion of the results and findings is provided further in this chapter.

5.2 Detector System Limitations

For the purposes of the qualitative and quantitative assay based on the gamma-ray spectroscopy, the high-resolution HPGe detectors are the natural choice. However, there are several factors that limit the performance of these detector systems for the delayed gamma-ray spent nuclear fuel assay:

- Intensity of the delayed gamma-rays of interest is low compared with the total photon flux incident on the detector.

- High radioactive background of the spent nuclear fuel leads to a high parasitic count rate in the detector that is characterized by a relatively low dead time limit.

- HPGe efficiency to high-energy photons decreases nonlinearly with energy, making it impractical for delayed gamma-ray lines above 5 MeV.

The size of the detector crystal is of critical importance for high count rate assay applications. Improved detection limits for relatively low-intensity delayed gamma-ray lines can be achieved by using larger Ge detectors, which result in better peak-to-background characteristics due to higher efficiencies and a higher peak-to-Compton ratio. The detector setup requires a carefully designed collimator and attenuation layers to reduce the count rate to tolerable levels.

For the preliminary estimations produced for this dissertation, a 130% relative efficiency coaxial HPGe detector system was adopted. Operational parameters and crystal dimensions provided in [55] were accurately replicated in the simulation algorithm for the detector response calculation. Assay parameters and the acquisition system configuration for this detector are discussed in the next section. Although it is conceivable that an elaborate setup for effective HPGe delayed gamma-ray spectrometry can be designed, it is still not clear how the real-world factors not accounted for in the modeling (detector stability across a dynamic range, resolution degradation, etc.) will affect system performance. The literature provides only scarce experimental data that are is not conclusive on this matter.

Among various possible substitutes to the germanium detectors, $LaBr_3$ scintillator solutions appear to be the most viable option. Made available commercially relatively recently, they demonstrate an increased efficiency for high-energy gamma-rays, high scintillation light output, and a fast decay time [56]. It is estimated that $LaBr_3$ detector electronics can tolerate 3 to 4 orders of magnitude higher count rates than HPGe systems. Despite the more coarse resolution (approximately 2% at 2 MeV), they can be used for assay applications. Using the 4-step modeling technique capabilities, individual peak contributions in the $LaBr_3$ spectrum can be accurately determined making the development of an appropriate analysis technique feasible.

5.3 Assay Instrument Parameters Evaluation

Preliminary parametric study of the delayed gamma-ray assay setup and configuration can be performed by utilizing the approximate analytical method provided in this section. These calculations were initiated in [57] and further developed to analyze the effect of the following parameters affecting the delayed gamma-ray response in the spent nuclear fuel assay:

- Strength of the interrogating neutron source.
- Dimensions of a collimator between the fuel assembly and the detector.
- Thickness of the attenuation layers between the fuel and the detector.

This analysis provides an approximate estimation; it uses simplifying assumptions, and physical data from the ENDF/B-VII libraries. Conclusions derived from these calculations are consistent with responses observed using the four-step modeling technique, as shown later in this chapter. Analytical estimations assume the conceptual assay instrument configuration as depicted in Figure 5.3, with the parameters as indicated below.

- The D-T neutron source, neutron spectrum tailoring and position that were used with the delayed neutron and differential die-away instruments were also used here. The source is located in the mid-length of the assembly.

- The spent fuel assembly inventory is obtained from NGSI library #1 with the average set of parameters: 45 GWd/t burnup, 4% initial enrichment, and 5 years cooling time. The assembly is submerged in water.

- The air-filled collimator opening on the fuel is a 1 cm-wide and 20 cm-long slot subtending the full side width of the assembly. The collimator converges on the front surface of the detector at a standoff distance of 1 m. The collimator is fabricated from lead.

- Attenuating filters are assumed to be lead with variable thickness. The primary filter is located at the fuel side and serves to control the contribution of the low-energy passive photon background. A thin 0.5 to 1 cm layer of lead is located in front of the detector to reduce the photon flux scattered from the collimator walls.

- The detector is a large high-purity Ge crystal. The front face of the detector is partially shielded by the collimator to an arbitrarily selected area of 6 cm^2.

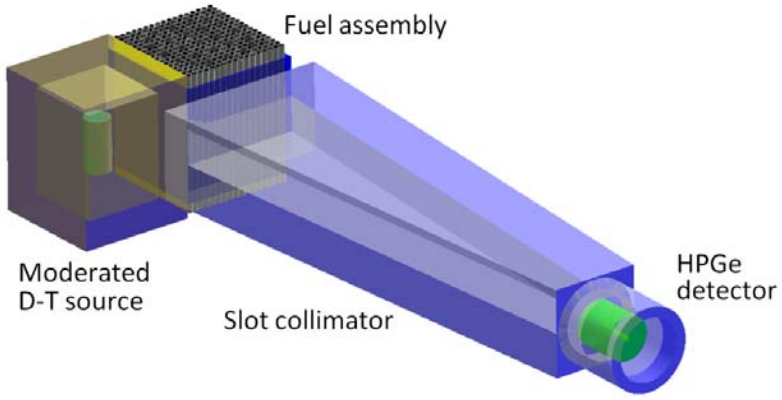

Figure 5.3. Assumed delayed gamma-ray assay setup for parametric study.

5.3.1 Delayed Gamma-Ray Response Rate Estimation

The intensity of the delayed gamma-ray peaks in the response spectra is primarily controlled by the output of the interrogating neutron source. This parameter can be estimated by considering a rate of production for an isolated peak and the effects of the assay setup configuration according to the calculation sequence shown in Figure 5.4.

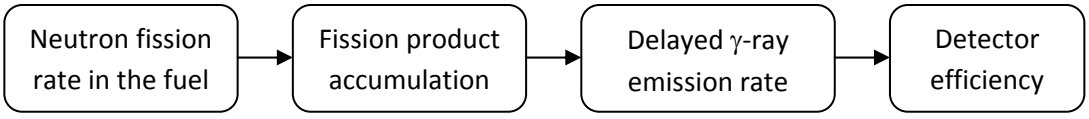

Figure 5.4. Calculation sequence for the delayed gamma-ray peak count rate.

Assume the target signature is the 3.577 MeV emission of Y-95 isotope ($T_{1/2}$ = 10.3 m), which is a prominent high-energy delayed gamma-ray line always considered in the assay response analysis. Under the thermal neutron interrogation, the Y-95 isotope is produced in the spent nuclear fuel in three primary ways: (1) as a direct fission product; (2) as a decay daughter of Sr-95 ($T_{1/2}$ = 23.9 s); and (3) as a decay daughter of Sr-96 ($T_{1/2}$ = 1.07 s). Considering the "long" interrogation mode, and the two main fissile isotopes U-235 and Pu-239, the cumulative yield of Y-95 can be estimated as the sum of three individual yields, as shown in Table 5.3.

Table 5.3. Cumulative yields of Y-59 used in analytical rate estimations [22].

Fissile isotope	Individual thermal fission yields			Assumed Y-95 cumulative fission yield
	Y-95	Sr-95	Sr-96	
U-235	1.11e-2	4.54e-2	3.57e-2	9.22e-2
Pu-239	1.68e-2	2.61e-2	1.82e-2	6.11e-2

According to the preliminary transport code estimations, distribution of the interrogating neutron flux intensity in the fuel pins is governed mostly by the assembly geometry and somewhat dependent on the multiplication of the assembly in the given media. Adopting a simplified assumption that a fuel pin located immediately near the center guide tube is representative of the average flux intensity across the assembly, the MCNPX calculated flux for the small fuel volume in the plane of the neutron source equals approximately 1.5e-3 neutrons/cm^2-s per source neutron. This calculation was performed for a 45 GWd/t burnup, 4% initial enrichment, 5 years cooling time assembly from spent fuel library #1, assuming water as the interrogation environment.

Assuming that the interrogating flux is primarily thermal and using the integrated thermal fission cross-sections for U-235 (585 barn) and Pu-239 (750 barn) [58], the fission reaction rate per unit volume for each isotope is calculated as:

$$RR_{fiss} = \varphi \cdot \sigma_f \cdot N, \tag{5.1}$$

where φ is neutron flux (neutrons/cm^2-s), σ_f is microscopic fission cross-section (barn), N is fissile isotope atom density (atoms/barn-cm).

From the assembly material inventory: $N_{U-235} \approx 1.76\text{e-}4$ (at./b-cm), $N_{Pu-239} \approx 1.2\text{e-}4$ (at./b-cm).
Therefore, assuming the 10^{10} n/s neutron source intensity, fission reaction rates are calculated as:

$$RR_{fiss}(U235) \approx 1.5\text{e-}3 \cdot 1\text{e+}10 \cdot 585 \cdot 1.76\text{e-}4 \approx 1.5\text{e}6 \text{ (fissions/cm}^3\text{-s)}.$$

$$RR_{fiss}(Pu239) \approx 1.5\text{e-}3 \cdot 1\text{e+}10 \cdot 750 \cdot 1.2\text{e-}4 \approx 1.35\text{e}6 \text{ (fissions/cm}^3\text{-s)}.$$

The rate of Y-95 isotope production on each fissile isotope is calculated by multiplying each fission rate by the appropriate fission yield calculated above:

$$R(Y95) = RR_{fiss} \cdot yield(Y95) \tag{5.2}$$

For U-235 fissions: $R(Y95) \approx 1.5\text{e+}6 \cdot 9.22\text{e-}2 \approx 1.38\text{e}5$ (atoms/cm^3-s).

For Pu-239 fissions: $R(Y95) \approx 1.35\text{e+}6 \cdot 6.11\text{e-}2 \approx 8.25\text{e}4$ (atoms/cm^3-s).

Total: $R(Y95) \approx$ 1.38e5 + 8.25e4 $\approx$ 2.21e5 (atoms/cm^3-s).

Assume that a 1 cm thick planar "slice" of the assembly is subtended by the detector. The volume of fuel in a 1 cm long pin with r = 0.41 cm is V_{pin} = 0.528 cm^3. There are 264 pins in the assembly. The mean free path of the 3.577 MeV photon in the fuel with density ρ = 10.45 g/cm^3 can be calculated using the mass attenuation coefficients at this energy for U: μ/ρ = 4.415e-2 cm^2/g, and O: μ/ρ = 3.31e-2 cm^2/g [59]:

$$\mu/\rho(UO_2) = w_U \cdot \mu/\rho(U) + \mu/\rho(O) = 0.88 \cdot 4.415\text{e-}2 + 0.12 \cdot 3.31\text{e-}2 = 4.282\text{e-}2 \text{ (cm}^2\text{/g)}.$$

$$\mu(UO_2) = \mu/\rho(UO_2) \cdot \rho = 4.282\text{e-}2 \cdot 10.45 = 0.447 \text{ (1/cm)}.$$

Then, the mean free path of a 3.577 MeV photon in spent fuel material can be obtained:

$$mfp(3.577) = \frac{1}{\mu(UO_2)} = \frac{1}{0.447} = 2.237 \text{ (cm)}.$$

This value corresponds to approximately 16 cm of an infinite fuel thickness layer at 3.577 MeV. Therefore, assuming arbitrarily that only half of the pins are

contributing to the detector, the total Y-95 production rate averaged over the 1 cm-thick assembly layer is:

$$R_{tot}(Y95) = V_{pin} \cdot \#\, pins \cdot R(Y95) \tag{5.3}$$

$$R_{tot}(Y95) \approx 0.528 \cdot 264/2 \cdot 2.21\text{e}5 \approx 1.539\text{e}7 \text{ (atoms/s)}.$$

The total production of Y-95 atoms during the assumed 15 minute interrogation period is calculated using the production-decay law and Y-95 decay constant calculated from the half-life $\lambda(Y95)$ = 1.122e-3 (1/s):

$$N(Y95) = \frac{R_{tot}(Y95)}{\lambda(Y95)}\left(1 - \exp(-\lambda(Y95) \cdot time)\right) \tag{5.4}$$

$$N(Y95) \approx \frac{1.539\text{e}7}{1.122\text{e}-3}\left(1 - \exp(-1.122\text{e}-3 \cdot 15 \cdot 60)\right) \approx 8.72\text{e}9 \text{ (atoms)}.$$

During the subsequent 15 minutes detection period (disregarding the short cooling time), this amount of Y-95 atoms undergoes the following number of decay disintegrations:

$$Decay = N(Y95) - N(Y95) \cdot \exp(-\lambda(Y95) \cdot time) \tag{5.5}$$

$$Decay \approx 8.72\text{e}9 - 8.72\text{e}9 \cdot \exp(-1.122\text{e}-3 \cdot 15 \cdot 60) \approx 5.54\text{e}9 \text{ (decays)}.$$

Considering that the 3.577 gamma-ray emission branching ratio *B.R. = 6.4%* in Y-95 decay, the total 3.577 MeV photon intensity can be calculated as:

$$I_{tot} = Decay \cdot B.R. \tag{5.6}$$

$$I_{tot}(3.577) \approx 5.54\text{e}9 \cdot 0.064 \approx 3.55\text{e}8 \text{ (emissions)}.$$

Geometric efficiency for the slot collimator and 1 m detector standoff, conservatively assuming 6 cm^2 area of the detector front face, can be approximated as:

$$\omega \approx \frac{d\Omega}{4\pi} \approx \frac{area}{4\pi \cdot (standoff)^2} \tag{5.7}$$

$$\omega \approx \frac{6}{4\pi \cdot (100)^2} \approx 4.775\text{e-}5.$$

Assume the detector as a 5 cm thick germanium crystal. Given this, the interaction probability in the detector is defined by using the mass-attenuation coefficient for Ge at 3.577 MeV: μ/ρ = 3.38e-2 cm^2/g, with ρ = 5.32 g/cm^3 [59]. Factoring in the peak-to-total ratio adopted as $r \approx 1/3$, an estimation of detector intrinsic efficiency to 3.577 MeV photons can be obtained by:

$$\varepsilon(Ge) = r \cdot \left(1 - \exp\left(-\mu/\rho \cdot \rho \cdot thickness\right)\right) \tag{5.8}$$

$$\varepsilon(Ge) \approx r \cdot \left(1 - \exp(-3.38\text{e-}2 \cdot 5.32 \cdot 5)\right) \approx 0.2.$$

Therefore, the number of 3.577 MeV photons detected in the setup without the attenuating filter at 1e10 neutrons per second interrogating source strength, 15 minutes interrogation time, and 15 minutes live detection time is estimated as:

$$I_{\text{det}} = \omega \cdot \varepsilon(Ge) \cdot I_{tot} \tag{5.9}$$

$$I_{\text{det}} \approx 4.775\text{e-}5 \cdot 0.2 \cdot 3.55\text{e}8 \approx 3.390\text{e}3 \text{ (counts/900 sec)} \approx 3.77 \text{ (counts/sec)}.$$

In the event that a lead filter is used, the attenuating factor is calculated assuming a Pb mass-attenuation coefficient of 3.577 MeV μ/ρ = 4.21e-2 cm^2/g with ρ = 11.34 g/cm^3 [59]:

$$a(Pb) = \exp\left(-\mu/\rho \cdot \rho \cdot thickness)\right) \tag{5.10}$$

For a 5 cm Pb layer: $a(5cm) \approx \exp(-4.21\text{e-}2 \cdot 11.34 \cdot 5) \approx 9.2\text{e-}2.$

For a 10 cm Pb layer: $a(10cm) \approx \exp(-4.21\text{e-}2 \cdot 11.34 \cdot 10) \approx 8.45\text{e-}3.$

Applied to the above number of counts, these attenuation coefficients provide modified count rates:

$$I_{\text{mod}} = a(Pb) \cdot I_{\text{det}}. \tag{5.11}$$

For a 5 cm Pb layer: $I_{\text{mod5}} \approx 9.2\text{e-}2 \cdot 3.390\text{e}3 \approx 311.9 \approx 0.35$ (counts/sec).

For a 10 cm Pb layer: $I_{\text{mod10}} \approx 8.45\text{e-}3 \cdot 3.390\text{e}3 \approx 28.7$ (counts/900 sec) ≈ 0.032 (counts/sec).

The resulting count rate estimations of the 3.577 MeV Y-95 lines are primarily affected by the (1) interrogating source strength; (2) detector geometry efficiency; and (3) thickness of attenuating filters. By adjusting any of these parameters in the above calculation, the relative effect on the signature intensity can be analyzed. Assuming the constant geometry, the effect of the neutron source strength and attenuation can be estimated as shown in Table 5.4. For a comparison of the estimated values in this table, Section 5.4 will show that the detailed calculation using the four-step modeling process resulted in a count rate of 14 counts/s for the case of a 6 cm thick lead filter and a 1e12 n/s interrogating source.

Table 5.4. Estimated detected count rate of the 3.577 MeV Y-95 delayed gamma-ray line (counts/sec).

Neutron source strength, n/s	**Thickness of the Pb attenuating filter, cm**		
	0	**5**	**10**
1e10	3.77	0.35	0.032
1e11	37.7	3.5	0.32
1e12	377	35	3.2

5.3.2 Passive Background Rate Estimation

The detector count rate is the primary limitation in the design of the delayed gamma-ray assay instrument. It is necessary to establish a balance between the intensity of the interrogating neutron source and the amount of attenuation in front of the detector, assuming that the detector geometry remains unchanged. As demonstrated above, the count rate of the delayed gamma-ray lines is effectively controlled by the source strength, and the attenuating filter is required in order to reduce the parasitic count rate from the low-energy passive background. This background is comprised of photon emissions from long-lived fission products and decay chains present in the spent nuclear fuel, and can be orders of magnitude higher in intensity than the induced gamma-ray lines. However, since the passive emissions are primarily below 2 MeV, their detector contribution can be effectively mitigated with the attenuating filters.

In order to estimate the detector count rate from the background emissions and the optimal amount of attenuation, assume the most prominent spent nuclear fuel passive signature – 661.7 keV gamma-ray line from Ba-137m in secular equilibrium with the Cs-137 fission product. The approximate analytical estimation follows the calculation scheme shown in Figure 5.5, for the same assembly setup parameters as before.

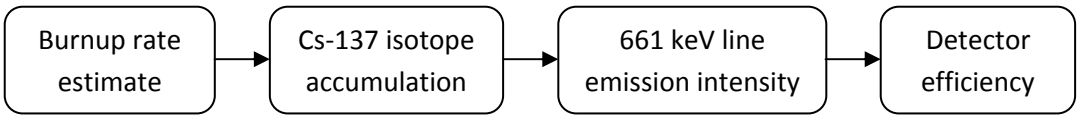

Figure 5.5. Calculation sequence for the passive background peak count rate.

Assume, on average, the amount of energy released per fission in the fuel during the reactor campaign to be 207 MeV. Cs-137 is produced in a reactor as a direct result of the fissions and as a decay daughter of the Xe-137 fission product with an assumed cumulative fission yield of 0.06 [22]. Its decay during the reactor campaign is disregarded. Then, for the 45 GWd/t (thermal) spent fuel burnup, the amount of Cs-137 atoms per ton of heavy metal is calculated as:

$$N(Cs137) = \frac{Burnup(Wd/t) \cdot time(s)/1.602e\text{-}19(eV/J)}{E_{fiss}(eV)} \cdot yield \tag{5.12}$$

$$N(Cs137) \approx \frac{45e9 \cdot 24 \cdot 3600/1.602e\text{-}19}{207e6} \cdot 0.06 \approx 7.035e24 \text{ (atoms/tU).}$$

Then, the specific activity of 661.7 keV gamma-ray emissions with Cs-137 decay branching ratio *B.R.* = 0.851 can be calculated as:

$$A(661.7) = B.R. \cdot \lambda \cdot N(Cs137) = B.R. \cdot \frac{\ln(2)}{T_{1/2}} \cdot N(Cs137). \tag{5.13}$$

$$A(661.7) \approx 0.851 \cdot \frac{\ln(2)}{30.07 * 365.25 * 24 * 3600} \cdot 7.035e24 \approx 5.14e15 \text{ (emissions/tU-s).}$$

Using the volume of a 1 cm section of the fuel pin as V_{pin} = 0.528 cm^3, fuel density ρ = 10.45 g/cm^3, and $w = 0.88$ weight fraction of uranium in UO_2, the heavy metal load in this volume is:

$$m(U) = w \cdot \rho \cdot V_{pin} \tag{5.14}$$

$$m(U) \approx 0.88 \cdot 10.45 \cdot 0.528 \approx 4.86 \text{ (g)} \approx 4.86e\text{-}6 \text{ (t).}$$

Then, the amount of total 661.7 keV emissions from the 1 cm segment of a single fuel pin is:

$$I_{tot}(661.7) = A(661.7) \cdot m(U) \tag{5.15}$$

$$I_{pin}(661.7) \approx 5.14e15 \cdot 4.86e\text{-}6 \approx 2.5e10 \text{ (emissions/s).}$$

The self-attenuation of the 661.7 photons in the nuclear fuel cannot be disregarded. Using the mass attenuation coefficients for U: μ/ρ = 0.1344 cm^2/g,

and O: μ/ρ = 7.77e-2 cm^2/g at this energy [59], the mass attenuation coefficient for the uranium dioxide matrix with ρ = 10.45 g/cm^3 can be calculated as:

$$\mu/\rho(UO_2) = w_U \cdot \mu/\rho(U) + \mu/\rho(O) = 0.88 \cdot 0.1344 + 0.12 \cdot 7.77\text{e-}2 = 0.128 \text{ (cm}^2\text{/g)}$$

$$\mu(UO_2) = \mu/\rho(UO_2) \cdot \rho = 0.128 \cdot 10.45 = 1.338 \text{ (1/cm).}$$

Then, the mean free path of the 661.7 photons in the spent fuel material can be obtained:

$$mfp(661.7) = \frac{1}{\mu(UO_2)} = \frac{1}{1.338} = 0.75 \text{ (cm).}$$

This value as well as the literature data suggest that 661.7 keV emissions coming from the very periphery of the assembly are contributing to the detector. According to semi-empirical results in [60], approximately 92% of the 661.7 keV signal collected with the HPGe detector originates in the outer three rows of pins. Using this value along with the slot collimator efficiency calculated above, the 661.7 keV photon count rate in the detector can be estimated as:

$$I_{tot} = \#pins \cdot \omega \cdot I_{pin} \approx (3 \cdot 17) \cdot 4.775\text{e-}5 \cdot 2.5\text{e}10 \approx 6.088\text{e}7 \text{ (photons/s)}$$

The interaction probability in a 5 cm Ge detector layer can be calculated for μ/ρ = 7.14e-2 cm^2/g at 661.7 keV and a peak-to-total ratio $r \approx 1/3$.

$$\varepsilon(Ge) = r \cdot \left(1 - \exp\left(-\mu/\rho \cdot \rho \cdot thickness\right)\right) \approx r \cdot \left(1 - \exp(-7.14\text{e-}2 \cdot 5.32 \cdot 5)\right) \approx 0.28.$$

Then the count rate of the 661.7 keV photons in the detector geometry without attenuating filters is:

$$I_{\det} = I_{tot} \cdot \varepsilon(Ge) \approx 6.088\text{e}7 \cdot 0.28 \approx 1.705\text{e}7 \text{ (counts/s).}$$

The effect of the Pb attenuating filters is calculated assuming μ/ρ = 0.1173 cm^2/g at 661.7 keV:

$$a(Pb) = \exp\left(-\mu/\rho \cdot \rho \cdot thickness\right). \tag{5.16}$$

For a 5 cm Pb layer: $a(5cm) \approx \exp(-0.1173 \cdot 11.34 \cdot 5) \approx$ 1.586e-3.
For a 10 cm Pb layer: $a(10cm) \approx \exp(-0.1173 \cdot 11.34 \cdot 10) \approx$ 2.5e-6.

Applied to the above number of counts, these attenuation coefficients provide modified count rates:

$$I_{\text{mod}} = a(Pb) \cdot I_{\text{det}} \tag{5.17}$$

For a 5 cm Pb layer: $I_{\text{mod}5} \approx 1.586\text{e-}3 \cdot 1.705\text{e}7 \approx 2.704\text{e}4$ (counts/sec).
For a 10 cm Pb layer: $I_{\text{mod}10} \approx 2.5\text{e-}6 \cdot 5.68\text{e}7 \approx 43$ (counts/sec).

The calculated count rates of the 661.7 keV line are sensitive to the thickness of the attenuating filters; however, this effect is lower for the photons emitted at higher energies. Although most of the intense background lines can be mitigated, it is possible that the total integrated passive count rate may be several times higher and approach the dead time limit of the HPGe detector.

The above estimations demonstrate that a number of delayed gamma-ray assay variables can be balanced to make the analysis practical and to target signatures retrievable with accuracy sufficient for the qualitative and quantitative analysis. Attenuating filters affect both the passive and delayed gamma-ray signals and have proven to be most effective in reducing the count rates from photons below 1 MeV. For the optimization process, two design limits of primary importance can be established:

- The average count rate in each of the isolated delayed gamma-ray peaks nominated for analysis should be no less than 1 count-per-second during

the spectrum acquisition period. In this case, statistically accurate peak areas can be determined during the sufficiently long detection time (900 seconds).

- The total detector count rate should be at the order of 1e5 counts-per-second for HPGe systems in order to avoid dead time, pile-up, and other effects detrimental to the resulting spectrum structure.

It is plausible that in a carefully designed setup, the above conditions can be satisfied for the neutron source strength of 1e11 neutrons per second assuming 900 seconds interrogation time. The non-optimized system assumed at this stage, indicates that a 1e12 neutrons per second generator operating for 900 seconds of interrogation time with 5 to 10 cm of lead attenuating filter will perform adequately. Given the count rate estimations provided by Equation 5.17, up to 10 cm of lead may be needed to keep the count rate at a tolerable level. As is indicated in Table 5.4, such a system would produce 3.2 counts/s in the 3.577 MeV Y-95 peak. A sufficiently strong source is required to overcome self-shielding limitations, low collimation efficiencies, and attenuation filters. Depending on the measurement constraints, increasing the interrogation time may be an option for improving the results. The efficiency of collecting the delayed gamma-ray signal can also be improved by increasing the number and type of detectors in the acquisition setup. In some cases, detector systems with faster response and higher dead time limits may also be an option.

5.4 Modeling Results

The high-fidelity delayed gamma-ray responses were calculated using the four-step modeling algorithm for a number of assemblies with simplified material inventories, as well as for several assemblies from spent nuclear fuel libraries #1 and #2. Only a subset of simulation results is included in this dissertation with more data provided in dedicated reports [61,62].

The assay geometry with the slot collimator was adopted following the analytical parametric study. Although not optimal, this setup configuration provides the total calculated count rate close to the detector limit of 1e5 counts per second, and sufficiently strong delayed gamma-ray lines. The exact model setup layout is shown in Figure 5.4, with the following parameters:

- Neutron source configuration and coupling with the assembly – as in the delayed neutron and differential die-away NGSI designs. Base case source intensity is 1e12 neutrons per second.

- Collimator slot opening on the fuel side – 21.4x2 cm, subtending the full width of the assembly; opening on the detector side – 3x2 cm.

- Thickness of the lead attenuating filters on the assembly side – 5 cm; on the detector side – 1 cm.

- Detector response is calculated for the 130% efficiency HPGe crystal, with resolution and energy broadening effects obtained from a real detector.

All simulations assume the base case assay time pattern: 900 seconds of interrogation, a 60 second cool-down period, and 900 live seconds of delayed gamma-ray spectrum acquisition time.

The results of spent nuclear fuel passive background spectrometry measurements in a similar setup were recently published by the CEA research group in France [63]. This work demonstrates a newly developed and deployed measurement station for high-count rate gamma-ray spectroscopy of spent nuclear fuel assemblies at the La Hague reprocessing plant. The system provides accurate gamma-ray spectra acquired at the event rate of several MHz using off-the-shelf HPGe detectors, with innovative signal processing electronics allowing for dynamic dead-time correction. An adaptive processing algorithm prevents resolution degradation with increased count rate resulting in accurate spectra for both quantitative and qualitative analysis. The configuration of the detector setup of this system is similar to the conceptual design of the delayed gamma-ray assay

system presented in this dissertation. Both systems are using a slot collimator converging on some fraction of a HPGe crystal surface area. Because of the focus on lower-energy passive peaks, the CEA setup is using collimators with an adjustable aperture rather than attenuating filters. A built-in calibration source introduced during measurements is used to calibrate the instrument for the changing collimation efficiency. The layout and operational results of the CEA system can be used to proof the concept of the active assay instrument design developed in this dissertation.

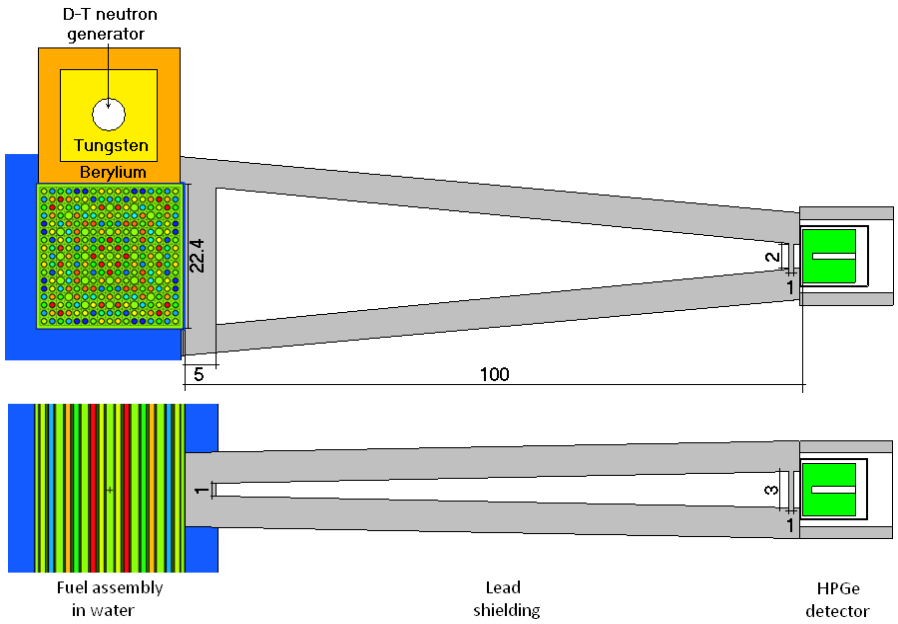

Figure 5.4. Assay setup layout adopted for high-fidelity delayed gamma-ray response modeling.

The delayed gamma-ray responses in each simulation case are obtained in the form of a calculated total spectrum acquired with the detector, along with individual partial contributions from four actinides undergoing fission: U-235, U-238, Pu-239, and Pu-241. In some cases, to save on the computation time, the resulting spectra were limited to the energy region above 2.5 or 3.0 MeV. As previously demonstrated, the passive continuum for the spent fuel library

assemblies above this threshold energy is negligible, and therefore was in some cases omitted from the results.

The calculated spectra were analyzed using originally developed scripts coupled with the four-step modeling algorithm and, in some cases, by transferring them to the ORTEC Maestro interactive peak analysis program. For each spectrum, select peak areas were extracted and observed peak ratios were calculated. Primary contributing gamma-ray lines for each peak area were identified from the discrete gamma-ray emission spectrum obtained in the 3rd step of the modeling algorithm.

Figure 5.5 (top) demonstrates the difference in passive and delayed gamma-ray responses between spent fuel libraries #1 and #2 calculated for the 45 GWd/t burnup, 4% initial enrichment, 5 years cooling time assembly. Figure 5.5 (bottom) also depicts an activated emission spectrum with a delayed gamma-ray component, for the assembly with the inventory of library #2. The top figure shows an overlay of two pairs of passive and activated spectra obtained for the assembly inventories from the two libraries. Deficiency in the passive spectrum calculated for the inventory of library #1 is clearly visible in the energy region between 1.5 and 3.5 MeV. In both activated spectra, the delayed gamma-ray response is considerably higher than the passive continuum in the energy range above 3 MeV. Therefore, delayed gamma-ray lines can be expected to be a dominating feature of the detected spectrum at high energies, with intensities proportional to the active source strength, as well as lengths of interrogation and detection periods. This observation is consistent with empirical results demonstrated in [19], and is illustrated in Figure 5.6. In the experiment performed at the Paul Scherrer Institute (Switzerland), a spent nuclear fuel pin was subject to neutron irradiation in a zero-power research reactor, with neutron flux estimated at 4e9 neutrons/($cm^{-2}s^{-1}$), and high-resolution spectra collected before and after irradiation. A comparison of these spectra demonstrates that the high-energy background is driven by activation from the interrogating source and that interference from the passive component is negligible.

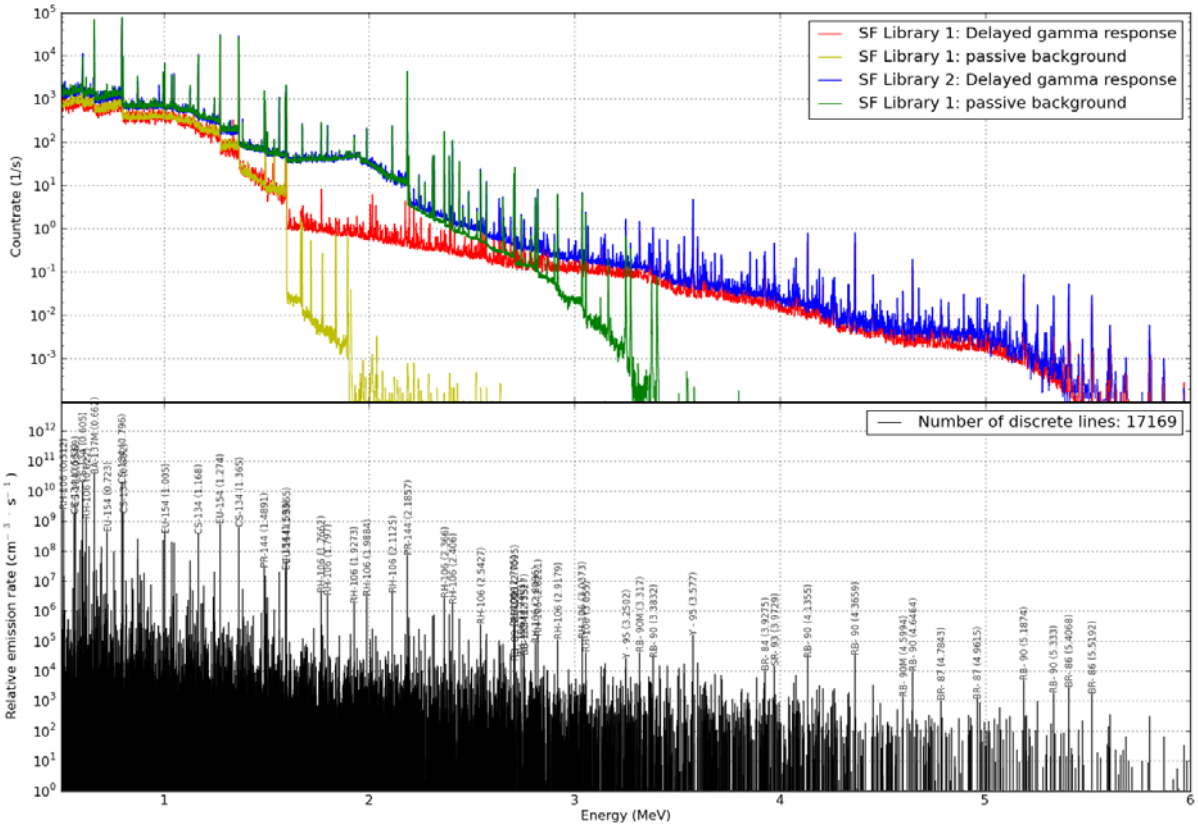

Figure 5.5. Calculated passive and activated HPGe spectra for the assembly from spent nuclear fuel library #1 and #2 with 45 GWd/t burnup, 4% initial enrichment, and 5 years cooling time (top). Calculated delayed gamma-ray emission spectrum for the same assembly from library #2 (bottom).

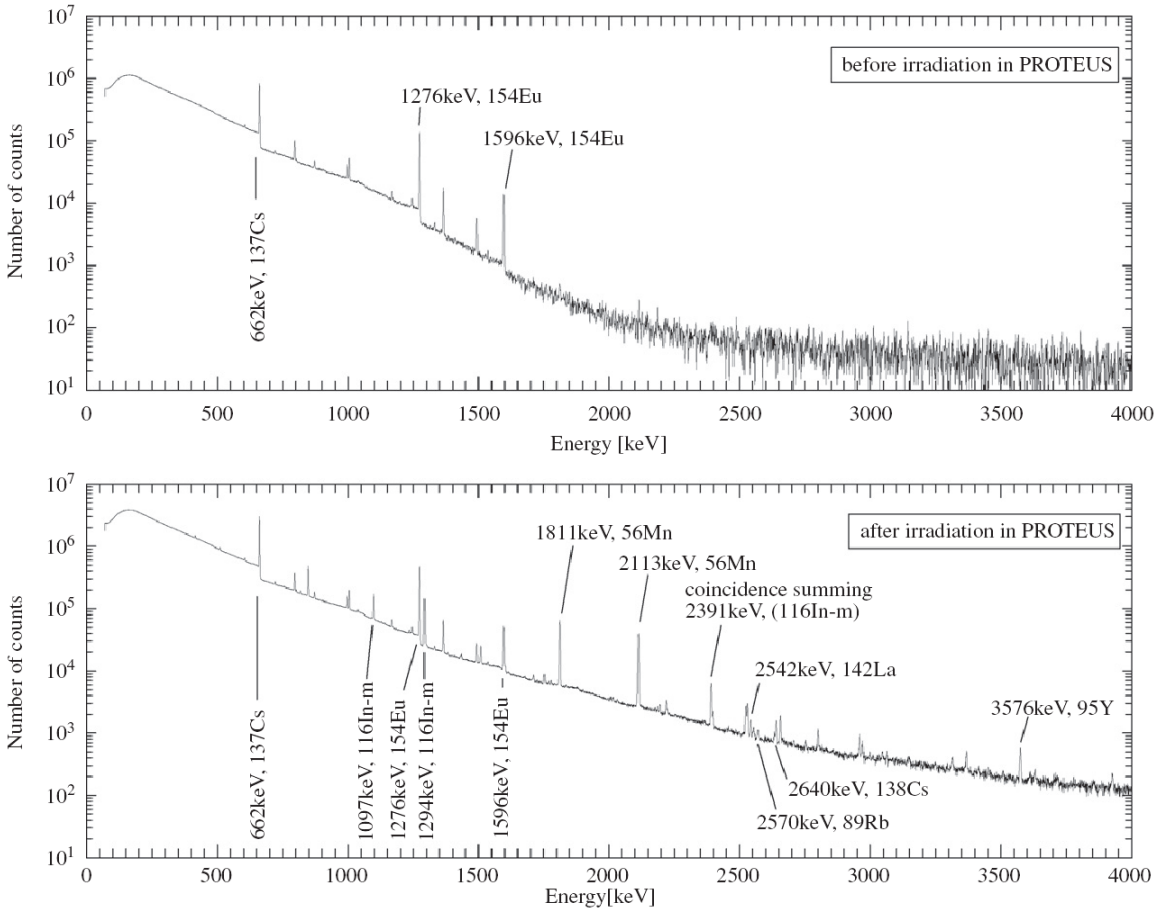

Figure 5.6. Gamma-ray spectra detected from a 36 GWd/t spent nuclear fuel pin before (top), and after 15-min irradiation period in a research reactor (both spectra are acquired on a zero-dead time HPGe system and are scaled to 6 hours acquisition time) [19].

The effects of collimation and attenuation in the detector setup were investigated by modeling a response from the same assembly with and without the acquisition setup around the detector. Simulations were accomplished for the inventory of library #1 for 45 GWd/t burnup, 4% initial enrichment, 5 years cooling time fuel assembly submerged in water and interrogated with the moderated 14.1 MeV neutron source with an intensity of 1e12 n/s. Two series of calculations were performed for the same 130% relative efficiency HPGe detector with an assumed

unconstrained count rate limit: (1) for an unshielded detector 5 cm away from the assembly, and (2) for a 1 m-long collimator converging on a front detector face of 6 cm^2. Two lead attenuating filters are used: 5 cm on the fuel side and 1 cm on the detector side of the collimator.

Figure 5.7 compares the resulting calculated spectra with partial contributions from the primary actinides in the fuel inventory and count rates. For the case of the unshielded detector, the total estimated count rate on the detector reaches 8e10 counts per second. The 661.7 keV peak area is 8.6e9 counts/s, and the 3.577 MeV peak area is 1.8e4 counts/s. In the case of the shielded detector, the total calculated count rate on the detector is 1.76e6 counts/s, including a passive only count rate at 1.32e6 counts/s. The 661.7 keV peak area is 5.46e4 counts/s, the 3.577 MeV Y-95 delayed gamma-ray peak area is 14 counts/s. Since the modeled setup is somewhat different, it was not expected that the simulated data would match the approximate estimations obtained in the previous section and shown in Table 5.4.

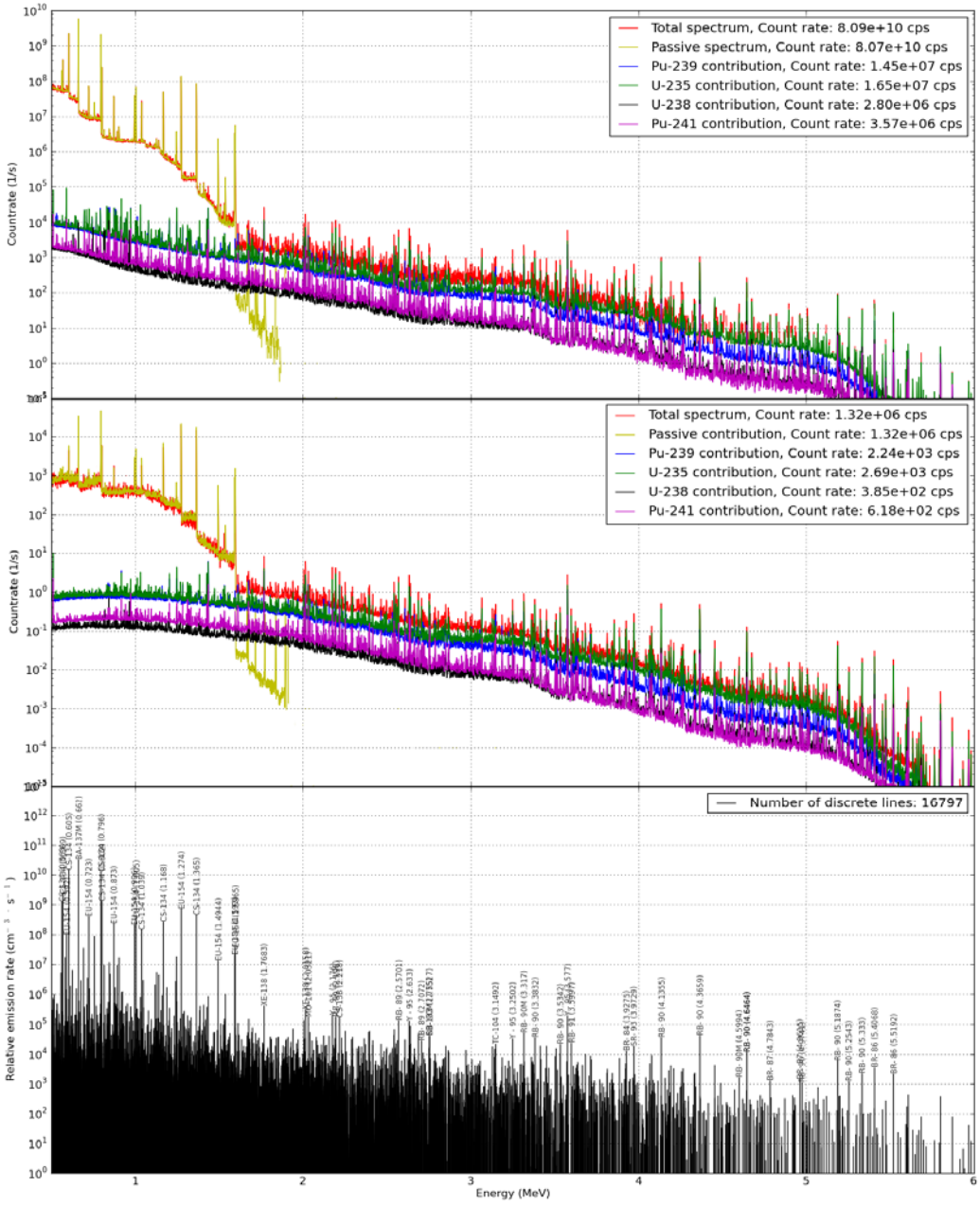

Figure 5.7. Simulated effect of the collimator and attenuating filters on the detector response for library #1 assembly with 45 GWD/t, 4 % initial enrichment, 5 years cooling time. Unshielded detector in the immediate vicinity of the assembly (top), slot collimator and 6 cm-thick lead attenuating filters (middle), and delayed gamma-ray emission spectrum (bottom).

The effects of the individual actinides in the spent fuel inventory were investigated using a set of assemblies with a simplified isotopic inventory. Figure 5.8 shows an example of the modeling results obtained for a UO_2 fuel material with 2.5 weight percent of U-235, 2.5 weight percent of Pu-239, and 0.5 weight percent of Pu-241. Spectra in this figure were generated to indicate the relative strengths of U-235 as compared with Pu-239 (note that the mass of Pu in this example is high relative to what would be expected for an end-of-life assembly). The calculated total spectrum demonstrates a considerable number of individual delayed gamma-ray peaks in the region above 3 MeV. Similar calculations were accomplished for a number of cases with inventories of the four actinides varied within ranges typical for the spent nuclear fuel. Automated processing of the resulting spectra was performed by extracting total and partial peak areas and analyzing peak ratios in various combinations.

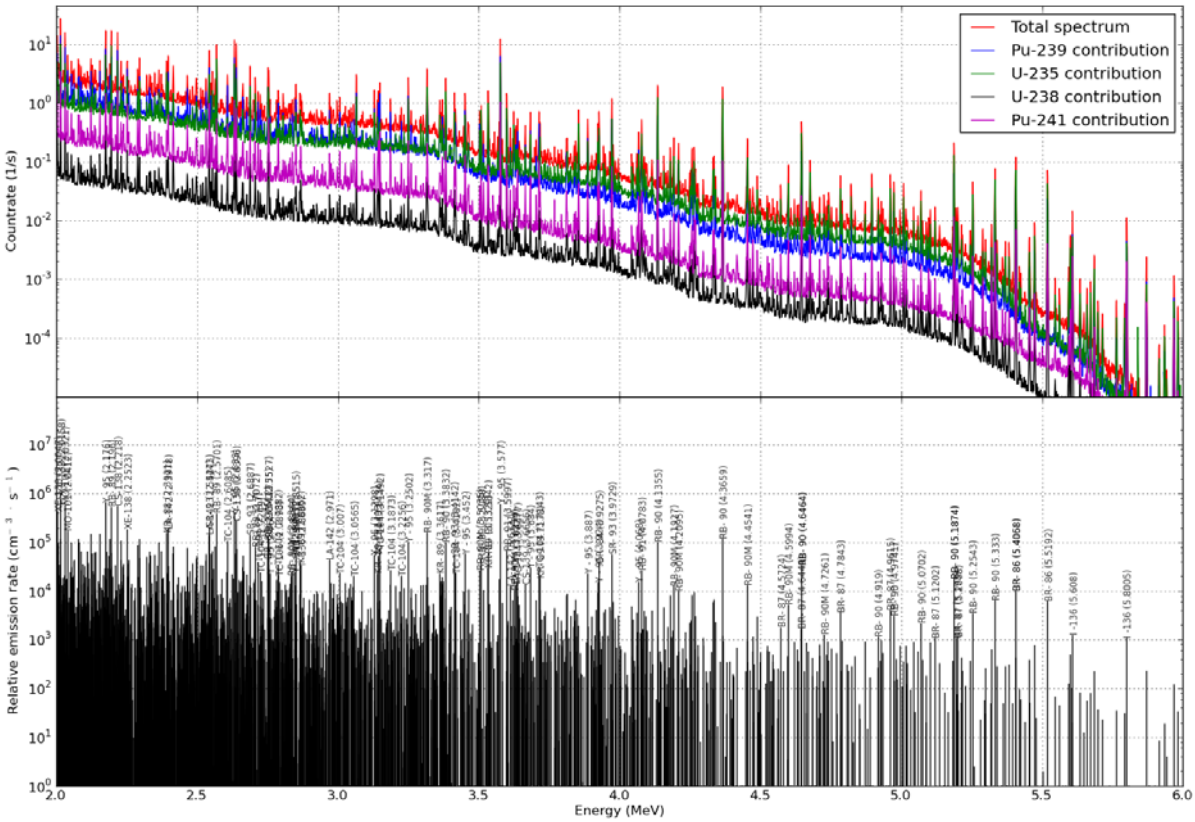

Figure 5.8. Delayed gamma-ray modeling results for the simplified assembly inventory.

A detailed analysis of the peaks and individual actinide contributions in these spectra demonstrates a high variability in delayed gamma-ray responses between the isotopes of U-235 and Pu-239. Although the integrated thermal fission cross-section for Pu-239 is higher than the cross-section for U-235, at the same isotopic content the delayed gamma-ray response of U-235 is more intense in the energy region between 3.5 and 5.5 MeV. This effect is a direct consequence of the higher U-235 thermal yields of fission products with $85 < A < 95$ (as shown earlier in Figures 2.4 and 2.9), dominating this part of the spectrum. As expected, relative intensities of the delayed gamma-ray peaks from Pu-239, U-238, and Pu-241 are mostly correlated in energy; however, several characteristic peaks for each of these isotopes were also identified. An abridged list of the most intense delayed gamma-ray peaks predicted in the energy region between 2.5 and 4.5 MeV is

shown in Table 5.5. An example of a typical automated data processing algorithm for the delayed gamma-ray response from Figure 5.8 is shown in Table 5.6. This table demonstrates some of the delayed gamma-ray peak areas extracted from the total calculated spectrum, along with the peak area fractions observed due to the presence of the four primary actinides. The actinide-specific peak area fractions were determined as a ratio between peak areas in the separately calculated individual and total delayed gamma-ray spectrum. Within the peak fitting uncertainty, the fractional contributions add up to the total peak area and directly quantify the importance of each actinide isotope in the detected delayed gamma-ray signature. The determination of such isotopic contributions to the peaks observed in the total spectrum comprises one of the objectives of the delayed gamma-ray response analysis discussed in Chapter 6.

Table 5.5. Selected peaks in simulated delayed gamma-ray spectrum for HPGe detector resolution.

Peak Position, MeV	**Primary contributing delayed gamma-ray emissions**	**Actinide response indicator**
2.532	Tc-104 (2.5329), Cs-139 (2.5318)	Pu-239
2.545	La-142 (2.5427), Sr-93 (2.5443), Tc-104 (2.5443), Te-133 (2.5418), Nb-99m(2.5437)	Pu-241
2.570	Rb-89 (2.5701)	U-235, U-238
2.608	Tc-104 (2.6085), Cs-139 (2.6057)	Pu-241
2.633	Y-95 (2.633), I-136 (2.6342)	
2.640	Cs-138 (2.6396), Nb-99m (2.6413)	
2.689	Sr-93 (2.6887)	
2.753	Rb-90m (2.7527), Sb-133 (2.755), Br-86 (2.7512)	U-238
3.149	Tc-104 (3.1492), Rb-90 (3.1486), Rb-91 (3.1473)	Pu-239, Pu-241
3.250	Y-95 (3.2502), Cs-140 (3.2491)	
3.317	Rb-90m + Rb-90 (3.317), Tc-104 (3.3187), Y-94 (3.3187), Kr-89 (3.3179)	Pu-241, U-238
3.383	Rb-90m + Rb-90 (3.3832)	U-238
3.577	Y-95 (3.577)	
4.135	Rb-90 (4.1355)	U-238
4.365	Rb-90 (4.3659)	U-238

Table 5.6. Script-generated simulated spectrum processing result.

Peak Position, MeV	Net area, counts/s	Fraction of the peak count rate due to actinide-specific response				Sum of the fractional contributions
		Pu-239	U-235	U-238	Pu-241	
2.177	41.69 ± 3.10	0.50 ± 0.00	0.41 ± 0.00	0.02 ± 0.00	0.09 ± 0.00	1.02 ± 0.01
2.196	36.57 ± 1.65	0.36 ± 0.01	0.56 ± 0.00	0.02 ± 0.01	0.06 ± 0.00	1.00 ± 0.01
2.218	37.66 ± 2.79	0.51 ± 0.00	0.32 ± 0.00	0.02 ± 0.00	0.10 ± 0.00	0.97 ± 0.01
2.253	15.76 ± 1.30	0.46 ± 0.01	0.33 ± 0.01	0.02 ± 0.00	0.20 ± 0.01	1.01 ± 0.02
2.289	7.09 ± 0.56	0.41 ± 0.05	0.38 ± 0.01	0.04 ± 0.00	0.16 ± 0.01	0.99 ± 0.04
2.392	11.69 ± 1.36	0.36 ± 0.01	0.58 ± 0.01	0.02 ± 0.00	0.06 ± 0.00	1.02 ± 0.01
2.416	6.59 ± 0.21	0.40 ± 0.01	0.43 ± 0.01	0.04 ± 0.01	0.15 ± 0.01	1.01 ± 0.02
2.532	3.41 ± 0.54	0.51 ± 0.03	0.37 ± 0.04	0.02 ± 0.01	0.12 ± 0.01	1.02 ± 0.02
2.545	16.95 ± 0.97	0.54 ± 0.00	0.39 ± 0.01	0.02 ± 0.00	0.09 ± 0.00	1.04 ± 0.02
2.570	26.29 ± 2.19	0.36 ± 0.00	0.56 ± 0.00	0.03 ± 0.01	0.05 ± 0.00	1.00 ± 0.00
2.608	7.42 ± 1.36	0.67 ± 0.02	0.21 ± 0.01	0.02 ± 0.01	0.16 ± 0.04	1.05 ± 0.03
2.633	27.40 ± 1.35	0.50 ± 0.03	0.40 ± 0.00	0.02 ± 0.00	0.09 ± 0.00	1.00 ± 0.03
2.640	18.53 ± 1.09	0.53 ± 0.00	0.34 ± 0.01	0.02 ± 0.00	0.11 ± 0.00	1.00 ± 0.01
2.689	9.81 ± 1.07	0.45 ± 0.01	0.46 ± 0.01	0.02 ± 0.00	0.08 ± 0.01	1.01 ± 0.02
2.753	8.94 ± 0.45	0.46 ± 0.01	0.47 ± 0.00	0.01 ± 0.00	0.05 ± 0.01	1.00 ± 0.01
3.149	5.21 ± 0.49	0.67 ± 0.01	0.15 ± 0.01	0.02 ± 0.01	0.16 ± 0.01	0.99 ± 0.02
3.250	6.77 ± 0.18	0.50 ± 0.01	0.41 ± 0.00	0.02 ± 0.00	0.08 ± 0.00	1.01 ± 0.01
3.317	10.61 ± 0.46	0.46 ± 0.01	0.48 ± 0.00	0.01 ± 0.00	0.05 ± 0.00	1.01 ± 0.02
3.383	6.91 ± 0.19	0.32 ± 0.01	0.60 ± 0.00	0.02 ± 0.00	0.06 ± 0.00	1.00 ± 0.01
3.577	36.50 ± 0.68	0.51 ± 0.00	0.40 ± 0.00	0.02 ± 0.00	0.08 ± 0.00	1.01 ± 0.00
4.135	6.13 ± 0.04	0.30 ± 0.00	0.62 ± 0.00	0.02 ± 0.00	0.05 ± 0.01	1.00 ± 0.01
4.365	6.29 ± 0.25	0.30 ± 0.02	0.61 ± 0.01	0.02 ± 0.00	0.05 ± 0.01	0.99 ± 0.03

As a part of the preliminary setup optimization studies, delayed gamma-ray modeling technique capabilities were used to investigate the spatial dependence of the response from a spent fuel assembly. Calculations of the delayed gamma-ray response were performed for the assembly with the inventory of spent fuel library #2 for 45 GWd/t burnup, 4% initial enrichment, and 5 years cooling time. An integrated delayed gamma-ray count rate in the energy region between 3 and 4.5 MeV was obtained for various zones of pins identified in the assembly lattice. Spatial contributions were then expressed as a percent fraction to the total

integrated delayed gamma-ray response count rate in the same energy region obtained from the whole assembly.

Figure 5.9 (top) shows spatial contributions to the total detected delayed gamma-ray count rate from rows of pins in the 17 x 17 assembly lattice located relative to the location in front of the slot collimator. Approximately 64% of the integrated count rate between 3 and 4.5 MeV originates in the four rows of pins closest to the collimator. This is explained by the higher geometrical efficiency of the detector to the outer pins and smaller self-attenuation of the delayed gamma-ray signal in the fuel material. The bottom part of the figure demonstrates corresponding delayed gamma-ray spectra calculated for this case.

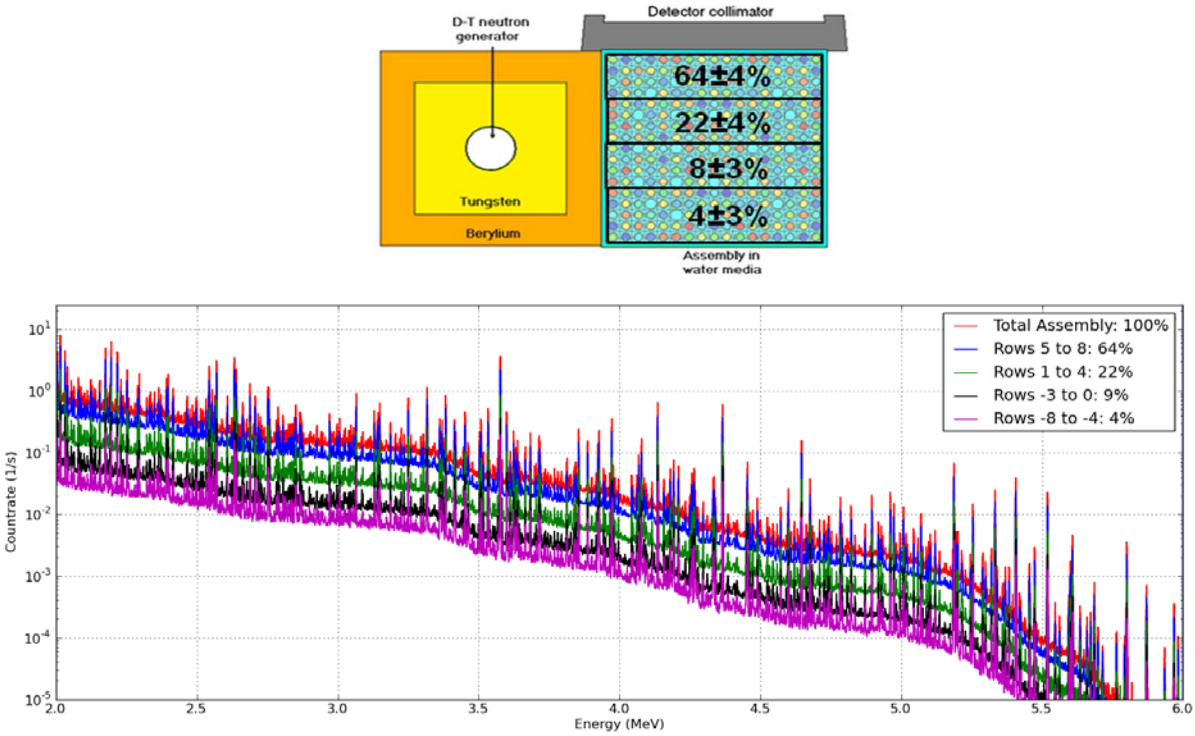

Figure 5.9. Spatial contributions to the integrated delayed gamma-ray response between 3 and 4.5 MeV from the assembly pin rows (top). Corresponding delayed gamma-ray spectra (bottom).

Figure 5.10 (top) shows a similar estimation of spatial contributions calculated for the quadrants identified in the 17 x 17 assembly lattice. The quadrant that is closest to the neutron generator and the detector collimator contributes approximately 60% of the integrated delayed gamma-ray response count rate between 3 and 4.5 MeV. This effect results from a higher geometric efficiency to the pins in this quadrant, both for the detector and the interrogating neutron source. Corresponding delayed gamma-ray spectra can be seen at the bottom of the figure.

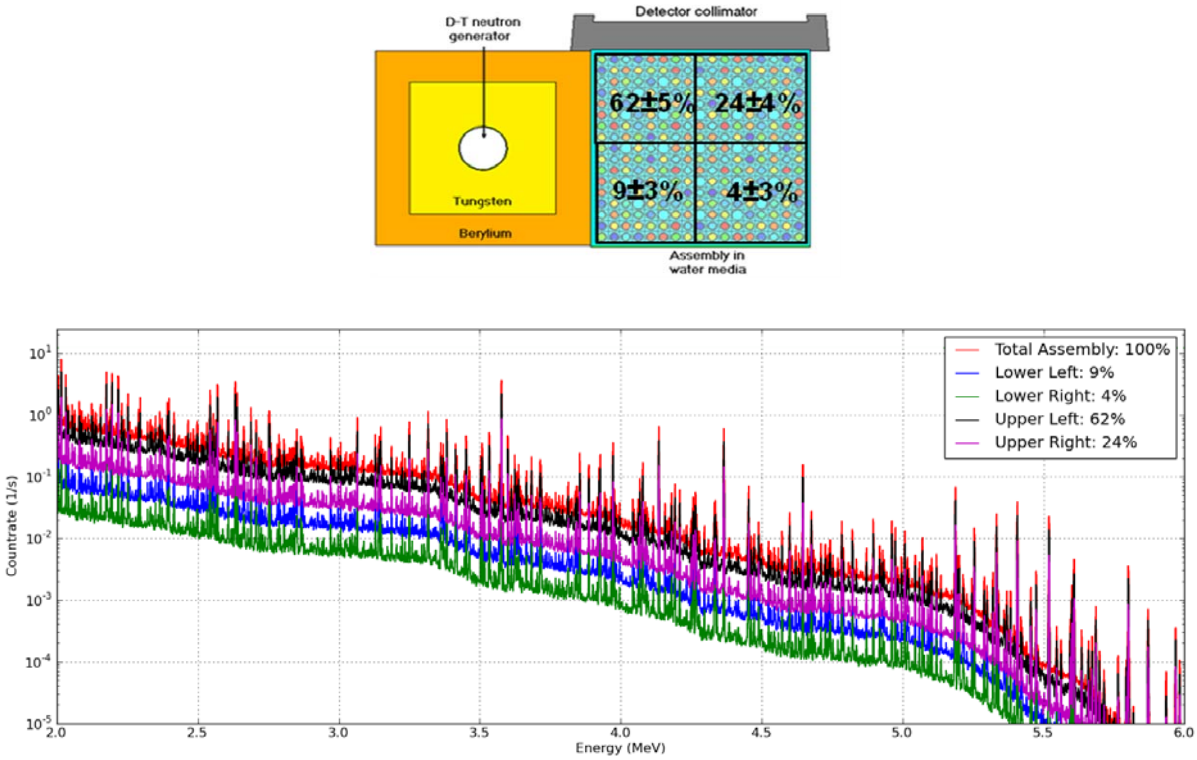

Figure 5.10. Spatial contributions to the integrated delayed gamma-ray response between 3 and 4.5 MeV from the assembly quadrants (top). Corresponding delayed gamma-ray spectra (bottom).

The effect of the spatial non-uniformity of the delayed gamma-ray response during spent nuclear fuel assembly interrogation should be considered in the further optimization studies of the assay setup. In real spent fuel assemblies,

isotopic concentrations vary considerably in axial and planar directions because of the asymmetric burnup during the reactor irradiation. The delayed gamma-ray instrument can be sensitive to these distributions, and therefore assay results can be different for the same assembly depending on its position relative to the irradiating source and the detector. Optimally, the efficiency of both source and detector coupling with the assembly should be increased to assay more pins in a single measurement. The simplest solution would be to introduce a second detector system on the side of the assembly opposite to the existing collimator. In this case, a combined signal from the two detector systems would provide a more uniform signal from the assembly, although pins in the center would still experience considerable shielding and signal attenuation. This could be partially addressed by bringing the interrogating source closer to the assembly side, and achieving higher neutron fluxes in the center pins. The combined effect of such modifications is still unclear, and the limits of the assay setup optimization will need to be the subject of further research.

As a part of the preliminary analysis of the delayed gamma-ray instrument, the ability to detect partial defects such as missing or replaced pins was investigated. One of the assumed scenarios considered substituting 24 pins from different locations in the 17 x 17 assembly lattice (center, mid-section, periphery) with pins containing depleted uranium consisting of 0.2 wt.% U-235. Delayed gamma-ray response modeling was performed for the assembly inventory from spent fuel library #2 with 45 GWd/t burnup, 4% initial enrichment, and 5 years cooling time. The results of the diversion simulations for the three cases is shown in Figure 5.11 indicating the diversion layout and the integrated delayed gamma-ray signal count rate between 3 and 4.5 MeV as a percent of the signal in the case of the original assembly.

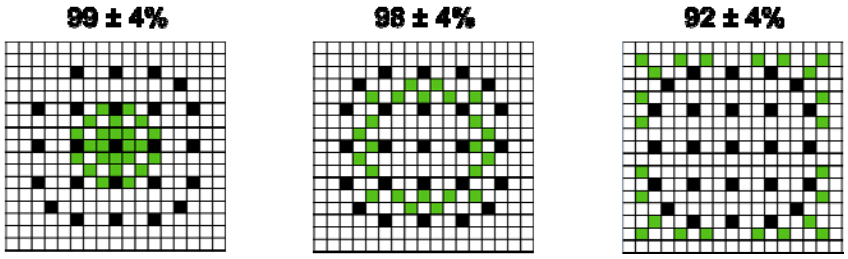

Figure 5.11. 24-pin diversion case layouts and change in the integrated delayed gamma-ray count rate between 3 and 4.5 MeV compared to the original assembly.

In the delayed gamma-ray assay, replacing a spent fuel pin with depleted uranium reduces the amount of fissile isotopes, and proportionally the magnitude of the activated signal. However, this effect is not linearly reflected in the detected response because of the non-linear spatial sensitivity of the assay setup discussed previously. In the present configuration of the instrument, only diversion from the pin rows closest to the detector can be determined with high confidence. Presently, the IAEA establishes the detection limit for partial defects as "at least half of the pins replaced or missing from the assembly" [5]. Despite this high level, the sensitivity to smaller diversions will become an important criterion in the further investigation of the delayed gamma-ray assay system.

Chapter 6

Delayed Gamma-Ray Response Analysis

6.1 Preliminary Considerations

As long as the delayed gamma-ray signatures can be confidently isolated and extracted under real assay conditions, multiple options for qualitative and quantitative analysis become available. The applicability of some techniques has been already demonstrated in the literature for simple materials and setups, and it is highly probable that similar principles can be successfully applied to spent nuclear fuel interrogation. By utilizing the four-step modeling algorithm capability to predict individual isotopic contributions to the detected peaks and energy regions of interest, a rigorous analysis approach can also be developed. Published experimental results and assay simulations performed for the NGSI spent fuel library demonstrate the ability of the delayed gamma-ray instrument to determine the total fissile content, fission rate, and both the relative and absolute fissile material quantities. The response analysis options that are discussed further in this chapter share the same inherent features of the delayed gamma-ray assay:

- *Direct signatures*. Analysis relies on actinide-specific fission fragment responses and does not require additional sample-specific inputs or previously defined parameter-space functions. As a result, high levels of precision are approached in some demonstration experiments.

- *Rigorous analysis*. All data manipulations, including the detected spectrum interpretation and subsequent computations, follow an exact calculation scheme that can be easily automated, without the need for manual control or input.

- *Simple calibration*. Only a few calibration measurements are required, primarily to experimentally determine the efficiency of the detector setup.

- *No background measurement*. For measurements of the relative sample characteristics, or in the event that the delayed gamma-ray energies of interest lie above interferences from the sample radioactivity, no pre-assay measurements are necessary. From the analysis of the passive spectra, no strong background peaks are expected above approximately 2 MeV. The background count rate decreases considerably for the assemblies with extended cooling time.

The analysis technique appropriate for the spent nuclear fuel assay that would account for the signal contributions of four isotopes: U-235, Pu-239, U-238, and Pu-241 is still being developed and only the initial findings are included in this chapter.

6.2 Total Fission Rate Methods

A simple and effective approach to total fissile content determination using the delayed gamma-ray assay can be derived from the discussion presented in [16]. The method is based on integrating the total number of photon counts in a wide high-energy interval, regardless of whether the events represent full or partial energy deposition. As demonstrated by the authors, because of the high density of the delayed gamma-ray lines in the detected spectra, a practical system based on this method does not require high-resolution detectors. The rate of delayed gamma-ray decay after interrogation is proposed as one of the assay signatures. Although the research presented in [16] was primarily qualitative, this method can be more quantitative and can be further extended to account for the contributions from several fissile isotopes and provide an accurate estimate of the total fissile content in spent fuel assemblies.

For this purpose the delayed gamma-ray assay response can be treated in a manner similar to the signals from the gross-counting neutron and photon detectors. The integrated photon counts collected in high-energy regions of the detected spectrum serve as a proportional signature of a total fissile rate in the assembly. In general, width and position of the energy region for the photon spectrum integration can be selected arbitrarily as long as they do not include the passive background interferences that obstruct the delayed gamma-ray signal.

The application of this response analysis approach was illustrated using the delayed gamma-ray response modeling technique and 11 assemblies from spent fuel library #1 with the total isotopic content of primary actinides shown in Table 6.1. Figure 6.1 depicts the numerical estimations of the gross delayed gamma-ray count rate between 3 and 4.5 MeV that was obtained by integrating the areas under each spectrum. Solid lines in this figure connect the count rate results obtained for assemblies with the same burnup, and varying initial enrichments. Individual contributions of the actinides to the total signal are shown in Table 6.2. The visible response distribution pattern, as well as its dynamic range is very similar to ones observed in other passive and active spent fuel assay instruments that are based on gross counts of the neutron or photon signatures. Although sensitivity to the fissile content is clearly demonstrated, there is no unique signature characterizing each individual inventory. Because of the non-linearity in the delayed gamma-ray response of the actinides, the same integrated counts value can correspond to a variety of inventories, depending on the relative concentrations of the contributing isotopes. This type of analysis is not self-sufficient and cannot be used without the preliminary knowledge of the assembly parameters, such as exact burnup and initial enrichment.

Table 6.1. Primary actinide content of the 11 spent fuel library #1 assemblies.

Assembly Parameters			Total isotope mass in the assembly, g			
Burnup, GWd/t	**Initial enrichment, %**	**Cooling time, years**	**U-235**	**Pu-239**	**Pu-241**	**U-238**
15	2	5	4,119.56	2,027.34	248.12	456,883
15	3	5	7,811.45	2,063.18	195.79	453,098
15	4	5	11,916.10	2,069.80	157.31	448,942
15	5	5	16,222.40	2,061.53	130.18	444,601
30	2	5	1,726.49	2,353.69	504.77	452,565
30	3	5	4,049.20	2,524.61	474.35	449,731
30	4	5	7,150.39	2,686.30	438.27	446,241
30	5	5	10,730.60	2,811.35	400.88	442,372
45	4	5	3,936.25	2,817.03	632.38	442,946
45	5	5	6,633.46	3,032.25	620.48	439,638
60	5	5	3,871.73	3,126.66	802.34	435,527

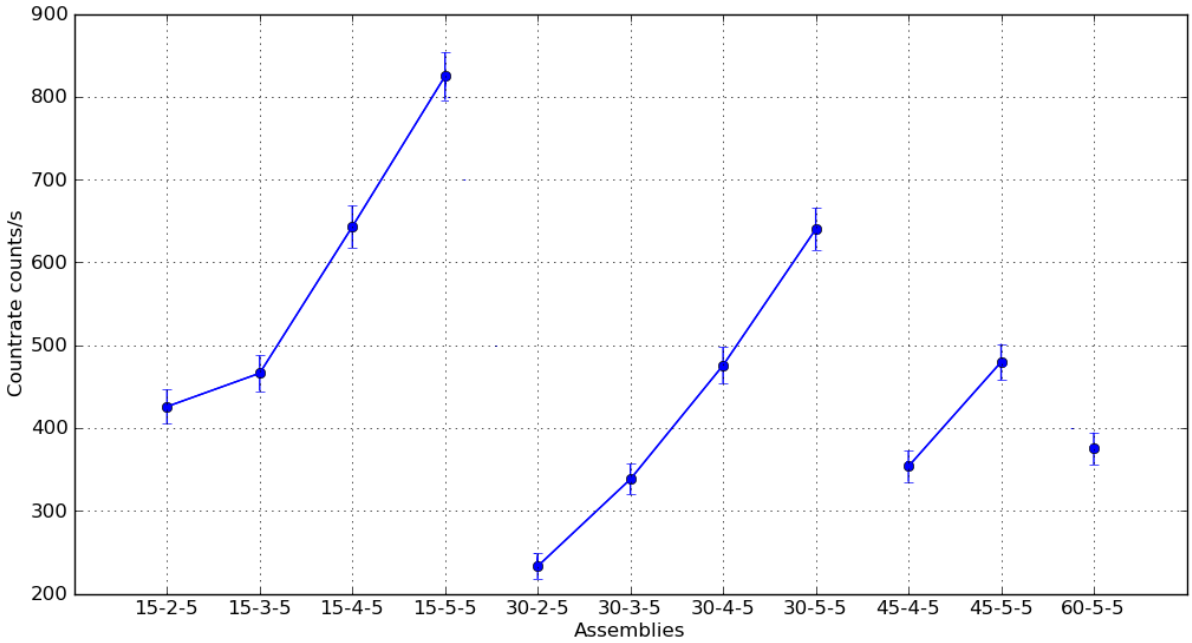

Figure 6.1. Integrated delayed gamma-ray count rates between 3.0 and 4.5 MeV for the 11 spent fuel library #1 assemblies.

Table 6.2. Isotope-specific contributions to the integrated delayed gamma-ray count rate between 3.0 and 4.5 MeV for the 11 spent fuel library #1 assemblies.

Library #1 assembly	Count rate contribution, %			
	U-235	Pu-239	Pu-241	U-238
15Gwd/t, 2%, 5yr.	62 ± 6	29 ± 4	4 ± 1	6 ± 2
15Gwd/t, 3%, 5yr.	73 ± 6	19 ± 3	2 ± 1	6 ± 2
15Gwd/t, 4%, 5yr.	82 ± 7	14 ± 3	1 ± 1	4 ± 1
15Gwd/t, 5%, 5yr.	86 ± 7	11 ± 2	1 ± 1	3 ± 1
30Gwd/t, 2%, 5yr.	35 ± 4	44 ± 5	10 ± 3	11 ± 3
30Gwd/t, 3%, 5yr.	56 ± 6	34 ± 4	4 ± 1	5 ± 1
30Gwd/t, 4%, 5yr.	67 ± 7	24 ± 4	4 ± 1	6 ± 2
30Gwd/t, 5%, 5yr.	74 ± 7	19 ± 3	3 ± 1	4 ± 1
45Gwd/t, 4%, 5yr.	50 ± 5	35 ± 4	8 ± 2	7 ± 2
45Gwd/t, 5%, 5yr.	62 ± 6	28 ± 5	6 ± 2	5 ± 1
60Gwd/t, 5%, 5yr.	48 ± 5	38 ± 4	8 ± 2	7 ± 2

Determining the total fission rate of spent fuel assemblies does not result in quantification of the fissile isotopic content. However, it is still a valuable characteristic of the assay response. It can be used as an additional signature to verify the declared fuel characteristics, and can be related to the total fissile content by means of calibration. While measurements of the integrated counts can be performed with relative ease and do not require an elaborate setup, this method does not take advantage of the information contained in the complex structure of the delayed gamma-ray response spectra.

Recently, a more robust fission rate measurement approach was experimentally demonstrated for the spent nuclear fuel pins in the already mentioned experiment at the Paul Scherrer Institute [19]. Here, fuel pins were irradiated in a reactor, and individual high-resolution delayed gamma-ray lines were analyzed to determine the total residual fission rate of the fresh and spent nuclear fuel. The fission rate during irradiation is derived from the net area of each measured peak by

accounting for the individual contributions from the fission product gamma-ray lines and temporal isotopic transmutations during the assay:

$$Fission\ Rate = \frac{N_{net}}{\varepsilon(E_\gamma)\cdot b(E_\gamma)\cdot C}, \tag{6.1}$$

where N_{net} is the net peak area, $\varepsilon(E_\gamma)$ is the energy-dependent efficiency of the detector setup, $b(E_\gamma)$ is the intensity of the gamma-ray line, and C is a correction factor for the fission product generation during interrogation and subsequent decay. The authors consider several high-energy delayed gamma-ray peaks and associated physical data required for the analysis, and obtain relative fission rate values with uncertainties of approximately a few percent. It can be assumed that a similar technique can be applied in the delayed gamma-ray interrogation of spent fuel assemblies. Further research is required to investigate the accuracy limits of this method in the realistic assay scenarios.

6.3 Individual Isotopic Content Method

Analyzing the individual structures in the delayed-gamma-ray spectra offers a more powerful way to determine spent fuel characteristics. Previously published research demonstrates several approaches to quantitative analysis of the fissile material isotopic content by means of the delayed gamma-ray assay. In an early work [17], authors applied principles of activation analysis for delayed gamma-ray measurements of uranium enrichment. This method relied on the so-called "internal standard" present in the sample with a known or constant concentration, in order to perform a flux-independent assay of fissile components. Under thermal neutron interrogation, uranium enrichment is given by ratios of U-235 fission product peak areas to the U-238 (n,gamma) Np-239 activation peak area, which is proportional to the uranium atoms ratio in the sample. Experimental results demonstrate a high dynamic range and sensitivity of this method and achieve a precision level of approximately 0.6% in the uranium isotopes ratio range of $20 < (\text{U-238/U-235}) < 200$, using readily available laboratory equipment. The

authors concluded that the precision of the method precision was limited primarily by counting statistics and peak integration errors. However, it is not yet clear whether a variation of this technique can be applied to the spent nuclear fuel assay. Since the U-238 activation lines are located in the low-energy part of the spectrum and overwhelmed by passive background radioactivity, appropriate high-energy "standard" lines have to be identified.

Experimental application of the high-precision delayed gamma-ray analysis is also demonstrated in a series of publications [14,15,64,65] dedicated to the characterization of waste packages. A similar approach is taken in [18] to achieve Homeland Security and forensics objectives. Both research groups consider separation of the delayed gamma-ray responses in the two-component U-235 and Pu-239 systems, and concentrate on analyzing the peak ratio in the low-energy range. Performed under regular laboratory conditions for a variety of complex samples, these experiments demonstrate delayed gamma-ray interrogation as a rigorous assay instrument.

A more practical isotopic analysis based on the delayed gamma-ray peak ratios was developed in [20]. This experimental research focused on 2-component U-235 and Pu-239 systems to develop assay principles that can potentially be extrapolated to more complicated cases such as spent nuclear fuel. The assay method involves preliminary measurements of the calibration samples containing a single fissile isotope in the assay configuration. Multiple delayed gamma-ray peak ratios characteristic for the particular fissile isotope can be obtained from these measurements. When a sample containing two components is assayed and corresponding peak ratios are determined, the weighting functions for each fissile isotope in the sample can be obtained from a simple "lever" rule:

$$W_{Pu} = \left(1 - \left|\frac{r_{meas} - r_{Pu}}{r_{Pu} - r_U}\right|\right) \cdot 100\% \quad \text{and} \quad W_U = \left(1 - \left|\frac{r_{meas} - r_U}{r_{Pu} - r_U}\right|\right) \cdot 100\%, \tag{6.2}$$

where r_{meas} is the measured peak ratio for a two-component system, r_{Pu} and r_U are the same peak ratios for the pure sample. This method offers the most straightforward experimental approach to the delayed gamma-ray assay and was

further investigated in application to spent nuclear fuel assemblies. Under real assay conditions, an additional calibration measurement may be required for each of the primary fissile isotopes in the assay-specific configuration. The analysis is compatible with the four-step modeling algorithm which allows for the calculation of fissile isotope-specific contributions to the delayed gamma-ray peaks.

Although various existing practical applications of the delayed gamma-ray interrogation were considered in the literature, none of them can be readily adopted for the quantitative assay of spent nuclear fuel. In the realistic assay conditions, the complexity of the analysis arises primarily from the following factors:

- A combination of contributions from several actinides to the delayed gamma-ray response has to be considered: U-235, U-238, Pu-239, and Pu-241.

- An intense passive background below the threshold of approximately 3 MeV requires a response analysis to be performed for high-energy delayed gamma-ray lines, about which little is known from previous research.

- The complex configuration of the spent nuclear fuel assembly and the assay setup make it difficult to account for the detector efficiency and self-attenuation of the delayed gamma-ray response in the system.

- Quantitative assay requires high precision in determining the contribution of the partial delayed gamma-ray lines to the detected peak areas.

Despite the generalized formulations, the effects of these factors can be reproduced in the modeling algorithm to the accuracy of the physical data libraries. As a result, a more precise analysis technique can be developed.

6.3.1 Derivation of the Exact Delayed Gamma-Ray Peak Ratio Expression

In order to further investigate the theoretical limits of the delayed gamma-ray analysis, an exact expression for quantifying the delayed gamma-ray response can be derived. By analyzing the parameters of the resulting equation, it is possible to characterize the combination of the physical library data inputs, information specific to the experimental setup, and the assumptions required to achieve various precision levels in the analysis.

Assume a standard case of the "long" interrogation time mode, when the delayed gamma-ray line of interest is emitted by an isotope that is directly produced in fission events and/or has short-lived precursors. Then, the rate of isotope production under neutron interrogation of a sample with several fissile nuclides can be calculated as:

$$R_{FP} = \phi \cdot N_{Av} \cdot \sum_i \left(\sigma_{f,i} \cdot y_i \frac{m_i}{A_i} \right), \tag{6.3}$$

where ϕ is the interrogating neutron flux in the sample (n/cm^2-s), N_{Av} is the Avogadro number (at./mol), i is the index of the actinide that undergoes fission with the following parameters: σ_f is the microscopic fission cross-section (cm^2), y_i is the summary (cumulative) yield of the fission product, m_i is the mass of the actinide (g), and A_i is the atomic mass of the actinide (g/mol). The summary yields in this expression include direct isotope yields in fission along with yields of short-lived precursors present in equilibrium with the isotope during interrogation.

Then, the total amount of fission product atoms produced during interrogation time t_i is:

$$N_p = \frac{R_{FP}}{\lambda} \cdot \left(1 - \exp\left(-\lambda \cdot t_i\right)\right), \tag{6.4}$$

where λ is the isotope decay constant. The number of isotope atoms at the end of the cooling period t_c is:

$$N_c = N_p \cdot \exp\left(-\lambda \cdot t_c\right), \tag{6.5}$$

and the number of decays during the delayed gamma-ray acquisition period t_{det} is:

$$N_d = N_c \cdot \left(1 - \exp\left(-\lambda \cdot t_{\text{det}}\right)\right). \tag{6.6}$$

The total number of decays is expressed as:

$$N_d = \frac{R_{FP}}{\lambda} \cdot \left(1 - \exp\left(-\lambda \cdot t_i\right)\right) \cdot \exp\left(-\lambda \cdot t_c\right) \cdot \left(1 - \exp\left(-\lambda \cdot t_{\text{det}}\right)\right) \tag{6.7}$$

Then, the general expression for the corresponding peak area (intensity) in the delayed gamma-ray spectrum, assuming the only contributing gamma-ray is:

$$I = \varepsilon \cdot B.R. \cdot N_d, \tag{6.8}$$

where ε is the detector efficiency to the gamma-ray line, and *B.R.* is the branching ratio for the line emission in the isotope decay. In the event that several significant gamma-rays are included in the peak, the total area is expressed as a sum of these contributions.

Assume now a simplified case when the signature gamma-ray peak "*A*" is formed by the emission of gamma-ray from fission product isotope that is produced in fissions from two actinides present in the system:

$$\left.\begin{matrix} Actinide\,1 \\ Actinide\,2 \end{matrix}\right\} (n, f) \rightarrow FP\ isotope\ A \rightarrow gamma\ peak\ A.$$

From the experiment, the rate of isotope *A* production during interrogation is calculated as:

$$R_A = \frac{I_A}{\varepsilon_A \cdot B.R._A \cdot \frac{1}{\lambda_A} \cdot \left(1-\exp\left(-\lambda_A \cdot t_i\right)\right) \cdot \exp\left(-\lambda_A \cdot t_c\right) \cdot \left(1-\exp\left(-\lambda_A \cdot t_{\det}\right)\right)} = \frac{I_A}{\varepsilon_A \cdot B.R._A \cdot f_A(t)} \tag{6.8}$$

where $f_A(t) = \frac{1}{\lambda_A} \cdot \left(1-\exp\left(-\lambda_A \cdot t_i\right)\right) \cdot \exp\left(-\lambda_A \cdot t_c\right) \cdot \left(1-\exp\left(-\lambda_A \cdot t_{\det}\right)\right)$.

The same production rate can be found through the fission reaction rates in both actinides:

$$R_A = \phi \cdot N_{Av} \cdot \left(\sigma_{f,1} \cdot y_{1,A} \frac{m_1}{A_1} + \sigma_{f,2} \cdot y_{2,A} \frac{m_2}{A_2} \right). \tag{6.9}$$

The mass of each actinide can be expressed as:

$$m_1 = \frac{A_1}{\sigma_{f,1} \cdot y_{1,A}} \cdot \left(\frac{R_A}{\phi \cdot N_{Av}} - \sigma_{f,2} \cdot y_{2,A} \frac{m_2}{A_2} \right). \tag{6.10}$$

$$m_2 = \frac{A_2}{\sigma_{f,2} \cdot y_{21,A}} \cdot \left(\frac{R_A}{\phi \cdot N_{Av}} - \sigma_{f,1} \cdot y_{1,A} \frac{m_1}{A_1} \right). \tag{6.11}$$

In order to perform the exact actinide mass calculation, assume a delayed gamma-ray peak from another fission product "*B*" in the same spectrum. Then, the mass of the second actinide expressed for this peak is:

$$m_2 = \frac{A_2}{\sigma_{f,2} \cdot y_{21,B}} \cdot \left(\frac{R_B}{\phi \cdot N_{Av}} - \sigma_{f,1} \cdot y_{1,B} \frac{m_1}{A_1} \right). \tag{6.12}$$

Substituting this equation in the above expression (6.10) for the first actinide mass results in the following exact solution:

$$m_1 = \frac{A_1}{\sigma_{f,1} \cdot y_{1,A}} \cdot \left(\frac{R_A}{\phi \cdot N_{Av}} - \frac{\sigma_{f,2} \cdot y_{2,A}}{A_2} \cdot \frac{A_2}{\sigma_{f,2} \cdot y_{21,B}} \cdot \left(\frac{R_B}{\phi \cdot N_{Av}} - \sigma_{f,1} \cdot y_{1,B} \frac{m_1}{A_1} \right) \right). \quad (6.13)$$

After rearranging:

$$m_1 = \frac{A_1}{\phi \cdot N_{Av} \cdot \sigma_{f,1}} \left(\frac{R_A \cdot y_{2,B} - R_B \cdot y_{2,A}}{y_{1,A} \cdot y_{2,B} - y_{2,A} \cdot y_{1,B}} \right), \quad (6.14)$$

and similarly,

$$m_2 = \frac{A_2}{\phi \cdot N_{Av} \cdot \sigma_{f,2}} \left(\frac{R_A \cdot y_{1,B} - R_B \cdot y_{1,A}}{y_{2,A} \cdot y_{1,B} - y_{1,A} \cdot y_{2,B}} \right). \quad (6.15)$$

These equations can be solved to exactly calculate the mass of each actinide.

For the real assay setup, estimations of the interrogating neutron flux can be obtained by means of transport code simulations. However, it is preferable to avoid such ambiguity in the analysis and to instead calculate the relative actinide content:

$$\frac{m_1}{m_2} = \frac{A_1 \cdot \sigma_{f,1}}{A_2 \cdot \sigma_{f,2}} \left(\frac{R_A \cdot y_{2,B} - R_B \cdot y_{2,A}}{R_A \cdot y_{1,B} - R_B \cdot y_{1,A}} \right) \quad (6.16)$$

The values of R_A and R_B are determined from the detected peak areas:

$$R_A = \frac{I_A}{\varepsilon_A \cdot B.R._A \cdot f_A(t)}, \quad R_B = \frac{I_B}{\varepsilon_B \cdot B.R._B \cdot f_B(t)}.$$

In these final expressions, m_i is the mass of an actinide in the interrogated material, A_i is the actinide atomic mass, $\sigma_{f,i}$ is the actinide fission cross-section,

$y_{i,X}$ is the actinide individual fission product yield, I_X is the detected peak area of a delayed gamma-ray, ε_X is the detection efficiency of the gamma-ray, $B.R._X$ is the branching ratio of the gamma-ray emission in the decay of the fission product, and $f_X(t)$ is the production and decay function of the fission product.

Following the same principles, this analysis can be expanded for three or more actinide contributions and for several individual delayed gamma-ray emissions contributing to the same peak area. Approximate parameter values can be obtained from the physical data libraries, and detected peak contributors can be found by applying the 4-step modeling technique. The detector setup efficiencies can be determined experimentally by using calibration targets fabricated from the fresh fuel material. The first approximation calculation requires an assumed value for the energy-integrated fission cross-section of each actinide that can be estimated using transport code calculations or from the literature with the thermal interrogating neutron flux assumption. The precision of these generalized calculations will be limited primarily by the statistical uncertainty in determining the detected peak areas. This calculation can be effectively used in conjunction with the purely empirical weighting functions method discussed previously.

The expression (6.16) demonstrates the rigorous nature of the delayed gamma-ray assay and that the spent fuel fissile content inventory values can be extracted from the response obtained in a single independent measurement. However, under real assay conditions, most of the contributing parameters will remain unknown or will be individual to the setup configuration. Application of this method will require setup-specific calibration measurements and more powerful techniques for the deconvolution of the delayed gamma-ray response.

6.3.2 Analysis of Delayed Gamma-Ray Peak Ratios

The isotope-specific information contained in the delayed gamma-ray spectra can be illustrated by comparing the calculated delayed gamma-ray spectra for pure U-235 and Pu-239 samples. This basic activation experiment simulation was

performed for a 15-minute thermal neutron interrogation, followed by a 1-minute cool-down interval, and a 15-minute detection period. The interrogation setup assumed a 25 cm standoff distance for a 3x2 in. coaxial HPGe detector with known energy and resolution calibration parameters. For the simulation results depicted in Figure 6.2, count rate limits for both detector types were disregarded, and response spectra were normalized to the amount of actinide present in each interrogated sample. The bottom part of this figure provides a close-up of four arbitrarily selected peaks with an apparent sensitivity to a specific fissile isotope.

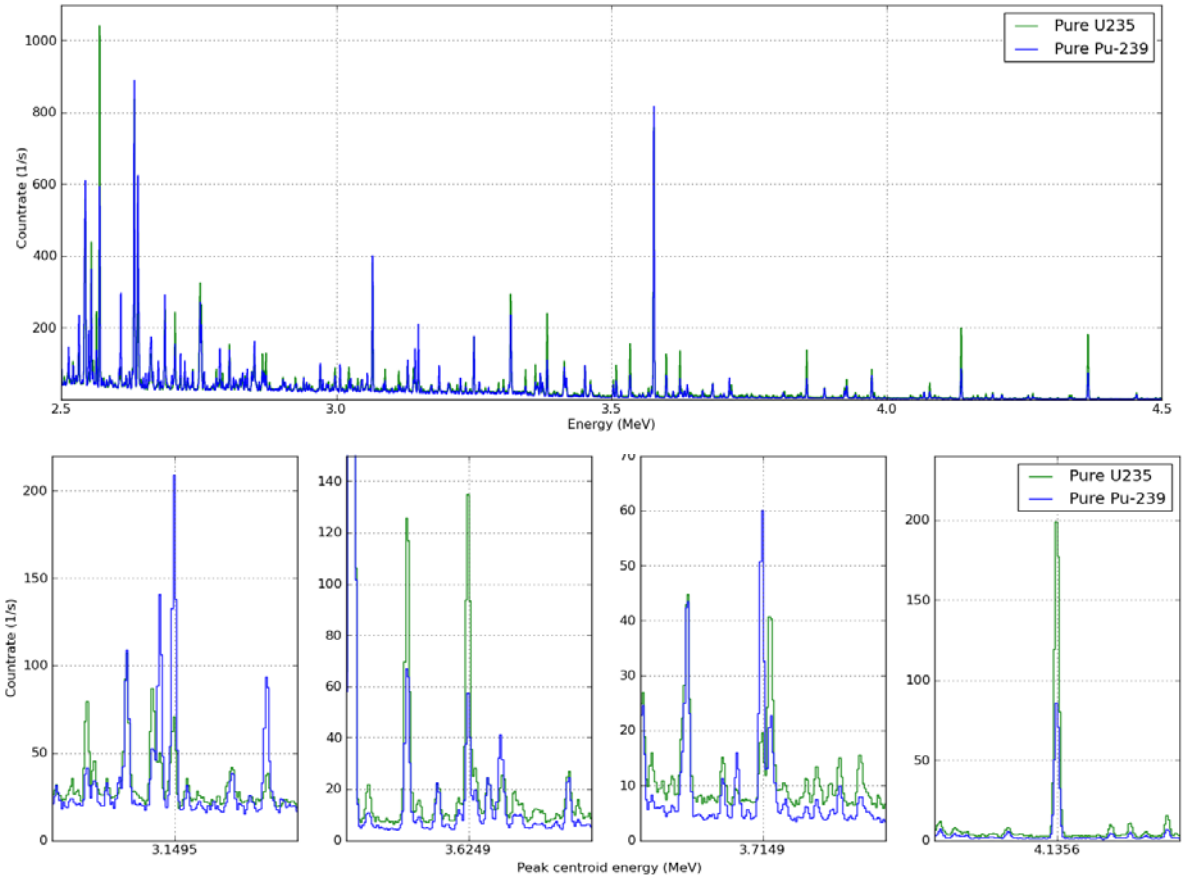

Figure 6.2. Delayed gamma-ray response spectra calculated for pure U-235 and Pu-239 samples in a simplified setup (top). Arbitrarily selected peaks with an apparent sensitivity to each isotope (bottom).

The area ratios of the four selected peaks change as a monotonic function with the isotopic composition of a binary system of the two isotopes and can serve as a direct measure of the relative U-235/Pu-239 content in a mixed sample. Figure 6.3 demonstrates the dynamic range of four calculated peak area ratios for various isotopic mixtures. In this figure and later in the text, the extracted peak areas are identified by the energy of each peak centroid. The areas of the delayed gamma-ray peaks and associated errors were obtained from the calculated delayed gamma-ray response spectra for each mixture using a specifically written post-processing code.

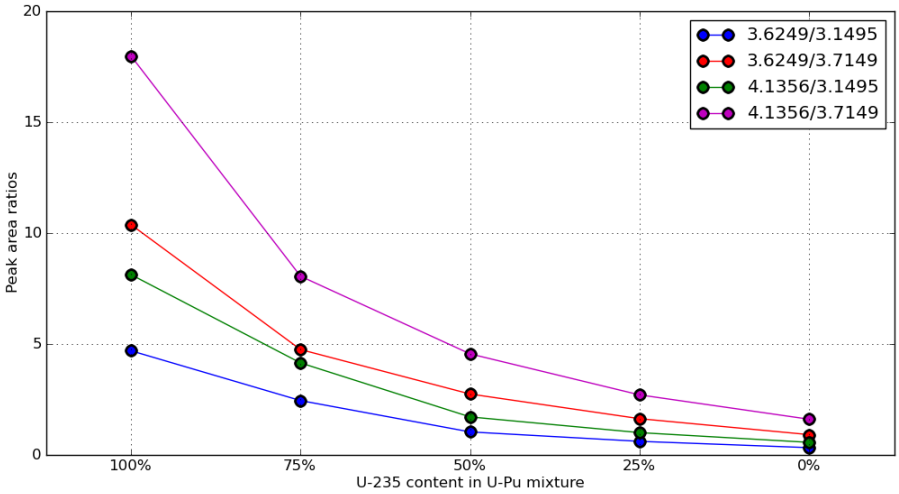

Figure 6.3. Calculated delayed gamma-ray peak area ratios for U-235/Pu-239 mixtures in the simplified setup.

The same effect of composition-specific delayed gamma-ray peak ratios was observed for the more complicated case of delayed gamma-ray spectra calculated for 17 x 17 assemblies from spent nuclear fuel library #1 with the parameters outlined in Table 6.1. These simulations were performed for the same assay instrument configuration and parameters as described in Section 5.4. A subset of peak ratios for the assemblies with various burnup, 5% initial enrichment, and 5 years cooling time is shown in Figure 6.4. Table 6.3 illustrates the relative fissile isotopic composition for these assemblies. The non-linear response in the case of

these assemblies is affected by the change in the Pu-241 content, while the variation in U-238 content is almost negligible.

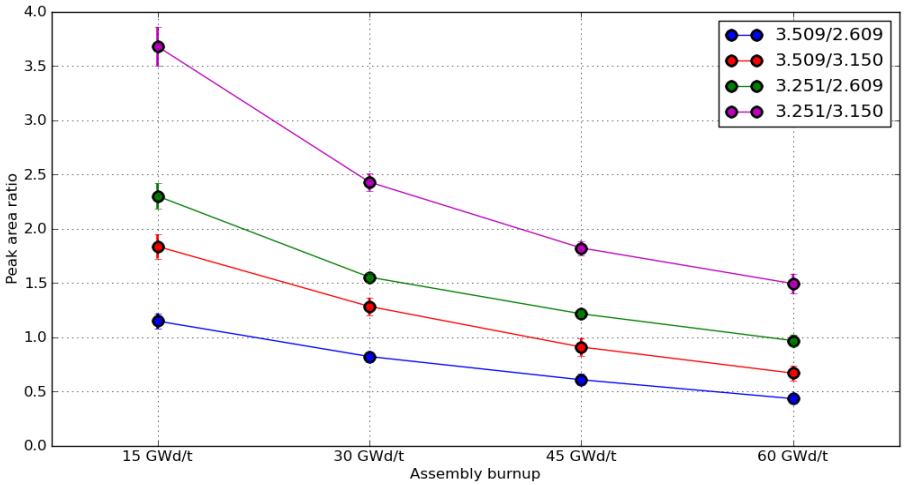

Figure 6.4. Ratios of four arbitrary peak areas extracted from the delayed gamma-ray spectra for spent fuel library #1 assemblies with various burnup, 5% initial enrichment, and 5 years cooling time.

Table 6.3. The relative composition of fissile isotopes for the assemblies from Figure 6.4.

Assembly	**Fissile content composition**		
	U-235	**Pu-239**	**Pu-241**
15 GWd/t	88%	11%	1%
30 GWd/t	77%	20%	3%
45 GWd/t	64%	29%	6%
60 GWd/t	50%	40%	10%

To investigate the potential of this analysis approach, the above peak ratios were determined for the whole set of 11 spent fuel library assemblies from Table 6.1. Individual peak areas were determined using a post-processing code from the total delayed gamma-ray response spectra calculated for the same setup configuration

as described in Section 5.4. Table 6.4 lists peak area ratios determined for 11 assemblies with 5 year cooling time and varying initial enrichment and burnup. The peak ratios from Table 6.4 are depicted in Figure 6.5, illustrating the response variability with the fuel inventory as represented by the assembly parameters. From this figure, it can be concluded that each assembly is characterized by a unique combination of peak ratios. Therefore, a simple empirical weight functions method can theoretically be applied for determining the relative composition of fissile isotopes. Such analysis can be performed by initially calculating the peak ratios from the individual actinide spectra, and then comparing these values to the same peak ratios obtained from the full inventory response. Multiple peak regions can be used to increase the accuracy of the delayed gamma-ray spectra deconvolution, however it still remains unclear whether a sufficiently high specificity can ultimately be obtained. Otherwise, the overall precision of this method is limited primarily by the statistical uncertainty in determining the detected peak areas.

Table 6.4. Delayed gamma-ray peak area ratios for 11 library #1 fuel assemblies.

Library #1 assembly	**Peak ratios**			
	3.509/2.609	**3.509/3.150**	**3.251/2.609**	**3.251/3.150**
15Gwd/t, 2%, 5yr.	0.430 ± 0.119	0.688 ± 0.192	0.857 ± 0.192	1.371 ± 0.311
15Gwd/t, 3%, 5yr.	0.825 ± 0.059	1.280 ± 0.098	1.145 ± 0.140	1.776 ± 0.222
15Gwd/t, 4%, 5yr.	1.007 ± 0.067	1.607 ± 0.116	1.793 ± 0.055	2.860 ± 0.122
15Gwd/t, 5%, 5yr.	1.147 ± 0.072	1.835 ± 0.112	2.299 ± 0.119	3.678 ± 0.181
30Gwd/t, 2%, 5yr.	0.385 ± 0.057	0.581 ± 0.113	0.895 ± 0.063	1.351 ± 0.196
30Gwd/t, 3%, 5yr.	0.521 ± 0.050	0.767 ± 0.080	1.098 ± 0.057	1.617 ± 0.108
30Gwd/t, 4%, 5yr.	0.685 ± 0.037	1.033 ± 0.071	0.976 ± 0.127	1.473 ± 0.201
30Gwd/t, 5%, 5yr.	0.820 ± 0.049	1.282 ± 0.081	1.552 ± 0.041	2.428 ± 0.079
45Gwd/t, 4%, 5yr.	0.491 ± 0.089	0.708 ± 0.129	1.063 ± 0.047	1.532 ± 0.074
45Gwd/t, 5%, 5yr.	0.606 ± 0.053	0.908 ± 0.082	1.214 ± 0.034	1.821 ± 0.065
60Gwd/t, 5%, 5yr.	0.432 ± 0.044	0.667 ± 0.068	0.967 ± 0.056	1.492 ± 0.091

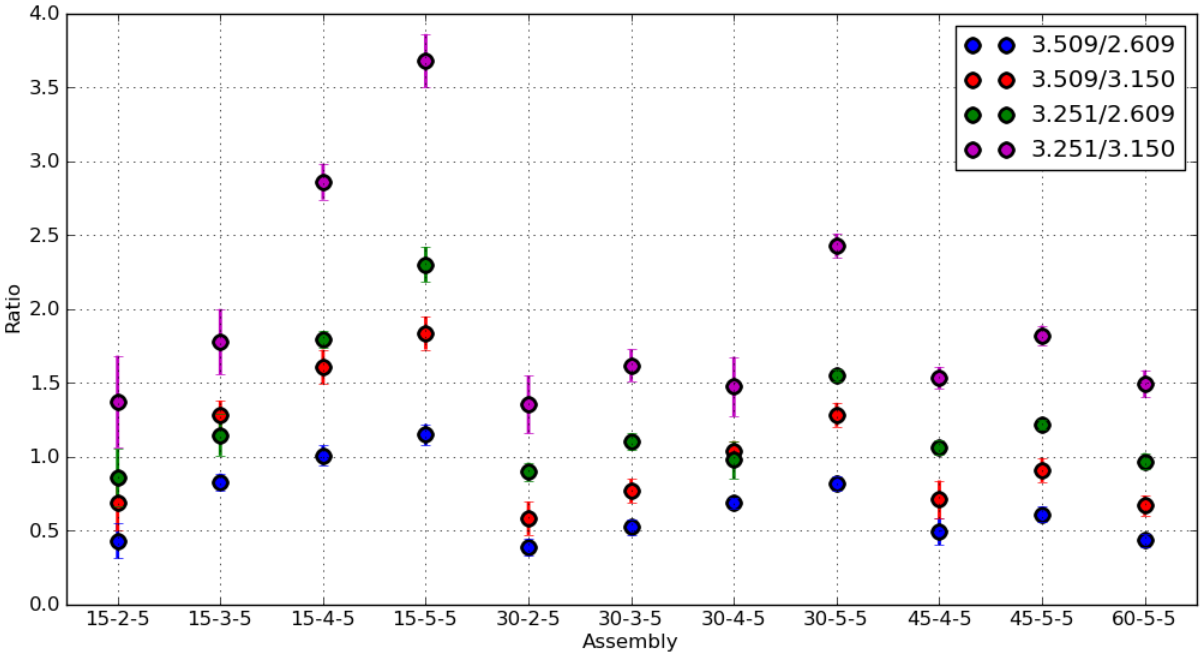

Figure 6.5. Calculated arbitrary peak ratios for 11 spent fuel library #1 assemblies.

6.3.3 Numerical Approach to the Response Analysis

Peak area ratios shown in Figure 6.5 were obtained from the delayed gamma-ray spectra calculated for 11 assemblies from spent fuel library #1. Figure 6.6 provides an example of a high-energy region of the response spectrum obtained for a fuel assembly with 45 GWd/t burnup, 4% initial enrichment, 5 years cooling time. The top spectrum in this figure is obtained for a HPGe detector resolution and demonstrates a number of isolated peaks that can be used in the peak area ratio analysis method. The middle spectrum was obtained for the $LaBr_3$ detector resolution with crystal dimensions and calibration parameters reported in [56]. Each spectrum shows individual isotopic contributions to the total delayed gamma-ray response from the primary actinides. Although the HPGe detector provides spectra with more resolved prompt and delayed gamma-ray lines, the resolution of the $LaBr_3$ detector is sufficient to observe several high-energy peaks and integrated continuum effects with apparent sensitivity to the isotopic content of the assayed fuel assembly. Analysis of individual isotopic contributions to the total response in HPGe and $LaBr_3$ spectra indicates that isotope-specific delayed

gamma-ray signatures are not limited to the isolated delayed gamma-ray peaks, but can also be observed in the continuum. For example, U-235 and Pu-239 produce approximately equal count rates in the energy region between 3.0 and 3.5 MeV (when normalized to the same concentration). However, above 4.0 MeV, the count rate is dominated by U-235 delayed gamma-ray emissions. The increased response in the upper energy region of the spectrum is explained by the emission lines of fission products with A around 90 that have higher yields for U-235. A similar effect of variable continuum contributions was observed for the isotopes of U-238 and Pu-241.

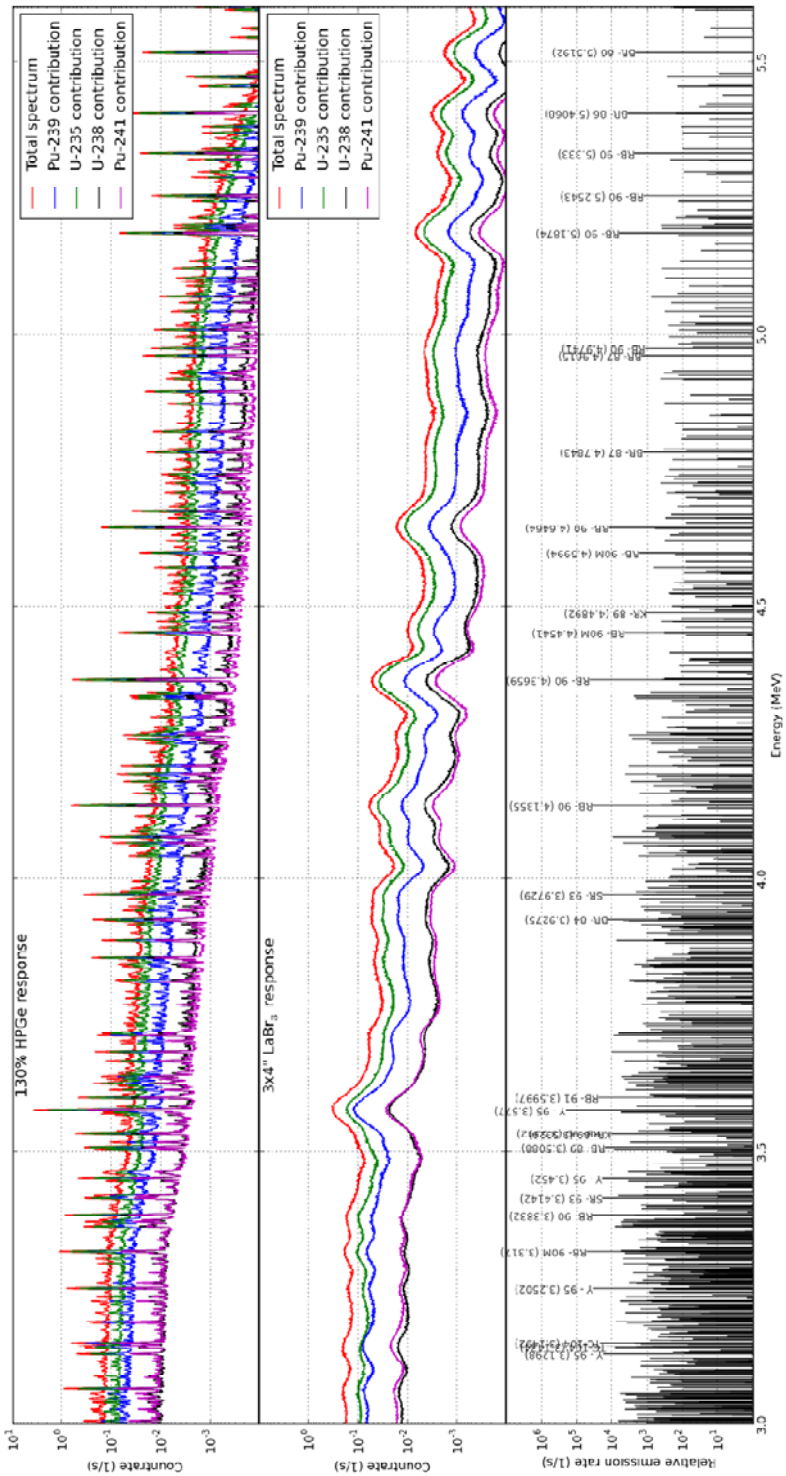

Figure 6.6. A high-energy region of the delayed gamma-ray spectrum calculated for the assembly from library #1 with 45 GWd/t burnup, 4% initial enrichment, and 5 years cooling time. High-purity germanium detector spectrum (top). LaBr3 detector (middle). Delayed gamma-ray emission spectrum in the fuel (bottom).

Accounting for the full variety of information contained in the delayed gamma-ray spectra can drastically improve the accuracy of the method and reduce the effect of statistical uncertainties. A preliminary study of the numerical spectrum deconvolution technique based on the orthogonal distance regression for linear combination of basis spectra has already proved promising. This method relies on obtaining individual setup-specific delayed gamma-ray spectra for each of the four primary actinide isotopes. The delayed gamma-ray response spectrum obtained in the assay is then treated as a linear combination of the four contributing spectra according to the following expression:

$$Response\ \ Spectrum\ = A \cdot U235 + B \cdot Pu239 + C \cdot U238 + D \cdot Pu241, \qquad (6.17)$$

where *A*, *B*, *C*, and *D* are the fitting parameters. By performing a fit of the isotope-specific spectra to the measured total response spectrum of the unknown sample, a contribution of each isotope corresponding to its relative composition in the mixture can be obtained.

A modeling study with simplified assay geometry has been performed to investigate the feasibility of such numerical fitting. A basic activation experiment model considered the interrogation of oxide actinide samples with a thermal neutron source. Actinide composition consisted of four isotopes (U-235, Pu-239, U-238, and Pu-241) with concentrations similar to spent nuclear fuel. Delayed gamma-ray spectra collection from these samples was simulated for consecutive 15-minute interrogation and detection time periods separated by a 1 minute cool-down interval. The interrogation setup assumed a 25 cm standoff distance for 3x2 in. coaxial HPGe and $LaBr_3$ detectors with known energy and resolution calibration parameters. Simulations were performed for three cases of the assayed material compositions. One of the cases was used to extract isotope-specific calibration spectra specific for each detector. These calibration spectra were then used to fit the total delayed gamma-ray response spectra obtained in the other two cases using the Levenberg-Marquardt orthogonal distance regression routine [66,67]. The fitting procedure was used to determine the fissile isotopes composition of the interrogated samples normalized relative to the U-235 content according to the expression:

$$Fissile\ Composition = U235 + C_1 \cdot Pu239 + C_2 \cdot Pu241, \quad (6.18)$$

where C_1 and C_2 are the isotope concentrations relative to U-235 content.

The deconvolution algorithm results are illustrated in Table 6.5 for two cases with different isotopic compositions of the assayed material and five scenarios developed for various interpretations of the delayed gamma-ray response spectra. The first scenario considered fitting the calibration and response spectra in the energy region between 3.0 and 5.0 MeV which was obtained with ideal resolution, i.e. without detector broadening effects. In the second and third scenarios, fitting of the same spectral regions was performed for HPGe and $LaBr_3$ detector resolutions. The fourth scenario considered fitting of the arrays containing peak areas extracted from the response and calibration spectra. The fifth scenario involved regions of spectra identified around the most intense peaks in the HPGe resolution. Results in this table provide a preliminary indication of the fitting technique's applicability for determining the relative composition of isotopes contributing to the delayed gamma-ray assay response. However, the accuracy of the fit decreases with the coarser resolution of the delayed gamma-ray spectra calculated for the $LaBr_3$ detector. Other potential limitations of this method have to be further investigated.

Table 6.5. Delayed gamma-ray response deconvolution results using the Orthogonal Distance Regression Method for simplified modeling cases.

Case 1 actinide composition: 5% U-235, 3% Pu-239, 2% Pu-241, 90% U-238	
Real fissile isotopes ratio	1 : 0.6 : 0.4
Response deconvolution results	
Scenario 1. Ideal resolution	1.0 : 0.592 (±0.003) : 0.410 (±0.002)
Scenario 2. HPGe resolution	1.0 : 0.603 (±0.004) : 0.399 (±0.003)
Scenario 3. LaBr3 resolution	1.0 : 0.687 (±0.017) : 0.350 (±0.013)
Scenario 4. Peak areas	1.0 : 0.606 (±0.017) : 0.407 (±0.013)
Scenario 5. Peak regions	1.0 : 0.606 (±0.016) : 0.405 (±0.012)
Case 2 actinide composition: 1% U-235, 3% Pu-239, 1% Pu-241, 95% U-238	
Real fissile isotopes ratio	1 : 3 : 1
Response deconvolution results	
Scenario 1. Ideal resolution	1.0 : 2.995 (±0.018) : 0.994 (±0.009)
Scenario 2. HPGe resolution	1.0 : 2.896 (±0.024) : 0.999 (±0.012)
Scenario 3. LaBr3 resolution	1.0 : 2.721 (±0.078) : 1.067 (±0.042)
Scenario 4. Peak areas	1.0 : 3.093 (±0.102) : 0.980 (±0.046)
Scenario 5. Peak regions	1.0 : 3.115 (±0.103) : 0.983 (±0.046)

Conclusions and Outlook

High-energy delayed gamma-ray spectroscopy provides the capability to directly assay fissile and fertile isotopes in the highly radioactive environment of the spent fuel assemblies and to achieve the safeguards goal of quantifying nuclear material inventories for spent fuel handling, interim storage, reprocessing facilities, and final disposal and repository sites. Preliminary results of the dedicated modeling and experimental efforts performed for this dissertation indicate that such measurements may be possible with presently available neutron generator and gamma-ray detection technology.

For a detailed analysis of the delayed gamma-ray responses in the spent nuclear fuel assay, an original modeling methodology has been introduced. The calculation process utilizes advanced capabilities of the modern transport and transmutation codes, along with a newly developed discrete gamma-ray source term reconstruction code. As a result, the modeling technique accounts for complex assay setup configurations and detailed material inventories and allows for accurate predictions of the spatially-dependent discrete gamma-ray source terms and detector responses. The delayed gamma-ray response modeling capability was benchmarked and verified in a series of specifically organized experiments involving samples of the fissile materials.

The scope of the current delayed gamma-ray instrument design was limited to a setup involving a moderated D-T interrogating neutron source, a “long” assay mode with extended irradiation and detection time periods, and a high-purity germanium detector. Analytical estimations and detailed model calculations performed for this assumed setup indicate that the delayed gamma-ray responses can be obtained with accuracy adequate for spent nuclear fuel assay. Individual isotopic signatures contained in these spectra can potentially be used to quantify the total fissile content and individual weight fractions of fissile nuclides. Several analysis techniques based on absolute detected delayed gamma-ray peak

intensities and peak area ratios can be implemented for fissile content quantification. Calculations performed for a number of spent fuel assemblies with varying burnup and initial enrichment demonstrate that each fuel assembly is characterized by a unique combination of delayed gamma-ray peak ratios from which fissile inventory can be derived.

The primary constrain for the delayed gamma-ray assay concept identified in this dissertation, is the HPGe detector count rate limitations combined with the high rate of spent fuel passive gamma-ray background extending up to 3.0 MeV. Passive background interference with the assay signatures can be avoided by analyzing delayed gamma-ray peaks with energies above this threshold. To a certain extent, the passive count rate can be reduced by the detector collimation and the use of the attenuating layers in front of the detector. Calculations indicate that the required intensity of the delayed gamma-ray peaks in the present non-optimized setup can be obtained with the interrogating neutron source intensity between 10^{11} n/s and 10^{12} n/s The assay response can be further improved by implementing the following measures: increasing the neutron source intensity, extending interrogation and detection time periods, and changing the detector parameters and configuration.

This dissertation establishes that unique actinide-specific signatures contained in the delayed gamma-ray spectra can be potentially used to non-destructively determine isotopic composition and content of nuclear materials. Energy and time variability of the delayed gamma-ray responses makes this interrogation method highly adaptable to specific assay scenarios. However, essential research is still required to fully assess the merits of this method for a range of safeguards applications. Specifically, it is imperative to evaluate the accuracy and completeness of isotope-specific delayed gamma-ray signature sets (particularly for short decay times and variable interrogating neutron energy distributions), to benchmark and validate computational tools, and to further establish a comprehensive theoretical basis for assay methodologies and instrumentation development.

Although the four-step modeling technique has performed satisfactorily in the limited benchmarking campaign conducted to date, an additional experimental effort is required to validate the calculation process for various assay conditions, in particular the pulsed interrogation. The consistency of the tabulated physical data used in the calculations (cross-sections, fission product yields, decay paths, photon emission rates, etc.) need to be examined specifically for short-time "pulsed" interrogation patterns. The modeling code package can be further refined and adapted to include additional features and capabilities necessary for the simulation of potential applications. Modeling can be effectively used to design experiments, to interpret the experimental measurements and to perform response sensitivity studies.

Additional experimental measurements are required to investigate the temporal patterns of delayed gamma-ray responses with particular emphasis being placed upon short-lived fission fragments with decay times from 100 milliseconds to minutes. The fast-decaying component of the delayed gamma-ray spectra potentially offers higher isotopic sensitivity of the assay, and can be collected in pulsed mode with a suitable time structure. Statistical limits and signal-to-background ratios of this method have to examined and compared to more conventional long interrogation methods.

Calculating isotopic content from the delayed gamma-ray measurements poses a challenging problem. The simplest approach is based on the analysis of isolated peak ratios, while more sophisticated algorithms take advantage of full information in the spectra and can potentially greatly improve assay accuracy. The development and testing of new analytical and numerical methods must be continued. An important aspect of the future research is to find algorithms and methods for determining isotopic fractions of spent nuclear fuel that account for cumulative contribution of U-235, Pu-239, U-238, and Pu-241, and can handle non-linear response behavior and multiplication effects.

For delayed gamma-ray assay scenarios that involve highly-radioactive materials such as spent nuclear fuel, detector signal throughput capabilities are critical. To date, studies have been based on conventional HPGe detectors but faster detector

options may be superior, especially in cases when regions of delayed gamma-ray spectra (rather than single peaks) are used to determine isotopic compositions. High-count rate detector systems for delayed gamma-ray assay in highly-radioactive environments need to be investigated. Fine energy resolution, efficiency to high-energy gamma-rays, and response linearity are important criteria that must be considered. HPGe detectors are the first choice for delayed gamma-ray spectroscopy, and fast signal processing electronics can be applied to increase data throughput. The trade-off limits between the energy resolution degradation and increased count rate limits can be established for specific assay scenarios. Modeling and simulation can be used as an effective tool for investigating application-specific configurations of detector setups, importance of collimators and attenuating filters, detector arrays, Compton suppression systems and other parameters.

The future research must therefore rely on a strong experimental component for measuring delayed gamma-ray responses from specific isotopes, isotopic mixtures, and nuclear materials, along with a closely linked modeling effort. Such experiments will provide data to verify and complement nuclear data libraries and to improve capabilities of the response modeling technique. As a result, the concepts of the delayed gamma-ray assay can be expanded to wider applications in the areas of nuclear safeguards, material control and accountancy, homeland security, and nuclear forensics.

Bibliography

1. "Atoms for Peace," Address by Mr. Dwight D. Eisenhower, President of the United States of America, to the 470th Plenary Meeting of the United Nations General Assembly, (8 December 1953).

2. INFCIRC/66 (Revision 2), "The Agency's Safeguards System," International Atomic Energy Agency (1965, as Provisionally Extended in 1966 and 1968).

3. INFCIRC/153 (Corrected), "The Structure and Content of Agreements Between the Agency and States Required in Connection with the Treaty on the Non-Proliferation of Nuclear Weapons," International Atomic Energy Agency (1972).

4. INFCIRC/540 (Corrected), "Model Protocol Additional to the Agreement(s) Between States and the International Atomic Energy Agency for the Application of Safeguards," International Atomic Energy Agency (1977).

5. "IAEA safeguards glossary. 2001 Edition," International Atomic Energy Agency (2002).

6. H. Feiveson, Z. Mian, M. V. Ramana, and F. von Hippel (ed.), "Spent Fuel from Nuclear Power Reactors. An Overview of a New Study by the International Panel on Fissile Materials, " International Atomic Energy Agency (2011).

7. J.R. Phillips, "Irradiated Fuel Measurements," in Passive Nondestructive Assay of Nuclear Materials, D.T. Reilly (ed.), Office of Nuclear Regulatory Research, NUREG/CR-5550 (1990).

8. S. J. Tobin et al., "Determination of plutonium content in spent fuel with nondestructive assay," Institute of Nuclear Materials Management 50th Annual Meeting, Tucson, AZ USA, LA-UR-09-03748 (2009).

9. A. Scheinman, "Calling for action: the next generation safeguards initiative," The Nonproliferation Review, Vol. 16, No. 2, (2009).

10. J. D. Chen A. F. Gerwing, R. Keeffe, M. Larsson, K. Jansson, L. Hildingsson, B. Lindberg, E. Sundkvist, U. Meijer, M. Thorsell and M. Ohlsson, "Long-Cooled Spent Fuel Verification Using a Digital Cerenkov Viewing Device," International Atomic Energy Agency Report, IAEA-SM-367/14/07, (2007).

11. P. M. Rinard and G. E. Bosler, "Safeguarding LWR Spent Fuel with the Fork Detector," Los Alamos National Laboratory Report, LA-11096-MS (1988).

12. A. Lebrun, M. Merelli, J-L. Szabo, M. Huver, R. Arlt, and J. Arenas-Carrasco, "SMOPY a new NDA tool for safeguards of LEU and MOX spent fuel," International Atomic Energy Agency Report IAEASM-367/14/03 (2003).

13. H. Rennhofer et al., "Detection of SNM by delayed gamma rays from induced fission," *Nucl. Instr. Meth. A* (2010).

14. N. Saurel, J. M. Capdevila, et al., "Experimental and simulated assay of actinides in a real waste package," *Nucl. Inst. Meth. Phys. Res. A*, 550 (2005).

15. M. Gmar, F. Jeanneau, et al., “Assessment of actinide mass embedded in large concrete waste packages by photon interrogation and photofission,” *Appl. Radiat. Isot.* 63 (2005).

16. E. B. Norman, S. G. Prussin, et al., “Signatures of fissile materials: high-energy γ rays following fission,” *Nucl. Instr. Meth. Phys. Res, A*, 521 (2004).

17. M. Mantel, J. Gilat, and S. Amiel, “Isotopic analysis of uranium by neutron activation and high resolution gamma ray spectrometry,” *J. Radioanal. Chem.* Vol. 2 (1969).

18. R. E. Marrs, E. B. Norman, et al., “Fission-product gamma-ray line pairs sensitive to fissile material and neutron energy,” *Nucl. Instr. Meth. Phys. Res. A*, 592, (2008).

19. H. Krohnert et al., “Freshly induced short-lived gamma-ray activity as a measure of fission rates in lightly re-irradiated spent fuel,” *Nucl. Instr. Meth. Phys. Res. A*, 624 (2010).

20. D. H. Beddingfeld, and F. E. Cecil, “Identification of fissile materials from fission product gamma-ray spectra,” *Nucl. Instrum. Phys. Res. A*, 417, 405 (1998).

21. T. Gozani, “Active Nondestructive Assay of Nuclear Materials,” Office of Standards Development, NUREG/CR-0602 (1981).

22. M. B. Chadwick, P. Oblozinsky, M. Herman, et al., "ENDF/B-VII.0: Next generation evaluated nuclear data library for nuclear science and technology," *Nuclear Data Sheets*, Vol. 107, (2006).

23. E. Crouch, “Fission Product Yields from Neutron-induced Fission,” Atomic Data and Nuclear Data Tables, 19 (1977).

24. B. J. Rider, T. R. England, "Evaluation of Fission Product Yields for the U.S.A. National Nuclear Data Files," Los Alamos National Laboratory Report, LA-UR-87-2462 (1987).

25. T. R. England et al. "Fission Product Yield Evaluation for the U.S.A. Evaluated Nuclear Data Files," Los Alamos National Laboratory Report, LA-UR-94-3318 (1994).

26. "Compilation and Evaluation of Fission Yield Data," Final report of a co-ordinated research project 1991-1996, IAEA-TECDOC-1168, International Atomic Energy Agency (2000).

27. A. Koning, R. Forrest, M. Kellett, R. Mills, H. Henriksson, and Y. Rugama, "The JEFF-3.1 Nuclear Data Library," JEFF Report 21,OECD/NEA, France, (2006).

28. K. Krane, "Introductory Nuclear Physics," Wiley Sons Inc. (1987).

29. W. Loveland, D. Morrissey, G. Seaborg, "Modern Nuclear Chemistry," Wiley Sons Inc. (2006).

30. L. B. Engle, P. C. Fisher, "Energy and Time Dependence of Delayed Gammas from Fission," Los Alamos National Laboratory Report, LAMS-2642 (1962).

31. G. Keepin et al., "Nuclear Safeguards Research and Development," Program status report, Los Alamos National Laboratory Report, LAMS-4794 (1971).

32. F. Dolatshahi et al., "The Air Transport of Radiation (ATR) Code," Defense Nuclear Agency, DNA-TR-89-14 (1990).

33. D. Beddingfeld, "Identification and Quantification of Pu and U from Fission Product Gamma-Ray Spectra," Ph.D. dissertation (1996).

34. T. R. England and B. F. Rider, “Fission product yield evaluation for the USA evaluated nuclear data files,” Los Alamos National Laboratory Report, LA-UR-94-3106 (1994).

35. W. B. Wilson et. al., “A Manual for CINDER’90 Version 07.4 Codes and Data,” Los Alamos National Laboratory, LA-UR-07-8412 (2008).

36. V. Mozin, and S. Tobin, “DGSDEF: Discrete gamma-ray source DEFinition code,” Los Alamos National Laboratory, LA-CC-10-083 (2010).

37. R. J. LaBauve, T. R. England, D. C. George, R. E. MacFarlane and W. B. Wilson, “DANDE - A linked general code system for core neutronics/depletion analysis ," *Nucl. Sci. Eng*. Vol. 95, 152 (1987).

38. D. B. Pelowitz et al., “MCNPX^{TM} User’s Manual. Version 2.6.0,” Los Alamos National Laboratory, LA-CP-07-1473 (2008).

39. ENDF/B-VI Decay Data http://t2.lanl.gov/data/decayd.html.

40. Klingensmith, J.J., Gauld, I.C., 2005. ORIGEN-S gamma decay spectra characterization and benchmarking. Transactions of the American Nuclear Society 93, 33–34.

41. T. R. England, W. B. Wilson and M. G. Stamatelatos, “Fission Product Data for Thermal Reactors, Part 1: A Data Set for EPRI-CINDER Using ENDF/B-IV," Los Alamos Scientific Laboratory report, LA-6745-MS (1976).

42. T. R. England, W. B. Wilson and M. G. Stamatelatos, “Fission Product Data for Thermal Reactors, Part 2: Users Manual for EPRI-CINDER Code and Data," Los Alamos Scientific Laboratory report, LA-6746-MS (1976).

43. T. R. England, “CINDER – A One-Point Depletion and Fission Product Program," Bettis Atomic Power Laboratory report, WAPD-TM-334 (August 1962; Rev. June 1964).

44. W.B. Wislon et al., “Accelerator Transmutation Studies at Los Alamos with LAHET, MCNP, AND CINDER'90,” Workshop on Simulating Accelerator Radiation Environments, Santa Fe, NM (1993).

45. J. W. Durkee, et. al., “Delayed-Gamma Signature Calculation for Neutron-Induced fission and activation using MCNPX, Part I: Theory,” *Progress in Nuclear Energy*, 51, pg. 813-817 (2009).

46. L.P. Ekström and R.B. Firestone, WWW Table of Radioactive Isotopes, database version 2/28/99, from URL http://ie.lbl.gov/toi/index.htm.

47. ORTEC Maestro-32 Vol. 6.04 MCA Emulator (2005).

48. V. Mozin, S. Tobin, J. Vujic, and A. Hunt, “Delayed gamma-ray instrument for determining plutonium mass in spent nuclear fuel,” 2010 ANS Annual Meeting, San Diego CA, LA-UR-10-00561 (2010).

49. V. Mozin, S. Tobin, and J. Vujic, “Delayed gamma-ray technique for fissile material assay,” 51st Annual Mtg. of the Institute of Nuclear Material Management, Baltimore MD, LA-UR 10-04701 (2010).

50. C. Freeman, V. Mozin, S. Tobin, et al., “Feasibility of X-Ray fluorescence for spent fuel safeguards,” Annual Mtg. of the Institute of Nuclear Material Management, Baltimore MD (2010).

51. M. L. Fensin, S. J. Tobin, N. P. Sandoval, M. T. Swinhoe, and S. J. Thompson, “A Monte Carlo linked depletion spent fuel library for assessing varied nondestructive assay techniques for nuclear safeguards,” *Advances in Nuclear Fuel Management IV*, Hilton Head Island SC (2009).

52. H.Trellue, M.Fensin et al., "Description of the Spent Nuclear Fuel Used in the Next Generation Safeguards Initiative to Determine Plutonium Mass in Spent Fuel," Los Alamos National Laboratory report, LA-UR 1100300 (2010).

53. P. Blanc, S. J. Tobin, T. Lee, J. Hu, J. Hendricks, and S. Croft, "Delayed neutron detection with an integrated differential die-away and a delayed neutron instrument," 51st Annual Mtg. of the Institute of Nuclear Material Management, Baltimore MD, LA-UR 10-04125 (2010).

54. T. Lee, H. O. Menlove, M. T. Swinhoe, and S. J. Tobin, "Differential die-away technique for determination of the fissile contents in spent fuel assembly," 51st Annual Mtg. of the Institute of Nuclear Material Management, Baltimore MD (2010).

55. S. Croft, and R. Venkataraman, "Larger detector crystals for safeguards application," Los Alamos National Laboratory and Canberra Industries Inc. memo, (2010).

56. A. Favalli et al., "Investigation of the PGNA using the $LaBr_3$ scintillation detector," *Appl. Radiat. Isot.* 68 (2009).

57. Dr. Stephen Croft, Los Alamos National Laboratory, personal communication September (2010).

58. J. Duderstadt, L. Hamilton, "Nuclear Reactor Analysis," Wiley Sons Inc. (1976).

59. C. Powell, A. Jablonski, "NIST Electron Effective-Attenuation-Length Database - Version 1.3," National Institute of Standards and Technology, Gaithersburg, MD (2011).

60. J. R. Phillips, and G. E. Bosler, "Calculated response contributions of gamma rays emitted from fuel pins in an irradiated PWR fuel assembly," Los Alamos National Laboratory, LA-9837-MS (1994).

61. V. Mozin, S. Tobin, J. Vujic, "NGSI Project Update – Delayed Gamma-Ray Instrument Modeling," Los Alamos National Laboratory Report, LA-UR 10-00558 (2010).

62. V. Mozin, S. Tobin et al., "Delayed Gamma-Ray Assay for Spent Nuclear Fuel Safeguards," Los Alamos National Laboratory report, LA-UR 11-00261 (2010).

63. P. Bin et al., "ADONIS, High Count Rate HPGe Gamma Spectrometry algorithm: Irradiated Fuel Assembly Measurement," ANIMMA 2011 International Conference, Ghent France (2011).

64. F. Carrel et al., "Detection of high-energy delayed gammas for nuclear waste packages characterization," *Nucl. Instr. Meth. A* (2010).

65. M. Gmar et al., "Use of delayed gamma spectra for detection of actinides (U,Pu) by photofission," *Nucl. Instr. Meth. A* 422 (1999).

66. D. Marquardt, "An Algorithm for Least-Squares Estimation of Nonlinear Parameters". *SIAM Journal on Applied Mathematics* 11 (2): 431–441. (1963).

67. K. Madsen, N.B. Nielsen, and O. Tingleff. "Methods for nonlinear least squares problems." Technical Report. Informatics and Mathematical Modeling, Technical University of Denmark. (2004).

68. G.F. Knoll, "Radiation detection and measurement," John Wiley Sons Inc. (2000)